Year : 2016

E2F1 inhibits circulating cholesterol clearance by regulating PCSK9 expression in the liver (PhD)

Lai Qiuwen

UNIL | Université de Lausanne

Faculté de biologie
et de médecine

Department of Physiology

**E2F1 inhibits circulating cholesterol clearance by regulating PCSK9
expression in the liver (PhD)**

Thèse de doctorat ès sciences de la vie (PhD)

présentée à la

Faculté de biologie et de médecine
de l'Université de Lausanne

par

QIUWEN LAI

PhD in Life Science

Jury

Prof. Francois Pralong, President Prof.
Prof. Lluis Fajas Coll, Directeur de these
Prof. Christian Widmann, expert
Prof. Von Eckardstein Arnold, expert

Lausanne 2016

Imprimatur

Vu le rapport présenté par le jury d'examen, composé de

Président·e	Monsieur	Prof.	François **Pralong**
Directeur·rice de thèse	Monsieur	Prof.	Luis **Fajas Coll**
Experts·es	Monsieur	Prof.	Christian **Widmann**
	Monsieur	Prof.	Arnold **Von Eckardstein**

le Conseil de Faculté autorise l'impression de la thèse de

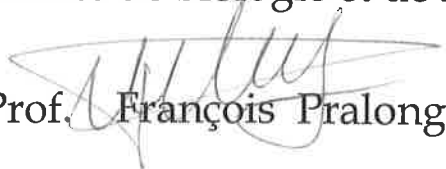## Madame Qiuwen Lai

Master in Life Sciences and Technologies Ecole Polytechnique Fédérale de
Lausanne

intitulée

E2F1 inhibits circulating cholesterol clearance
by regulating PCSK9 expression in the liver (PhD)

Lausanne, le 3 octobre 2016

pour le Doyen
de la Faculté de biologie et de médecine

Prof. François Pralong

Acknowledgements

Table of Contents

Table of Contents

Abstract

Abstract

The metabolic syndrome has become a worldwide epidemic. It includes obesity, dyslipidemia, diabetes and nonalcoholic fatty liver disease (NAFLD). The metabolic syndrome is caused, amongst others, by alterations in lipid metabolism, that lead to aberrant whole body energy homeostasis and thus disease development. Hence, understanding how cells regulate lipid homeostasis is key to treat lipid deregulation. Recently, novel regulators of metabolic processes, including cell cycle regulators like cell cycle dependent kinase 4 (CDK4) and E2F transcription factors 1 (E2F1) have been identified. Here, we show that E2F1 plays a crucial role in maintaining cellular cholesterol homeostasis through the regulation of cholesterol uptake via the proprotein convertase subtilisin/kexin type 9 (PCSK9); an enzyme that upon activation promotes low-density lipoprotein receptor (LDLR) degradation.

We found that the E2F1-/- mice have reduced total plasma cholesterol and elevated cholesterol content in the liver, suggesting an increase of cholesterol uptake. Following these observations, we showed that E2F1 deletion leads to a marked decrease in PCSK9 expression and to an increase in LDLR expression. In addition to the upregulation of LDLR, we also demonstrated that E2F1-/- hepatocytes have increased LDL uptake. Moreover, ChIP-seq and PCSK9 reporter experiments confirmed that E2F1 binds and transactivates PCSK9 promoter. Consistent with this, E2F1-/- mice fed a high cholesterol diet (HCD) displayed a fatty liver phenotype, confirming our hypothesis that E2F1 controls cholesterol uptake.

Collectively, our results suggest that E2F1 plays a physiological role in maintaining cholesterol balance via the control of PCSK9 expression, which in turn controls LDLR stability. The newly identified E2F1-PCSK9 axis is likely the first report to define the role of E2F1 in cholesterol metabolism and to improve therapeutic strategies to counteract dyslipidemia.

Résumé

E2F1 inhibe l'absorption du cholestérol circulant en régulant l'expression de PCSK9 dans le foie

Les maladies métaboliques constituent actuellement l'épidémie mondiale du 21ème siècle. L'altération du métabolisme lipidique peut conduire à des altérations de l'homéostasie du corps en entier, qui résultent dans le développement de maladies telles que le diabète, la stéatose hépatique et l'athérosclérose. Par conséquent, comprendre comment les cellules régulent l'homéostasie lipidique est clef pour fournir des connaissances pour lutter contre les dérégulations lipidiques. Au cours des années, la recherche à permis de mettre en évidence de nouveaux régulateurs des processus métaboliques, tels que des facteurs du cycle cellulaire comme CDK4 (Cell Cycle Dependent Kinase 4) et E2F1 (E2F transcription factor 1). Nous avons mis en évidence que le facteur de transcription E2F1 joue un rôle crucial dans le maintien de l'homéostasie cellulaire du cholestérol, via la régulation de son incorporation, par l'intermédiaire de PCSK9 (Proprotein convertase subtilisin/kexin type 9) ; une enzyme qui induit une dégradation des LDLR (Low density lipoprotein receptor).

Les souris E2F1-/- ont un taux de cholestérol plasmatique diminué et une augmentation du contenu de cholestérol dans le foie, suggérant une augmentation de l'absorption du cholestérol. Suite à cette observation, nous avons démontré que l'inactivation du gène E2F1 entraîne une diminution marquée de l'expression de PCSK9, et une augmentation de l'expression du LDLR. Ainsi, les hépatocytes E2F1-/- sont caractérisés par une augmentation de l'absorption de LDL. De plus, des expériences de ChIP-seq, et l'utilisation de rapporteurs d'activité de promoteurs, démontrent que E2F1 se lie au promoteur de PCSK9 en activant ainsi l'expression de ce gène. De façon intéressante, les souris E2F1-/- ayant subi un régime riche en cholestérol (HCD-High cholesterol diet) développent une stéatose hépatique, confirmant notre hypothèse que E2F1 contrôle l'absorption du cholestérol. Dans l'ensemble, nos résultats suggèrent que E2F1 joue un rôle physiologique dans le maintien de

l'homéostasie du cholestérol par le contrôle de l'expression de PCSK9, qui à son tour contrôle l'absorption optimale des stérols.

Notre travail aura un impact important, car il identifie un nouveau rôle pour le facteur de transcription E2F1, connu pour son implication dans le cycle cellulaire et le cancer, dans le contrôle du métabolisme du cholestérol.

Abbreviations

ABCA1	ATP-binding cassette A1
ABCG1	ATP-binding cassette G1
ABCG5	ATP-binding cassette G5
ABCG8	ATP-binding cassette G8
ACAT	Acyl-CoA acyl-transferase
ACC	Acetyl-CoA carboxylase
BA	Bile acid
BSEP	Bile acid salt export pump
CA	Cholic acid
CDCA	Chenodeoxycholic acid
CDK4	Cell cycle dependent kinase 4
CDK6	Cell cycle dependent kinase 6
CE	Cholesterol ester
CETP	Cholesteryl ester transfer protein
ChIP-seq	Chromatin immunoprecipitation-high-throughput DNA sequencing
ChREBP	Carbohydrate responsive element binding protein
CM	Chylomicron
CVD	Cardiovascular diseases
CYP7A1	Cytochrome P450 Family 7 subfamily A member 1
CYP7B1	Cytochrome P450 Family 7 subfamily B member 1
DCC	3, 5- diethoxycarbonyl-1, 4-dihydrocollidine
DHFR	Dihydrofolate reductase
DP	Dimerization protein
E2F1	E2F transcription factor 1
ER	Endoplasmic reticulum
FAS	Fatty acid synthase
FH	Familial hypercholesterolemia
FHBL	Familial heterozygous hypobetalipoproteinemia
FXR	Farnesoid X receptor

GK	Glucokinase
GLUT2	Glycolytic glucose transporter 2
HCC	Hepatocellular carcinoma
HCD	High cholesterol diet
HDL	High density lipoprotein
HMGCR	3-Hydroxy-3-methylglutaryl-CoA reductase
HNF1	Hepatocyte nuclear factor 1
HSC	Hepatic stellate cells
IDL	Intermediate density lipoprotein
Insig	Insulin-induced gene
IPP	Isopentenyl pyrophosphate
IRS	Insulin receptor substrate family
KC	Kupffer cells
LCAT	Lecithin:cholesterol acyltransferase
LDL	Low density lipoprotein
LDL-C	Low density lipoprotein cholesterol
LDLR	Low density lipoprotein receptor
L-PK	Liver glycolytic pyruvate kinase
LPL	lipoprotein lipase
LRH-1	Liver receptor homologue-1
LRP1	LDL related protein 1
LXR	Liver X receptor
MEF	Mouse embryonic fibroblasts
MS	Mass spectrometry
NAFLD	Nonalcoholic fatty liver disease
NASH	Nonalcoholic steatohepatitis
NLRP3	NOD-, LRR and pyrindomain-containing 3
NPC1L1	Niemann-pick type C1-like 1
NTCP	Sodium taurocholate cotransporter polypeptide
PCSK9	Proprotein convertase subtilisin/kexin type 9
PDH	Pyruvate dehydrogenase
PDK1	Phosphoinositide dependent kinase 1

PDK4	Pyruvate dehydrogenase kinase 4
PI3K	Phosphoinositide 3-kinase
PKB	Protein kinase B
PPARγ	Peroxisome proliferator-activated receptor γ
RB	Retinoblastoma protein
RCT	Reverse cholesterol transport
RXR	Retinoid X receptors
SCAP	SREBP cleavage activating sensing protein
SCD1	Stearoyl CoA desaturase
SHP	Small heterodimer partner
SRE	SREBP response element
SREBP1c	Sterol regulatory element binding proteins 1c
SREBP2	Sterol regulatory element binding proteins 2
SCARB1	Scavenger receptor class B member 1
TG	Triglyceride
TGFβ	Tumor growth factor β
TK	Thymidine kinase
TNFα	Tumor necrosis factor α
TRL	Triglyceride rich lipoprotein
VLDL	Very low density lipoproteins
WAT	White adipose tissue
α-SMA	α-Smooth muscle actin

Chapter 1. Introduction

Chapter 1. Introduction

Deregulated cholesterol levels are a known risk factor for atherosclerosis. In humans, long-term intake of dietary cholesterol in excess raises serum cholesterol and increases the risk of cardiovascular diseases (CVDs). CVDs are one of the leading causes of death worldwide, resulting in approximately 17.5 million deaths in 2012. In the past 20 years, the management of CVDs relied on the use of statins. However, recent studies have shown that long-term statins use could increase the risk of diabetes and produce other undesired side effects (Thompson et al. 2016). In this context, understanding novel pathways regulating cholesterol metabolism is essential for the development of new therapies against CVDs.

The transcription factor E2F1 has well-established roles in cell proliferation, differentiation, and apoptosis (Wu et al. 1994, Richon et al. 1996, Biswas et al. 2012). Emerging evidence has demonstrated that E2F1 also plays an important role in glucose, oxidative and fatty acid metabolism (Annicotte et al. 2009, Denechaud et al. 2016, Lagarrigue et al. 2016) . A previous study by Hsieh and co-workers has shown that E2F1-/- mice have lower plasma cholesterol, raising the possibility that E2F1 could also be implicated in the regulation of cholesterol homeostasis (Hsieh et al. 2008).

In this thesis, I focused primarily on understanding and deciphering the role of E2F1 in the control of cholesterol metabolism. In this chapter, I will first summarize the key processes involved in maintaining cholesterol homeostasis, follow by introducing the well-established functions of E2F1 in cell cycle as well as its recently reported functions.

I.   Cholesterol metabolism

In mammals, cholesterol is an essential building block for cell membranes, important metabolites (e.g. bile acids (BAs), steroid hormones and oxysterols), which play important biological functions in all living organisms (Wallace et al. 2015). Cholesterol can be obtained from exogenous dietary

Figure. 1   **Structural composition of lipoprotein.**

Legend

Apolipoprotein

Phospholipid

Free cholesterol
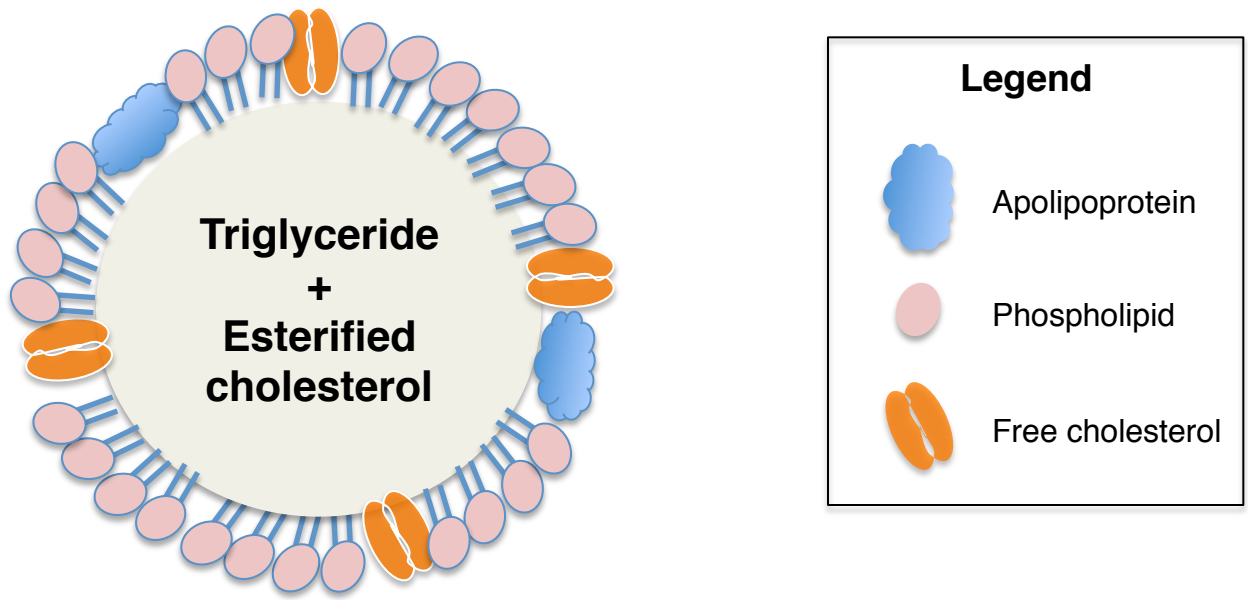
Table. 1   **Main class of lipoprotein .**

Lipoprotein Class	TG	PL	Free-chol	E-chol	Protein	Main apolipo-protein
Chylomicron	80-95	3-6	1-3	2-4	1-2	A-I, A-IV, A-V, B-48, C-I, C-II, C-III.E
VLDL	45-65	15-20	4-8	16-22	6-10	B-100, E, C-I, C-II, C-III
LDL	4-8	18-24	6-8	45-50	18-22	B-100
HDL	2-7	26-32	3-5	15-20	45-55	A-I, A-II, E

VLDL: very low density lipoprotein, LDL: low density lipoprotein, HDL: high density lipoprotein, TG: triglyceride, PL: phospholipid, Free-chol: free cholesterol, E-chol: esterified cholesterol. Values are expressed as % of lipoprotein weight.

sources or can be endogenously synthesized by the tissues. In this section, I will focus on the endogenous and exogenous pathways for cholesterol homeostasis.

1. Cholesterol homeostasis

1.1 Lipoproteins

Cholesterol is a lipophilic and highly insoluble molecule, therefore it has to be transported in the form of lipoproteins, which are constituted by a hydrophobic core containing phospholipids, apolipoproteins, triglycerides (TG), esterified and free cholesterol (figure 1). Cholesterol homeostasis is maintained by complex lipoprotein metabolism that involves a cascade of activities between apolipoproteins, enzymes, and cellular receptors. There are four main types of circulating lipoproteins namely chylomicrons (CMs), very low-density lipoproteins (VLDLs), low-density lipoproteins (LDLs) and high-density lipoproteins (HDLs). Lipoproteins can be classified based on their size, density, composition and function as summarized in table 1 (Hegele 2009).

1.2. Cholesterol circulation

The lipid content present in the diet consists of triglycerides (TG), cholesterol and phospholipids. Dietary TG and cholesterol are first emulsified in the intestine by bile salts and hydrolyzed into monoglycerides, free fatty acids, and cholesterol by pancreatic lipases in order to penetrate the intestinal cell. Emulsification increases the surface area, allowing lipases to digest TG into monoglycerides and fatty acid. Once absorbed by the enterocytes in the small intestine, monoglycerides, and fatty acids, as well as free cholesterol and esterified cholesterol, are packaged into chylomicrons which enter the circulation via the lymphatic system (van der Wulp et al. 2013). In the circulation, chylomicrons are hydrolyzed by lipoprotein lipase (LPL), releasing fatty acid and monoglycerides, which can be taken up by the adipocytes or muscle cells for usage or storage respectively. The depletion of triglycerides

Figure. 2   **Metabolism of cholesterol: central role of the liver.**
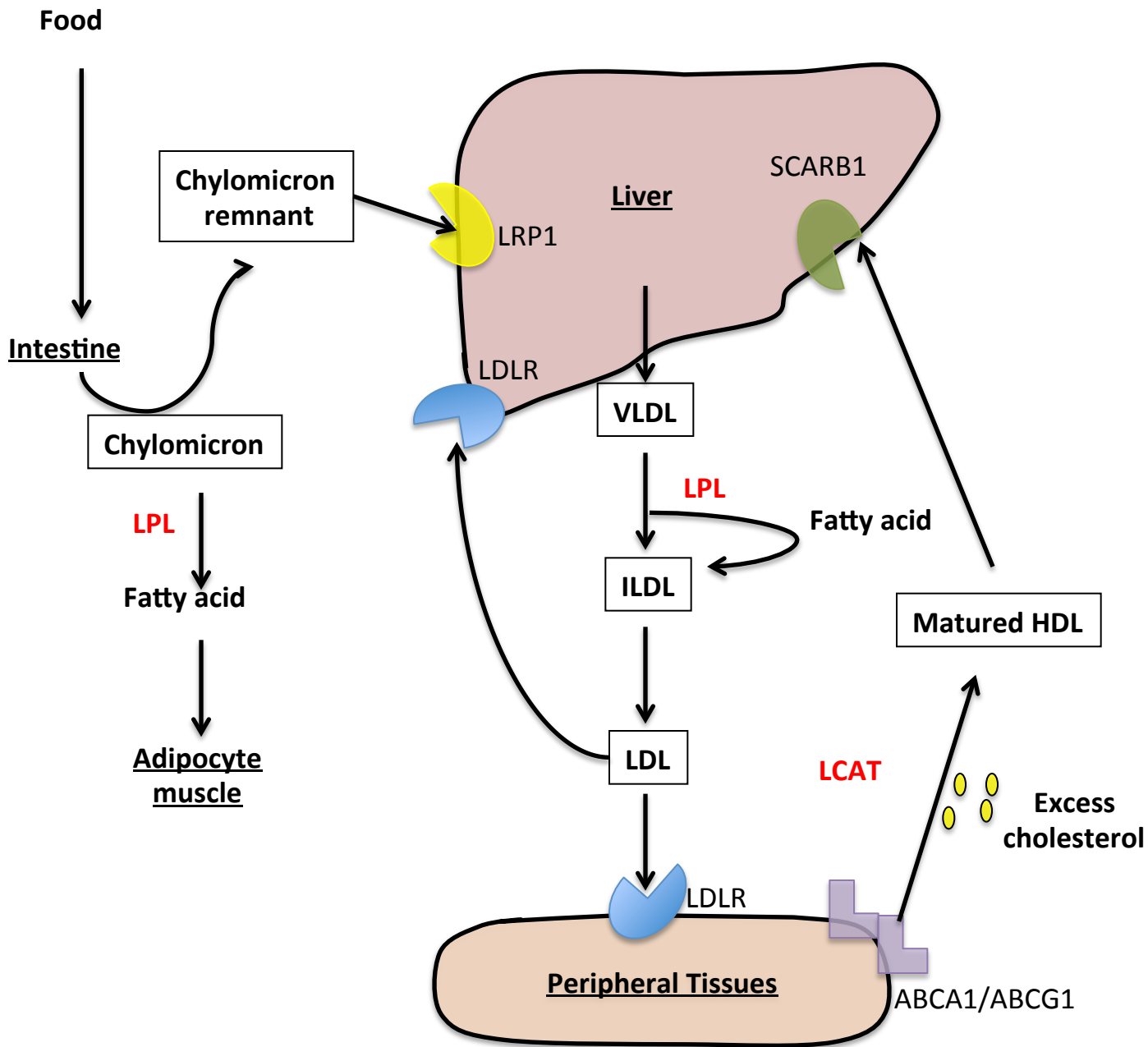
Exogenous lipoproteins metabolism. Dietary lipid is digested and emulsified into free fatty acid by pancreatic lipase and absorbed by the enterocytes of the small intestine. Once in the enterocytes, free fatty acid, monoglycerides and cholesterol are packaged into chylomicrons and enter the circulation. **Endogenous lipoproteins metabolism**. VLDL is synthesized in the liver and enters into the circulation. In the circulation, VLDL is converted to IDL in the muscle and then further transformed to LDL and are uptake by peripheral tissues. **RCT**. Excess cholesterols from the peripheral tissues are loaded into nascent HDL forming a matured HDL. Matured HDL returned to the liver, where excess cholesterol is converted into bile for excretion. VLDL: very low density lipoprotein, IDL: intermediate density lipoprotein, LDL: low density lipoprotein, HDL: high density lipoprotein, TG: triglyceride, PL: phospholipid, Free-chol: free cholesterol, E-chol: esterified cholesterol, LPL: lipoprotein lipase, LCAT: lecithin:cholesterol acltransferase, RCT: reverse cholesterol transport, SCARB1:scavenger receptor class B member 1, ABC:ATP-binding cassette transporters LRP1: LDL related protein 1.

from the chylomicrons forms smaller particles known as chylomicron remnants. In comparison to chylomicrons, the chylomicron remnants contain more cholesterol and are pro-atherogenic (Feingold et al. 2000). Thereafter, chylomicron remnants need to be taken up by the hepatocytes via LDL-related protein 1 (LRP1) (Ferns et al. 2008) (figure 2).

In contrast, the endogenous lipoprotein pathway begins in the liver with the production of VLDLs. The TG content in the VLDLs is metabolized in muscle and adipose tissue by lipoprotein lipases forming an intermediate density lipoproteins (IDLs), which are enriched with cholesterol. The IDLs are further converted to LDLs, which are taken up by the liver and other peripheral tissues via the LDL receptor (LDLR) (figure 2).

Excess cholesterol from the peripheral tissues is removed through a process known as reverse cholesterol transport (RCT). RCT begins with the synthesis of nascent HDLs in the liver and in the intestine. The HDLs acquire excess cholesterol from peripheral tissues, which leads to the formation of mature HDLs (figure 2). The mature HDLs are then transported back to the liver, where excess cholesterol can be excreted directly into the feces or eliminated after conversion into bile acids. Bile acids serve as signaling molecules for key biological functions and are also important for the solubilization of dietary intake. Up to 95% of the bile acids are reabsorbed in the ileum and returned to the liver. The enterohepatic circulation of bile acids provides an efficient mechanism to conserve the bile acid pool in the intestinal and hepatobiliary tract (Ferrebee et al. 2015) (figure 2).

2. *Cellular cholesterol metabolism*

Cholesterol homeostasis is a tightly regulated process at the cellular level. Broadly, homeostasis requires a balance between endogenous synthesis, lipoprotein uptake and excretion (figure 3).

2.1. *Cholesterol synthesis*

16

Figure. 3   **Cellular cholesterol metabolism.**
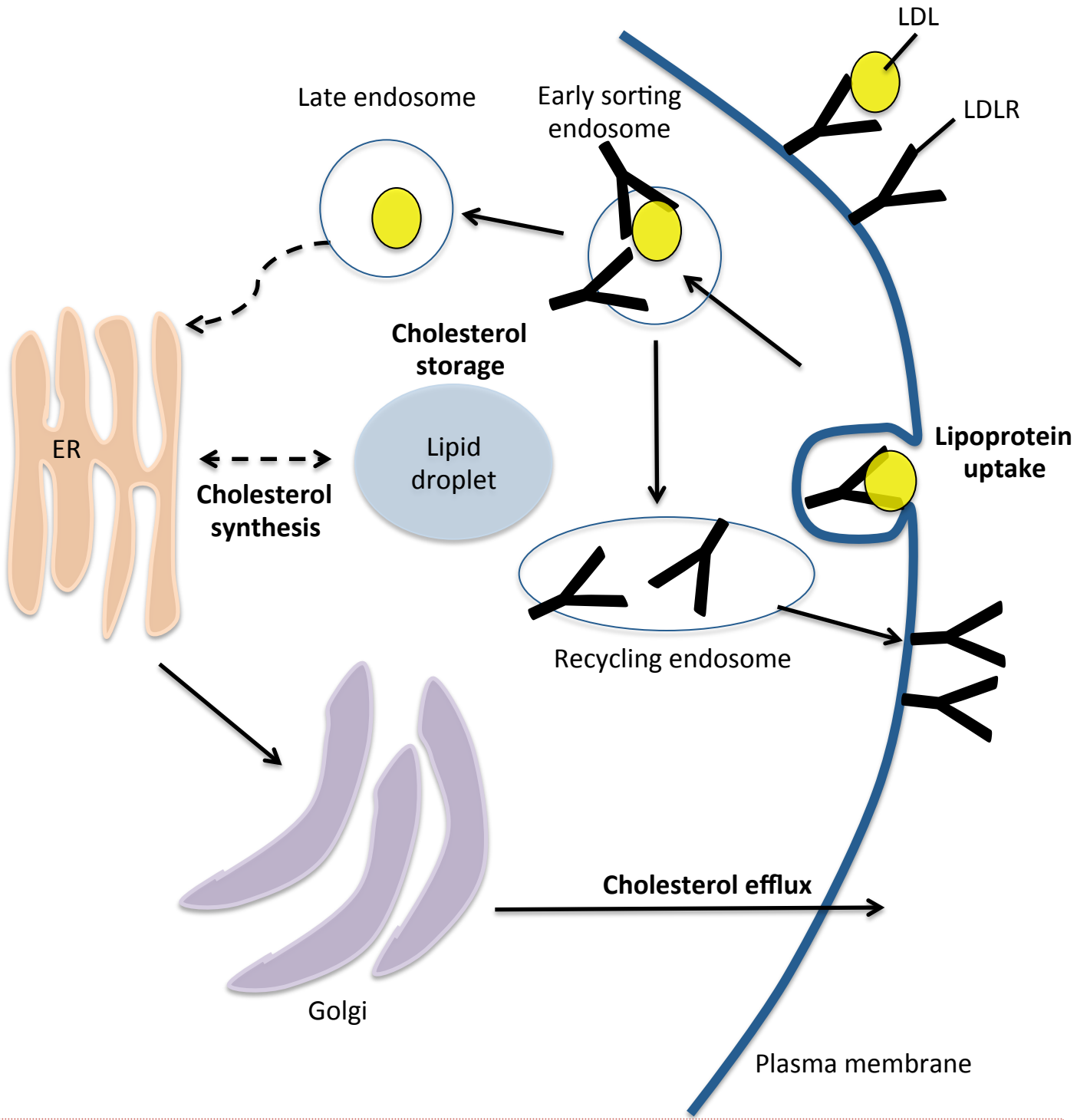
Lipoprotein uptake. LDL uptake is mediated by LDLR and dispenses to endosomes. The acidic condition in endosome induces the release of LDL from the receptor. The LDLR is recycled back to the plasma membrane while LDL is delivered to the ER or the lipid droplet for storage. **Cholesterol synthesis.** Synthesis takes place in the ER and cholesterol is stored in lipid droplet or transported to other intracellular compartment. **Cholesterol efflux.** A process whereby excess cholesterol is loaded to nascent HDL and return to the liver for excretion. LDL: low density lipoprotein, ER: endoplasmic reticulum, LDLR: low density lipoprotein receptor.

While all cells can synthesize cholesterol, the liver is the main organ that produces the majority of the cholesterol required by the body. *De novo* cholesterol biosynthesis play important roles in both cellular and developmental pathways. Intermediate metabolites produced during this process serve as building blocks for several end products e.g. dolichol, coenzyme Q, isopentenyl-tRNA. The importance of cholesterol is evident from the discovery of an increasing number of genetic disorders that are associated with mutations in different cholesterol biosynthetic enzymes (Nwokoro et al. 2001)

Cholesterol biosynthesis takes place at the endoplasmic reticulum (ER) and begins with the substrate Acetyl-CoA, which is mainly produced from the oxidation reactions that occur in the mitochondria (figure 4). The entire process involves over 30 different enzymes. The key rate-limiting enzyme of this pathway is 3-hydroxy-3-methylglutaryl-CoA reductase (HMGCR), which catalyzes the reaction from HMG-CoA to mevalonate. The inhibition of HMGCR activity is a common target for cholesterol-lowering drugs, such as statins. During the process of cholesterol synthesis, all reductive reactions require the use of NADPH, as a cofactor. Mevalonate then undergoes a series of phosphorylations and decarboxylations reactions, producing isoprenoid and isopentenyl pyrophosphate (IPP). A condensation reaction then occurs in the presence of squalene synthase, leading to the formation of squalene, which is subsequently converted to lanosterol, the first sterol produced in the reaction. From lanosterol, cholesterol formation requires an additional 19 steps reactions (van der Wulp et al. 2013). Because excessive free cholesterol is toxic for cells, the majority of the cholesterol is esterified into cholesterol esters (CEs) by an enzyme known as acyl-CoA acyl-transferase (ACAT) and is stored as lipid droplets or transported into other intracellular compartment (Brown et al. 1980).

2.2. LDL Cholesterol uptake

Figure. 4   **Cholesterol biosynthetic pathway.**
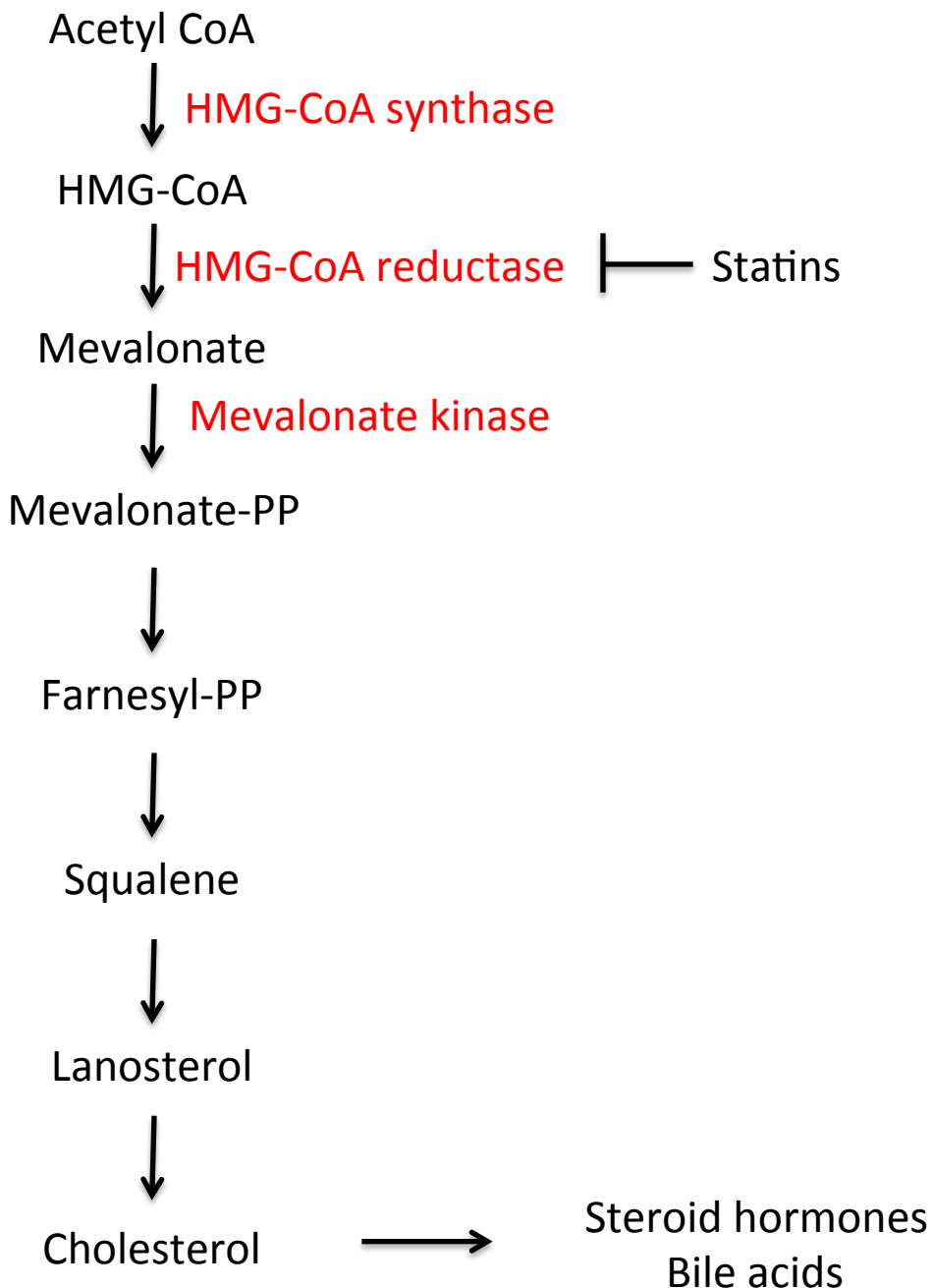
Acetyl CoA is converted to cholesterol in a series of enzymatic steps. Statins inhibit cholesterol synthesis by inhibiting the rate limiting enzyme, HMG-CoA reductase, and is widely used as a drug to treat hyperdyslipidemia. CoA: coenyzme, HMG-CoA: 3-hydroxy-3-methylglutaryl-coenzyme A.

Cells can also obtain cholesterol through the uptake of circulating plasma lipoproteins via LDLR dependent pathway (figure 2). The uptake of the LDLs and other ApoE/ApoB lipoproteins are mediated by LDLR. LDLs bind to the LDLRs and are endocytosed into a clathrin-coated vesicle and transported to the acidic endocytic compartment, where cholesterol esters are hydrolyzed by hormone-sensitive lipases (Brown et al. 1986). The LDLRs are then dissociated from the LDLs and are recycled back to the plasma membrane by a reaction mediated by small Rab GTPases (Holtta-Vuori et al. 2002). The cholesterol remaining in the early endosome forms the late endosome, which are responsible for the delivery of cholesterol to other membranes, such as the plasma membrane, endoplasmic reticulum (ER) and lipid droplets for storage (figure 3).

The degradation of LDLRs is regulated by the enzyme, proprotein convertase subtilisin/kexin 9 (PCSK9). The 25kb PCSK9 gene is constituted of 12 exons and 11 introns (de Almeida et al. 2013). Structurally, the PCSK9 protein is composed of a signal sequence, an N-terminal prodomain, a catalytic domain, and a C-terminal domain. PCSK9 is mainly expressed and synthesized in the liver, with lower expression in the intestine, kidney, and brain (Seidah et al. 2003). PCSK9 is initially produced as an inactive precursor form, that undergoes autocatalytic processing to release an N-terminal prodomain segment. The N-terminal segment functions as a folding chaperone and as a catalytic site inhibitor. The degradation of LDLR is initiated by the interaction with the catalytic sites of secreted PCSK9 and the epidermal growth factor domain of LDLR. The PCSK9-LDLR complex enters the lysosome where degradation of LDLR occurs (Zhang et al. 2007) (figure 5). Loss of PCSK9 in humans has no known adverse effects; in fact, a nonsense mutation in PCSK9 lowered LDL levels by approximately 30% (Cohen et al. 2005, Cohen et al. 2006, Hallman et al. 2007). In mouse models, the deletion of PCSK9 caused an increase of LDLRs levels, resulting in significantly lower LDL in the plasma (Rashid et al. 2005). As a result, PCSK9 inhibitors have emerged as a new class of drugs used to treat hypercholesterolemia.

Figure. 5

Degradation of LDLR by PCSK9.
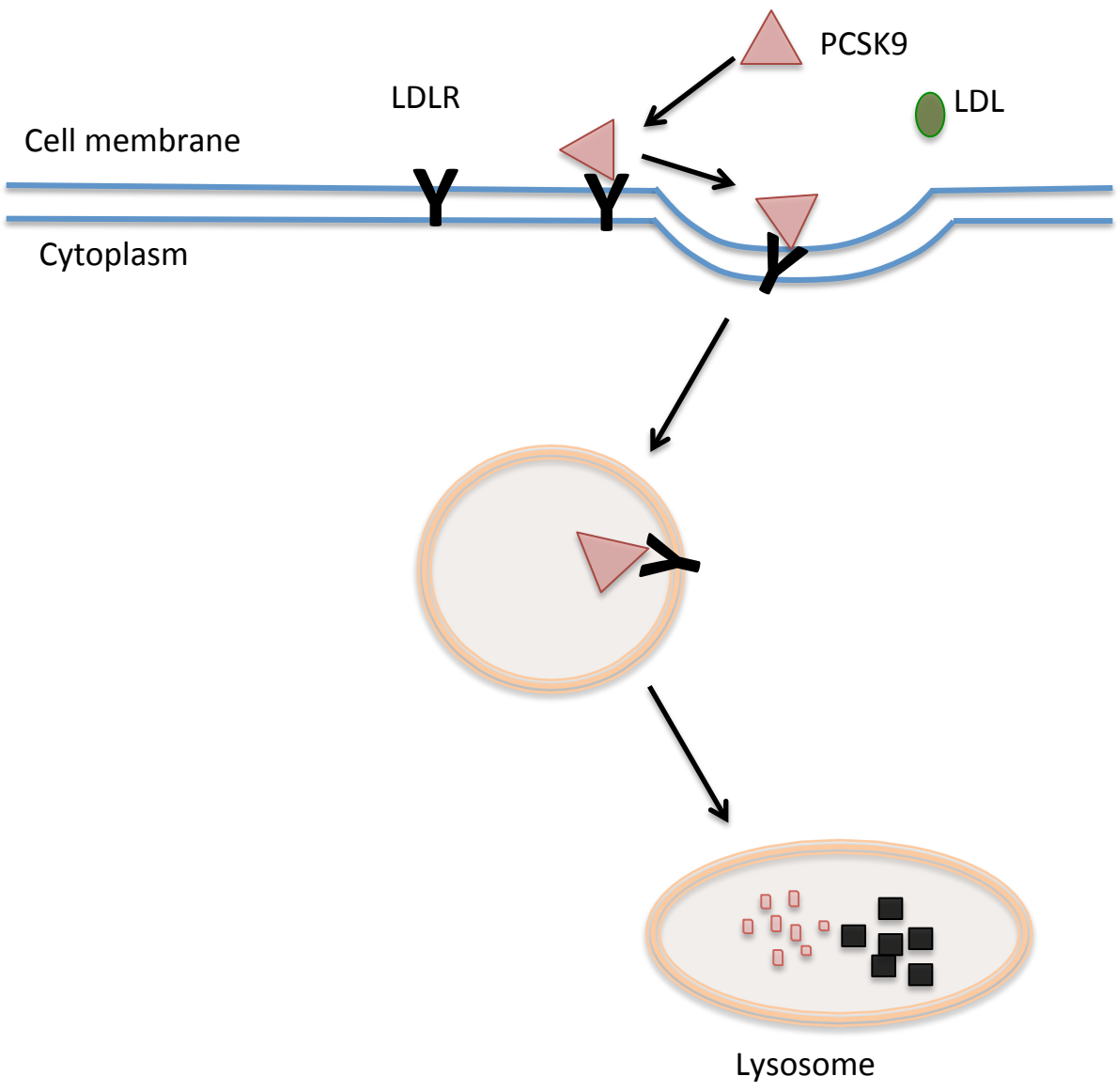
PCSK9 binds to the LDLR and facilitate endocytosis into the lysosome where degradation of LDLR occurs. LDLR: low density lipoprotein receptor, PCSK9: proprotein convertase subtilisin/ kexin 9, LDL: low density lipoprotein. Image is adapted Mullard, A., 2012.

2.3. Excretion via bile acid

Bile acids (BAs) synthesis is a multistep process that begins with the conversion of cholesterol to 7α-hydroxycholesterol by cytochrome P450 Family 7 subfamily A member 1 (CYP7A1), the rate-limiting enzyme of bile acid synthesis. The final products of the BA synthesis pathway are chenodeoxycholic acid (CDCA) and cholic acid (CA), which are also termed as primary bile acids. BAs are stored in the gallbladder and secreted into the intestine where they interact with TGs, phospholipids, and cholesterol to form micelles. Micelles improve the digestion and absorption of dietary triglycerides and cholesterol. Subsequently, 95% of the bile acids are reabsorbed, while 5% are excreted in the feces (Cohen 2008, Spinelli et al. 2016).

Many factors are involved in reverse cholesterol transport (RCT) and among them, lecithin:cholesterol acyltransferase (LCAT) and cholesteryl ester transfer protein (CETP) are the most critical. Functionally, LCAT is an enzyme that is found at the surface of HDLs. This enzyme converts free cholesterol into cholesterol esters. The cholesterol esters produced are packed into the core of the HDLs and bind to the scavenger receptor class B member 1 (SCARB1) localized on the surface of the hepatocytes. CETP also facilitates RCT by increasing the transfer of cholesterol esters from the HDLs to LDLs and VLDLs, which later are removed via LDLR-mediated pathway or directly converted to bile acids for excretion in the liver. Although CETP plays a significant role in cholesterol clearance, the conversion of esterified cholesterol from non-atherogenic lipoproteins (HDLs) to atherogenic lipoproteins (LDLs or VLDLs) suggests that it may be proatherogenic. This could explain why mice are less prone to atherosclerotic lesions, that unlike in humans, they lack CETP activity (Marotti et al. 1993).

ATP-binding cassette (ABC) transporters are also crucial mediators of cholesterol secretion into the bile. ABCG5/8 are expressed mainly in the liver and intestine, which mediate the conversion of cholesterol into bile acid. In the ABCG5/8 knockout mouse model, there is a 75% reduction in biliary cholesterol secretion (Yu et al. 2002). An overexpression of ABCG5/8 leads to an increase in cholesterol secretion (Dikkers et al. 2015). These data suggested that

19

Figure. 6   The process of SREBP proteolytic cleavage.
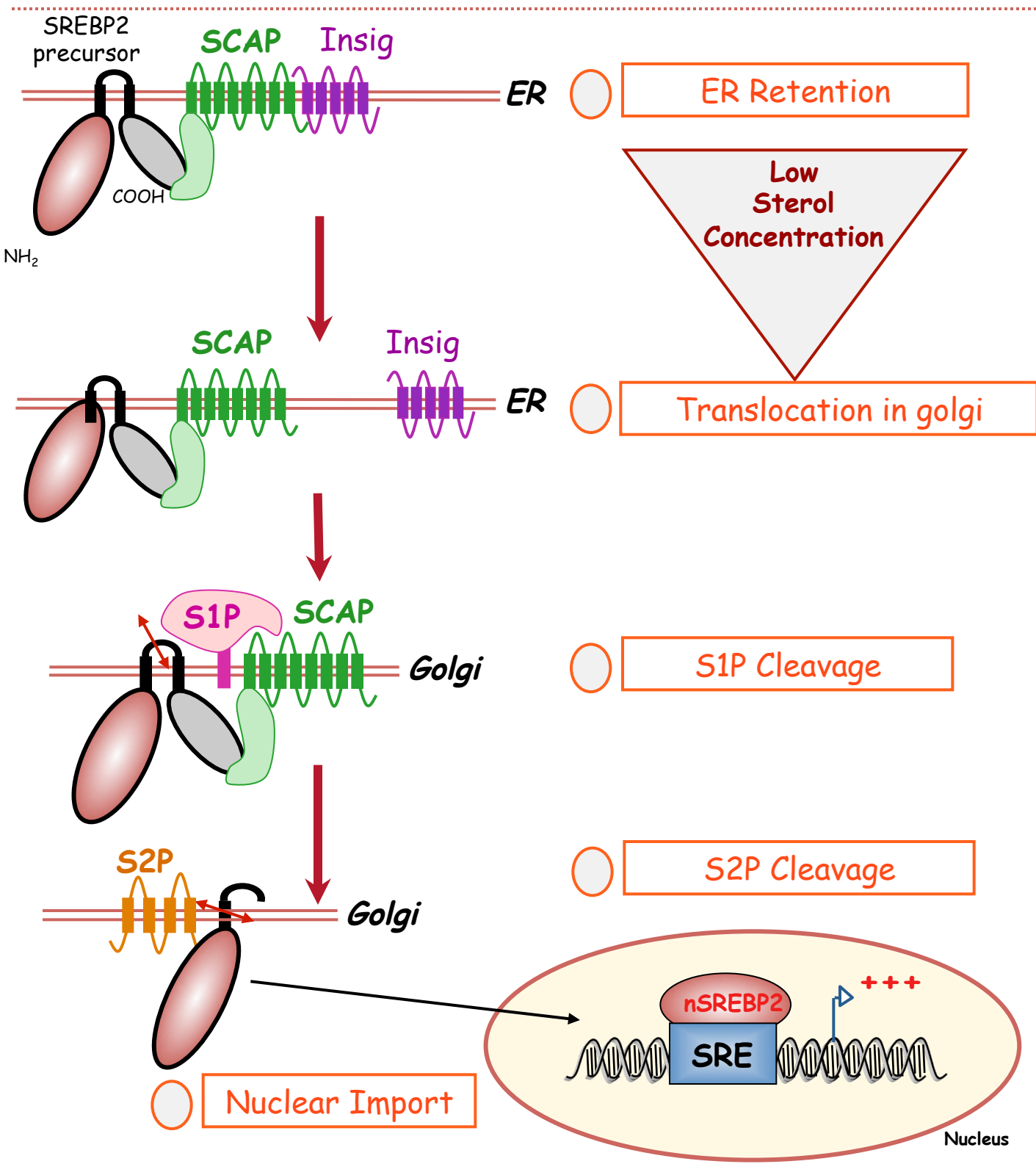
At low sterol concentration, Insig is released from SCAP. SCAP then transport SREBP2 to the Golgi where it is cleaved by S1P and S2P. The active form of SREBP2 binds to the SRE in the nucleus and activate genes involved in cholesterol synthesis and uptake. SCAP:SREBP cleavage activating sensing protein, Insig: insulin-induced gene, ER: endoplasmic reticulum, S1P: site-1 protease, S2P:site-2 protease, SRE: SREBP responsive element. Image adapted from Yabe et al. 2002.

mutation of ABCG5/8 is associated with an increased of dietary cholesterol absorption and defective biliary excretion. ABCA1 is also central in regulating cholesterol efflux. ABCA1 is required to initiate the first stage of RCT, by transferring cholesterol to lipid-poor apolipoprotein, apoAI (Yamauchi et al. 2016). A mutation in ABCA1 leads to Tangier Disease, a disorder characterized by HDL deficiency and by the accumulation of cholesterol in macrophages (Oram et al. 2001).

3. *Transcriptional regulation of cholesterol homeostasis*

Cholesterol homeostasis is regulated at the transcriptional level. In this section, I will describe the various regulators involved in cholesterol biosynthesis, cholesterol uptake and the major nuclear receptors involved in regulating cholesterol and bile acid metabolism.

3.1. *Control of cholesterol synthesis*

Cholesterol homeostasis is a tightly regulated process that involves both positive and negative regulation, in response to the corresponding metabolic flux. There are three SREBP isoforms, namely SREBP1a, SREBP1c and SREBP2. Functionally, SREBP1a is an inducer of all SREBP-responsive genes, SREBP1c selectively regulates the transcription of genes involved in the fatty acid metabolism while SREBP2 governs the genes that participate in cholesterol synthesis and uptake (e.g. HMGCS, HMGCR, LDLR) (Horton et al. 1999, Horton et al. 2002).

SREBP2 is also regulated at the transcriptional and post-transcriptional levels. SREBP2 contains a sterol response element in the promoter region and upon sterol sensing, SREBP2 can induce its own expression. In the inactive state, SREBP2 is bound to SREBP cleavage-activating sensing protein (SCAP) and insulin-induced gene (Insig) at the ER. SCAP is a transmembrane protein that contains a sterol-sensing domain and is responsible for transporting SREBP2 to the Golgi (Yang et al. 2002). On the other hand, Insig is an ER membrane protein that mediates SCAP-SREBP2 retention at the ER, in response to sterol signaling (Yabe et al. 2002). At low cholesterol levels, Insig is released from the SCAP-SREBP2 complex, allowing SCAP to interact with the

COPII trafficking complex, which guides SREBP2 to the Golgi, where it is processed by two membrane-bound proteases (site-1 protease (S1P) and site-2 proteases (S2P)). Active SREBP2 then enters the nucleus to induce the expression of cholesterol synthesis and uptake genes such as HMGCR, LDLR and PCSK9 (Brown et al. 2002, Goldstein et al. 2006) (Figure 6). Moreover, SREBP2 can be modified by ubiquitination and be directed for degradation by the proteasomes. It has been also established that SREBP2 can be negatively regulated by sumoylation (Hirano et al. 2003). In addition to SREBP2, HMGCR is also tightly regulated so that cholesterol synthesis is inhibited when cells detect high cholesterol levels. For example, sterol intermediates such as lanosterols and oxysterols serve as signaling molecules that drive HMGCR degradation. The degradation of HMGCR is mediated by Insig. In the presence of high levels of sterol intermediates, the HMGCR-Insig interaction is induced, promoting the HMGCR ubiquitination and subsequent degradation (Song et al. 2005).

3.2. Control of LDL cholesterol uptake

During cholesterol depletion, SREBP2 induces the transcription of LDLR and PCSK9 in parallel. The increase of LDLR enhances the clearance of LDL from the circulation, whereas a high level of secreted PCSK9 degrade LDLR. Thus, activating PCSK9 and LDLR simultaneously, produce an opposing effect that is governed by a single metabolic signal, SREBP2 (Peterson et al. 2008). It was proposed that the aim of such a regulation is to transiently down-regulate LDLR via PCSK9, to permit sufficient time to unload newly synthesized cholesterol to peripheral tissues (Peterson et al. 2008). This mechanism prevents an overwhelming of cholesterol derived from LDL uptake and synthesis simultaneously in the cells, keeping whole body cholesterol balance.

Apart from SREBP2, it was found that SREBP1c and hepatocyte nuclear factor (HNF1) also function as transactivators of PCSK9 gene expression. It has been reported that PCSK9 contains an SREBP response element (SRE), where SREBP1c binds in response to insulin (Costet et al.

21

2006) and induces PCSK9 expression. In HNF1 knockdown mouse model, PCSK9 plasma and transcript levels in the liver were reduced, suggesting that HNF1 is a positive regulator of PCSK9 transcription (Li et al. 2009).

3.3. Control of bile acid metabolism

The nuclear receptors are also important regulators of cholesterol and bile acid homeostasis. These receptors are liver X receptor (LXR), farnesoid X receptor (FXR), liver receptor homologue-1 (LRH-1) and small heterodimer partner (SHP).

- *LXR*

The LXR family includes LXRα and LXRβ. LXRα is expressed in metabolically active tissues such as liver, kidney, intestine, WAT and macrophages, whereas LXRβ is ubiquitously expressed. The ligands for LXR are oxysterols (24(S)-hydroxycholesterol, 22(R)-hydroxycholesterol) (Janowski et al. 1999). Thus, LXR acts as a cholesterol sensor. In situations when hepatocytes have an excess of cholesterol, many oxysterols will be generated and bind to LXR. Activated LXR then forms a heterodimer with retinoid X receptors (RXR) and induces the expression of genes that are involved in cholesterol catabolism, absorption and transport such as CYP7A1, ABCA1, ABCG1, ABCG5/8, ApoE (Lu et al. 2001) (figure 7). This process has been confirmed using *LXRα* knock mice, which have an excessive accumulation of hepatic cholesterol (Peet et al. 1998). It has been hypothesized that humans are more sensitive to dietary cholesterol, resulting in a greater increase of plasma cholesterol as compared to mouse and rat models (Peet et al. 1998). This difference is speculated to be due to the presence of a mutated LXR response element located in the promoter of the human CYP7A1 gene. Unlike in humans, high dietary cholesterol induces mouse CYP7A1 through activation of LXR transcription factor, which then binds to a functional LXR response element in the CYP7A1 promoter (Agellon et al. 2002). The activation of CYP7A1

increases the catabolism of cholesterol into bile acids, facilitating efficient cholesterol clearance from the circulation and maintaining plasma cholesterol levels within an optimal range.

In contrast to the liver, other tissues do not have the capacity to excrete excess cholesterol via the bile-fecal route; hence they rely on storing it within the cells or pumping cholesterol out of the cell and channelling it to the HDLs, which carry them back to the liver for excretion. LXRs facilitate these events through the activation of SREBP1c, which is the master regulator of fatty acid synthesis. The increase of fatty acid production facilitates the esterification of cholesterol for storage purposes and increases the abundance of phospholipids that serve as a building block for lipoproteins that transport excess cholesterol (Lu et al. 2001). ABC transporters are also direct targets of LXR activation. LXR prevents the accumulation of cholesterol in macrophages by driving ABCA1 and ABCG1 transcription in order to enhance efflux of cholesterol to lipid-poor lipoprotein (figure 7). Similarly, in the intestine, dietary input or secreted biliary cholesterol induce LXR activation, which in turn activates ABCG5/8 and ABCA1 transporters. The activation of these transporters in the intestine increases cholesterol efflux into the intestinal lumen and minimizes sterol absorption.

- *FXR, LRH-1 and SHP*

The FXR is a bile acid receptor which governs feedback repression of bile acid synthesis. The major target gene of FXR is SHP that, upon activation, forms an heterodimer with LRH-1. The SHP/LRH1 heterodimer inhibits CYP7A1 transcription and the transcription of other target genes that are involved in BA synthesis, including SHP itself (figure 7). Apart from regulating BA synthesis, FXR is also involved in the regulation of BA transport to avoid their accumulation. The two main transporters for BA are sodium taurocholate cotransporter polypeptide (NTCP) and bile acid salt export pump (BSEP). Activated FXR down-regulates NTCP, a transporter responsible for mediating BA uptake. On the contrary, FXR induces BSEP, which facilitates bile

acid efflux into bile (Sinal et al. 2000). Beside BA synthesis, LRH-1 is also involved in RCT by inducing SCARB1 expression. In the LRH-1+/- mouse model, SCARB1 expression is lower, supporting the idea that SCARB1 is regulated by LRH-1. LRH-1 also mediates the suppression of CETP through FXR mediated pathway (Luo et al. 2001).

Altogether, cholesterol homeostasis requires the cooperation of various transcriptional regulators that sense cholesterol cues and react accordingly. Deregulation of these transcription factors leads to an imbalance of cellular cholesterol and BAs and can contribute to disease development.

4. Cholesterol deregulation and associated diseases

Cholesterol imbalance leads to high levels of plasma LDL and low levels of HDL. It is considered as a risk factor for CVDs. Besides CVDs, cholesterol imbalance also leads to liver injuries, such as NAFLD. In this section, I will discuss the various diseases associated with cholesterol deregulation as well as the current treatments available.

4.1. Cardiovascular vascular diseases (CVDs) in the market, which acts by inhibiting

Among the many existing lipoprotein metabolism disorders, familial hypercholesterolemia (FH) is the most common disorder due to mutation in LDLR. As a result of defective LDLR function, circulating LDLs are accumulated and deposited in the blood vessels, leading to complications such as atherosclerosis. Intervention aiming at decreasing plasma LDL cholesterol has thus become an efficient strategy to treat coronary artery disease. Among all, statins are the most common drug found HMGCR (Bou Malham et al. 2016). The ultimate outcome of statins is decreasing endogenous cholesterol synthesis and enhancing LDL cholesterol uptake. The second class of drugs, such as Ezetimibe, act by inhibiting the intestinal absorption of cholesterol. Ezetimibe

binds selectively to the Niemann-pick type C1-like 1 (NPC1L1), a key transporter of cholesterol localized mainly in the intestine and the liver (Pirillo et al. 2016). Blocking NPC1L1 limits the intestinal absorption of cholesterol and drives increased dietary cholesterol excretion. Alternatively, there are also drugs available in the market that bind to bile acids, which are commonly termed as a bile acid sequestrant (e.g. Cholestyramine or colestipol). As a consequence, bile acids do not circulate back to the liver. As a feedback mechanism to maintain an optimal bile acid levels in the circulation, there is an increase of LDLR-mediated cholesterol uptake for bile acid synthesis. The final outcome is a reduction in plasma cholesterol and an increase in the conversion of cholesterol to bile acids for excretion. Most recently, the FDA has approved a new class of drug known to inhibit PCSK9 (Alirocumab and Evolocumab). The inhibition of PCSK9 prevents LDLR degradation, which facilitates LDL clearance from the circulation. Based on the outcome of a clinical trial, it was shown that PCSK9 inhibitor is well tolerated in patients with no adverse effects, suggesting that PCSK9 inhibitors are a valuable drug option, particularly for patients who are intolerant to statin treatments (Kastelein et al. 2015).

4.2. NAFLD diseases

Deregulation of lipid and lipoprotein metabolism is also associated with Nonalcoholic fatty liver disease (NAFLD) (Fon Tacer et al. 2011). NAFLD is the most common liver disease found in the Western countries and affects around 30% of the US population. The pathology of NAFLD encompasses various stages. NAFLD is characterized by lipid accumulation in the liver (simple/mild steatosis), followed by chronic inflammation leading to nonalcoholic steatohepatitis (NASH). The advanced stage of NAFLD includes the development of hepatic fibrosis, cirrhosis or hepatocellular carcinoma (Arguello et al. 2015). Although the underlying mechanisms inducing inflammation and fibrosis remain unclear, several evidences have well established that perturbed cholesterol homeostasis is central to the development of NASH (Musso et al.

2013, Ioannou 2016). Many factors have been recently uncovered to play a role in modulating liver injury. Among them, Kupfer cells (KC) and hepatic stellate cells (HSC) are new key players in NASH development. KCs are macrophages residing in the liver, whereas HSCs are hepatic cells that are required for the fibrogenesis of the liver. In response to high concentration of cholesterol, KCs activates NOD-, LRR and pyrindomain-containing 3 (NLRP3) inflammasome resulting in the production of proinflammatory cytokines and chemokines (Eguchi et al. 2014). The accumulation of inflammatory signalings such as tumor necrosis factor α (TNFα) and tumor growth factor β (TGFβ), drives the transformation of HSCs into collagen-producing myofibroblasts and contributes to fibrosis (Wallace et al. 2015).

II.   The transcription factor E2F1

Eight E2F genes (E2F1-8) have been identified to date, which can be classified based on their protein structures, their interaction partners, and their transcriptional properties (Biswas et al. 2012). E2F1 is the most studied member of the family. The role of E2F1 was first described as a key player in the control of the G1/S transition during the cell cycle progression. Nevertheless, it is now evident that cell cycle regulation represents only a subset of E2F1 roles, which include the regulation of apoptosis, senescence, DNA damage response and most recently, its participation in metabolism. In this section, I will discuss some of the well-known functions of E2F1 as well as the new emerging roles of this transcription factor.

1.   E2F1 and cell cycle

The E2F transcription factors have been identified as proteins that are able to bind to the promoters of the adenoviral gene E2 (Kovesdi et al. 1986). E2F1 was the first member of the E2F family to be identified because of its ability to bind the retinoblastoma protein (RB) (Bagchi et al. 1991). The activity of E2F1 is dependent on its binding partners, which include dimerization protein (DP) or the retinoblastoma family proteins, composed of the RB1, RBL1, and RBL2 (Dyson 1998). In the inactive state, E2F1 interacts with RB family members. The E2F1-RB interaction blocks the transcriptional activation domain of E2F1-DP and prevents recruitment of co-activators to the promoters of target genes (Frolov et al. 2004). During cell cycle progression, cyclin-dependent kinases (CDKs) 4/6 phosphorylate RB, leading to the release of E2F1. E2F1 is then available to bind with DP1 to modulate the expression of genes such as *c-MYC*, *cyclin D*, and *cyclin E*, which are necessary for S phase entry (figure 8). E2F1 also controls the expression of genes implicated in DNA synthesis such as dihydrofolate reductase (DHFR) and thymidine kinase (TK).

27

The deletion of dE2F1 in *Drosophila* results in S-phase arrest and growth retardation (Dimova et al. 2003). In mice, the loss of E2F1, E2F2 and E2F3 diminished the ability of embryonic fibroblast to enter S-phase and block mitosis and cell proliferation (Wu et al. 1994). Conversely, the overexpression of E2F1 drives ectopic S-phase entry in Drosophila and Arabidopsis (Asano et al. 1996). All these data support that the E2F/RB pathway is necessary for S phase entry. Despite the critical function of E2F1 in cell proliferation, E2F1-/- mice undergo normal development and reproduction and are widely used as an experimental model to understand the *in vivo* functions of E2F1. While E2F1-/- mice develop normally, they are prone to develop tumors with aging, suggesting that E2F1 also plays a pro-apoptotic role. Indeed, this is confirmed by the fact that thymocytes of E2F1-/- mice fail to undergo apoptosis leading to an excess of mature T cell lymphocytes in E2F1-/- mice (Yamasaki et al. 1996).

Depending on the cellular context, the overexpression of E2F1 can also induce senescence in human primary fibroblast (Dimri et al. 2000) and apoptosis in various cell types (Du et al. 1996, DeGregori 2002). For example, E2F1 can influence p53 stability through the activation of p14/Arf tumor suppressor gene, thus leading to cell cycle arrest and apoptosis (DeGregori et al. 1997). In addition, several studies have indicated that E2F1 has a functional role in DNA damage response. During DNA damage, cells either undergo apoptosis or activate the cell repair mechanism. For instance, when cells are exposed to a genotoxic agent, the expression of E2F1 was increased to mediate apoptosis and/or cell repair processes (Stevens et al. 2004). Consistent with this view, it was shown that DNA damage increases the expression and the activity of E2F1, culminating the increase of the transcript levels of genes participating in DNA-repair and checkpoint regulation (Stevens et al. 2004).

2. E2F1 and metabolism

There are emerging evidences that cell cycle regulators such as E2F1 play a critical role in lipid, oxidative and glucose metabolism. Fajas and co-workers first uncovered the link between E2F1 and adipogenesis; they validated

Figure. 8   Control of cell cycle G1-S transition by CDK-Rb E2F1 pathway.
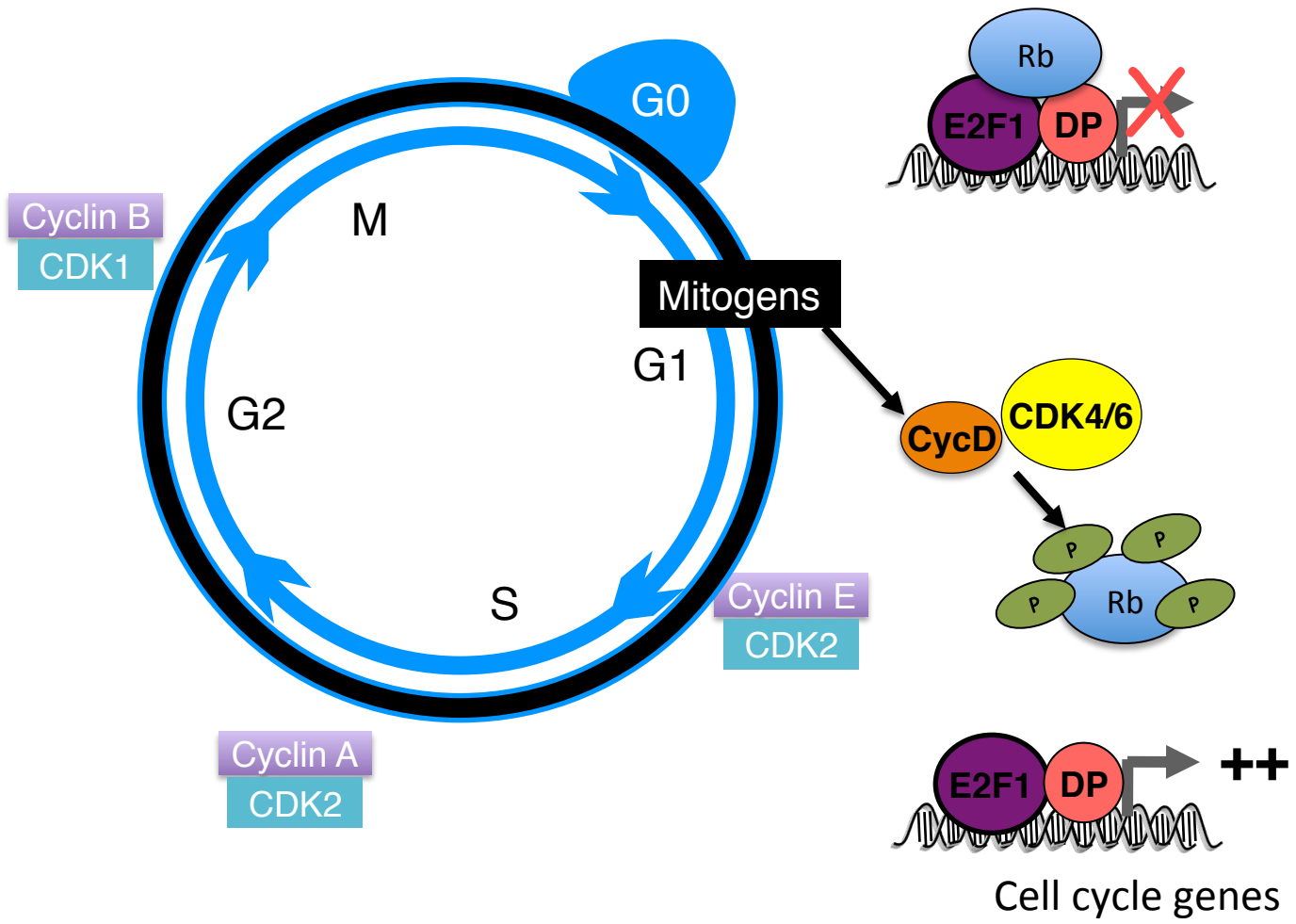
Inactive state of E2F1. E2F1 binds to Rb, which blocks the transcriptional activation domain of E2F1-DP. **Transition of G1-S phase.** Rb is hyperphosporylated by CycD-CDK4/6 complex, thereby induces E2F1-Rb dissociation. E2F1 is then available to bind with DP1 to modulate the expression of cell cycle genes. CDK: cyclin dependent kinases, Rb: retinoblastoma protein, DP: dimerization protein.

in both mouse models and mouse embryonic fibroblasts (MEFs), that the E2F1 deletion leads to a decrease in adipocyte differentiation (Fajas et al. 2002). The authors also observed that E2F1-3 and E2F4 have opposing effects on adipocyte differentiation and this was explained by their differential regulation of a key master regulator of adipocyte differentiation, peroxisome proliferator-activated receptor γ (PPARγ). In fact, E2F1, RB, and histone deacetylase HDAC3 constitute a repressor complex that inhibits PPARγ, preventing it from activating the transcriptional program required for adipocyte differentiation (Fajas et al. 2002). At the physiological level, E2F1-/- mice fed a high fat diet were resistant to obesity, highlighting the importance of E2F1 in adipogenesis (Fajas et al. 2002).

In addition, it was identified that E2F1-/- mice also present a resistance to exercise-induced fatigue and cold exposure, these evidences reveal the role of E2F1 in oxidative metabolism in brown adipose tissue (BAT) and muscle (Blanchet et al. 2011). E2F1 has also been demonstrated to regulate insulin secretion by binding directly to the promoter of the K+ ATP channel Kir6.2 and controlling its expression. K+ ATP channel Kir6.2 plays an important role in regulating glucose-induced insulin secretion through modulating membrane polarization (Miki et al. 1999). As a result, E2F1-/- mice showed impaired insulin secretion and are glucose intolerant (Annicotte et al. 2009). Most recently, It has been also shown, that E2F1 mediates nutrient sensing and modulates glucose utilization in the heart by regulating pyruvate dehydrogenase kinase 4 (PDK4), an inhibitor of pyruvate dehydrogenase (PDH), which catalyzes the conversion of pyruvate to Acetyl-CoA (Hsieh et al. 2008). Moreover, the authors also showed that E2F1-/- mice have reduced plasma cholesterol, suggesting that E2F1 is also implicated in cholesterol metabolism.

Altogether, these results provide a direct support that in addition to cell cycle regulation, E2F1 is also involved in the control of key metabolic processes and that the modulation of E2F1 might provide new perspectives in the control of metabolic diseases.

III. Project aims

Several lipids lowering drugs are available in the market for treatment of cardiovascular diseaease (CVDs). However, CVDs remains the number one cause of death globally. Therefore, in this project, we aim to identify a new potential therapeutic target for CVDs. As mentioned in the previous chapter, increasingly, there are data to support that cell cycle regulators particularly the E2F1/CDK4/Rb axis are major regulators of metabolic processes. In this context, we aim to determine the role of E2F1 in cholesterol metabolism using E2F1 full knock-out mouse model. The overall aims of the project is as follow:

1) To phenotype cholesterol metabolism in E2F1+/+ and E2F1-/- mouse models.

2) To examine the molecular mechanism by which E2F1 regulate cholesterol metabolism.

3) The contribution of E2F1 to the regulation of cholesterol metabolism in normal physiology and physiopathological (fed a high cholesterol diet) conditions.

Chapter 2: Brief results and contribution to each article

Chapter 2: Brief result and contribution to each article

During my PhD training, I had the privilege to participate in several projects as highlighted below, of which I will briefly describe the findings and my contribution to each article.

1) Denechaud, PD, Lopez-Mejia IC,Giralt A, **Lai Q**, E. Blanchet, B. Delacuisine B, Nicolay BN, Dyson NJ, Bonner C, Pattou F, Annicotte JS and Fajas L (2016). "E2F1 mediates sustained lipogenesis and contributes to hepatic steatosis." <u>J Clin Invest</u>.

2) Lagarrigue S, Lopez-Mejia IC, Denechaud PD, Escoté X, Castillo-Armengol J, Jimenez V, Chavey C, Giralt A, **Lai Q**, Zhang L, Martinez-Carreres L, Delacuisine B, Annicotte JS, Blanchet E, Huré S, Abella A, Tinahones FJ, Vendrell J, Dubus P, Bosch F, Kahn CR, Fajas L (2016) "CDK4 is an essential insulin effector in adipocytes." <u>J Clin Invest</u>.

3) **Lai Q**, Denechaud PD, Cédric LM, Fajas L (2016). E2F1 inhibits circulating cholesterol clearance by regulating PCSK9 expression in the liver. <u>JCI insight</u>. (Manuscript under revision)

1.   *Article 1: E2F1 mediates sustained lipogenesis and contributes to hepatic steatosis*

In this article, we have revealed that E2F1 plays an essential role in the liver physiopathology via the regulation of glycolysis and lipogenesis. It is known that liver glycolysis and lipogenesis are regulated at the transcriptional level by signaling molecules such as insulin and glucose. Insulin induces the activity of transcription factors such as sterol regulatory element binding protein 1c (SREBP1c) to promote downstream gene activation to initiate glycolysis program. SREBP1c targets are among of others, glycolytic glucose transporter (GLUT2), glucokinase (GK) and liver glycolytic pyruvate kinase (L-PK). Likewise, glucose induces carbohydrate responsive element binding protein (ChREBP), a master regulator of lipogenesis, which upon activation,

Figure. 9   E2F1 controls glucose and lipid metabolism in liver.

A

B

Breeding of db/db mice x E2F1-/- mice

db/db mice

db/db E2F1-/- mice

Hepatic steatosis

Hepatic steatosis
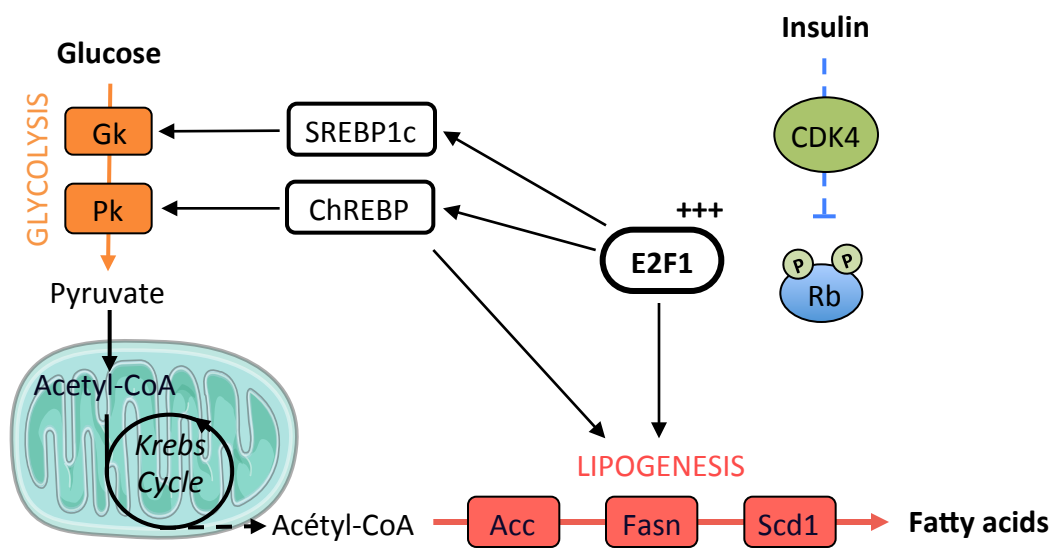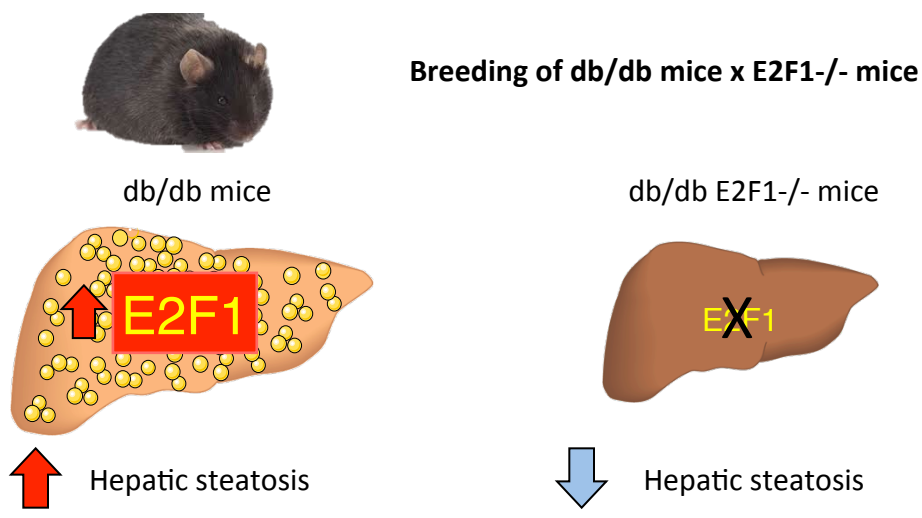
(A) The E2F1 transcription factor binds directly to the promoters of its target genes (SREBP1c, ChREBP, Acaca, Fasn, Scd1) and thus controls the glycolytic and lipogenic pathway in the liver. Under the action of insulin, CDK4 phosphorylates Rb and thus raises his repressive effect on E2F1. **(B)** E2F1 deletion in the db/db mouse model protects from hepatic steatosis via a decrease in de novo synthesis of fatty acids. Gk: glucokinase, Pk: pyruvate kinase, SREBP1c:sterol regulatory element binding protein 1c, ChREBP: induces carbohydrate responsive element binding protein, CDK4: cyclin dependent kinases 4, Acc: acetyl-CoA carboxylase, FAS: fatty acid synthase, Scd1: stearoyl CoA desaturase.

induces lipogenic genes such as acetyl-CoA carboxylase (ACC), fatty acid synthase (FAS) and stearoyl-CoA desaturase (SCD1).

Interestingly, we showed here that E2F1 plays a role as a key positive regulator of glycolysis and lipogenesis (figure 9A). Using chromatin immunoprecipitation-high-throughput DNA sequencing (ChIP-seq) analysis, we identified a new class of E2F1 target genes related to the cellular metabolic process and demonstrated that E2F1 binds directly to the promoters of glycolytic and lipogenic genes. We also showed that E2F1 expression and activity are increased in response to feeding through canonical activation of the CDK4-RB pathway via insulin stimulation.

Strikingly, in different mouse models of hepatic steatosis (mice fed a high fat diet and db/db mice) and in glucose intolerant human liver samples, we observed an increased of hepatic E2F1 expression during the disease state. We also illustrated that E2F1 deletion in the db/db mouse model caused protection from hepatic steatosis, suggesting that E2F1 deficiency prevents hepatic lipid accumulation. Therefore, E2F1 inhibition could be used as an intervention against steatosis (figure 9B). In summary, we have placed E2F1 as a key transcription factor in the regulation of hepatic lipid synthesis and glycolysis.

-Contribution: Performed and analyzed gene expression in hepatocytes.

2. Article 2: CDK4 is an essential insulin effector in adipocytes

Insulin is a hormone produced by pancreatic beta cells in response to dietary intake. Defects in insulin signaling pathway is a typical characteristic of type 2 diabetes. The release of insulin triggers glucose utilization in the metabolic tissues such as liver, adipose tissue and muscle. In the adipose tissue, insulin binds to its receptor, which has a tyrosine kinase domain. Upon insulin stimulation, the insulin receptor undergoes autophosphorlyation, resulting in the recruitment and phosphorylation of the proteins in the insulin

Figure. 10   CDK4 controls glucose and lipid metabolism in adipose tissue.

A
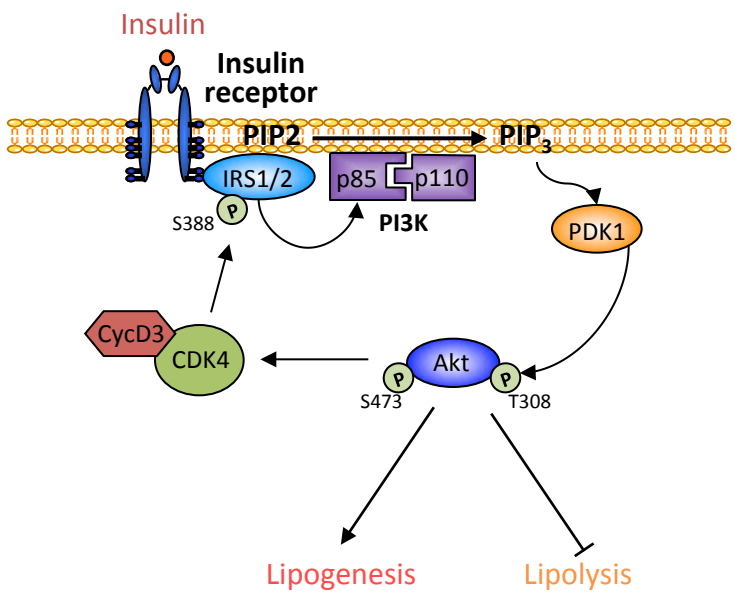
B

Role of CDK4 in the physiopathology of obesity
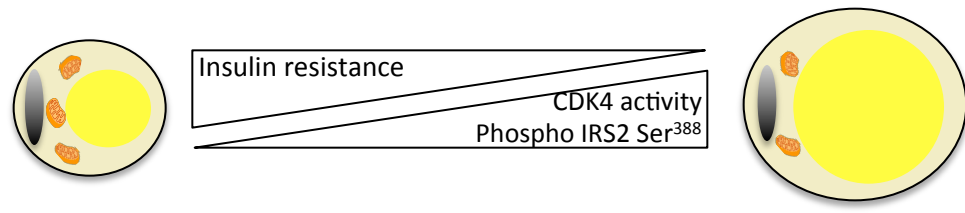
(A) Insulin activates CDK4 which phosphorylates IRS2 on Ser388 and thus supports the active insulin signaling. **(B)** CDK4 activity in adipose tissue of obese people is positively correlated with body fat, as well as the activation of the insulin signaling pathway through Ser 388 phosphorylation of IRS2. IRS: insulin receptor substrate family, PIP: phosphatidylinositol 4, 5-bisphosphate, PDK1: phosphoinositide dependent kinase 1, PI3K: phosphoinositide 3-kinase, CDK4: cyclin dependent kinase 4, CycD3: cyclin D3.

receptor substrate family (IRS), particularly IRS1 and IRS2. The activation of IRS1 and IRS2 then stimulates downstream kinases such as phosphoinositide 3-kinase (PI3K), phosphoinositide dependent kinase 1 (PDK1) and protein kinase B (PKB), also known as AKT, to control lipogenesis and lipolysis in adipocytes. The pathways of lipogenesis and lipolysis are finely regulated by insulin signaling in the adipose tissue. Insulin signaling induces lipogenesis and simultaneously inhibits lipolysis thereby providing a mechanism to maintain lipid balance.

Here, we found that CDK4 is a major regulator of insulin signaling in white adipose tissue (WAT). We used three strains of transgenic mouse model: (1) CDK4 whole knockout mice (CDK4-/-), (2) Constitutively hyperactive Cdk4 mutant mice (CDK4^{R24C}) (3) CDK4 specific knockout mice model in adipose tissue via infection by viral vector expressing Cre recombinase (CDK4$^{flox/flox}$). In these animals, we observed that the kinase activity of CDK4 in adipose tissue is positively correlated with body fat. The absence of CDK4 led to a "lean" phenotype and was also correlated with decreased lipogenesis and increased lipolysis in adipose tissue. Conversely, hyperactivation of CDK4 observed in the CDK4^{R24C} led to weight gain and was correlated with increased lipogenesis and a suppression of lipolysis in the adipose tissue.

To understand the function of CDK4 in adipose tissue, we studied the glucose metabolism in these mouse models. Surprisingly, the Cdk4^{R24C} mice, which have a greater weight gain, exhibit an improvement in insulin sensitivity and glucose tolerance. Conversely, CDK4 adipose specific knockout mice exhibit a decrease in insulin sensitivity. Moreover, a global kinome analysis of the adipocytes in CDK4 deficient mice following insulin stimulation showed that insulin signaling was impaired, with a lower AKT kinase activity in CDK4-deficient mice as compared to the control; underscoring that CDK4 plays an important role in insulin signaling upstream of AKT.

In response to insulin, the activity of CDK4 increases and it phosphorylates IRS2 at Ser388, creating a positive feedback loop for insulin signaling activation (figure 10A). In conclusion, our results provide evidences that CDK4 is a regulator of insulin signaling in adipocytes, providing new

34

insights in the context of metabolic diseases such as obesity and diabetes (figure 10B).

-Contribution: Performed and analyzed tissue sections of the different mouse models.

3.   Article 3: E2F1 inhibits circulating cholesterol clearance by regulating PCSK9 expression in the liver

In this article, we reported that E2F1-/- mice have reduced total plasma cholesterol and increased hepatic and colon cholesterol content as compared to wild-type mice. To identify potential E2F1 target genes implicated in cholesterol metabolism, we analyzed E2F1 ChIP-seq data from primary cultures of hepatocytes infected with adenovirus-E2F1. This led to the finding that E2F1 binds directly and transactivates the promoter of the PCSK9 gene. Consistently, when E2F1 is deleted, we observed a reduction of PCSK9 gene expression in all the studied models (mice, mouse primary hepatocytes and human cell lines). The repression of PCSK9 in E2F1-/- models resulted in an increased LDLR protein expression. This contributes to more LDL uptake in E2F1 deleted cells, leading to an accumulation of cholesterol in these cells.

To study the function of E2F1 in cholesterol homeostasis, we challenged E2F1+/+ and E2F1-/- mice with high cholesterol diet (1.25% HCD) for five weeks. Similarly, we observed that the E2F1-/- mice have increased liver cholesterol content, reduced PCSK9 expression and an increase of hepatic LDLR expression. The master regulator of cholesterol synthesis genes, SREBP2 was also significantly reduced. This could be a secondary response as a result of an increase sterol uptake. In addition, we also showed that E2F1-/- mice displayed a fatty liver phenotype evidenced with ballooning hepatocytes; positive trichrome staining and increased expression of α-collagen and α-smooth muscle actin (α-SMA). In comparison to the E2F1+/+ mice treated with HCD, E2F1-/- mice have a modest reduction of bile acid in the feces, indicating

that deletion of E2F1 not only had an impact on LDLR uptake, that the catabolism of cholesterol was affected too. The net result of E2F1 deletion was an increase of hepatic sterol accumulation in the liver, leading to liver injury.

In summary, our data support the idea that E2F1 plays a crucial role in regulating cholesterol homeostasis through mediating sterol uptake (via upregulation of PCSK9). Our findings also emphasize that although PCSK9 inhibitors are effective against hyperdyslipidemia, it is important to ensure that these patients present a healthy and efficient sterol excretion system to avoid over accumulation of sterol in the tissues.

-Contribution: Defined the project, performed the experiments, analyzed the data, wrote the manuscript.

Chapter 3: Discussion and Perspectives

Chapter 3: Discussion and Perspectives

Reducing circulating LDL is an effective strategy against CVDs. Understanding the underlying mechanistic underpinnings of LDL homeostasis is necessary for the development of new and more effective therapeutic initiatives against the rising metabolic syndrome. For instance, the recent discovery of PCSK9 in LDL homeostasis has lead to the development of PCSK9 inhibitors in the management of CVDs. There is now several PCSK9-based therapeutics in the clinics (Kastelein et al. 2015). Despite their efficacy as a LDL controlling agent, the effects of PCSK9 suppression is not completely understood. Defining the upstream and downstream regulators of the PCSK9 function will be necessary for more effective prediction of the pharmacological activity and toxicity of PCSK9-modulating agents. In this chapter, I will discuss our findings (article 3) about the role of the E2F1-PCSK9 axis in the control of cholesterol metabolism. I will then provide a perspective for future research in cholesterol metabolism and cancer.

1. E2F1 is critical for cholesterol homeostasis

In addition to its established roles in cell cycle control, a growing body of evidence have shown that E2F1 is a critical regulator of energy metabolism (Annicotte et al. 2009, Denechaud et al. 2016, Lagarrigue et al. 2016). Phenotypic characterization of E2F1-/- mice in this thesis has shown that cholesterol balance is perturbed in the absence of E2F1. Indeed, E2F1-/- mice have reduced plasma cholesterol and increased hepatic as well as colon cholesterol content. These observations could be due to an increase in cholesterol uptake, an increase of cholesterol biosynthesis, or both. In support of the former, we observed that there was a decrease in the rate of cholesterol synthesis in E2F1-/- hepatocytes cells relative to E2F1+/+ cells. Moreover, SREBP2, a major regulator of cholesterol biosynthesis, was significantly reduced in HCD-fed E2F1-/- mice, whereby cholesterol is in excess (appendix, figure 1). To further rule out the possibility that E2F1 has a direct effect on cholesterol

biosynthesis, we checked the expression of cholesterol biosynthesis genes such as mevalonate kinase (MVK), farnesyl diphosphate farnesyl transferase 1 (FDFT) etc. and confirmed that none of the cholesterol biosynthesis genes were modulated in E2F1-/- mice livers fed a chow diet or HCD as compared to the wild-type mice (appendix, figure 2). Thus, the reduced cholesterol biosynthesis in E2F1-/- mice is a secondary effect of excessive cholesterol resulting from enhanced cholesterol uptake.

2.   E2F1: a new transcriptional regulator of PCSK9

Based on our ChIP-seq data, we found that E2F1 binds to the promoters of many cholesterol-related genes. Among the genes, PCSK9 has been described as a major regulator of LDL uptake. Renilla-based reporter analysis has also confirmed that E2F1 binds directly to transactivate the PCSK9 expression. Interestingly, the cholesterol metabolic phenotypes of E2F1-/- mice were also reminiscent of PCSK9 inhibition. PCSK9 (Rashid et al. 2005) and E2F1 deleted mice have reduced plasma LDL and elevated LDLR protein expression. As such, a novel E2F1-PCSK9 axis could explain the observed cholesterol phenotypes of the E2F1-/- mice. In agreement with this view, the hepatic PCSK9 and E2F1 expression are induced in fed mice and is repressed in fasted mice. Similar results were obtained in mouse and human hepatocytes, whereby, both PCSK9 mRNA and protein expression were reduced when E2F1 was deleted. Thus, hepatic E2F1 is a positive regulator upstream of PCSK9 expression.

Paradoxically, when we challenged the wild-type mice with a HCD, the expression of E2F1 was significantly higher relative to chow diet, whereas PCSK9 level is lowered relative to the chow diet. These findings raise the possibility that E2F1 may function in addition to SREBP2 to provide dynamism in the regulation of PCSK9 expression in response to different cholesterol diets. Indeed, several other transcription factors such as SREBP1c and HNF1 have been implicated in PCSK9 regulation. In mouse liver and hepatocytes, E2F1 controls SREBP1c gene expression (Denechaud et al. 2016). Separately, it was reported that E2F1 interacts with SREBP1c. Using mass spectrometry analysis

on the pull-down fraction of triple RB knockout (RB, p130, p107) in hepatocellular carcinoma cell line (HCC), the authors demonstrated that SREBP1c protein is bound to E2F1 (Tarangelo et al. 2015). Thus, E2F1 can also control PCSK9 indirectly via SREBP1c. In light of our findings, future studies should consider the role of E2F1 together with other known regulators of PCSK9 activity in the characterization of LDL homeostasis.

3.   The impact of E2F1 deletion in sterol excretion

Excess of cholesterol in the liver is converted into bile acids (BAs), which are excreted in the feces (Cohen 2008). Hence, more BAs are expected in the feces of E2F1-/- mice. However, we did not observe any changes in the levels of bile acids and neutral sterols in the feces of chow-fed E2F1+/+ and chow-fed E2F1-/- mice. Given that E2F1-/- mice displayed elevated cholesterol content in the liver, these data suggest that the animals had impaired response to excess cholesterol. In order to understand the implication of E2F1 in cholesterol homeostasis, we challenged the E2F1-/- mice with a HCD. E2F1-/- mice had more hepatic cholesterol content as compared to E2F1+/+ mice. The levels of fecal neutrals sterol remained unchanged between E2F1+/+ and E2F1-/- mice, while a modest reduction in bile acids levels was observed in the feces of E2F1-/- mice as compared to E2F1+/+. This suggested an aberrant BA and cholesterol excretion in the absence of E2F1 function.

Correspondingly, E2F1 has been previously studied in the context of bile acid regulation in a cholestatic liver fibrosis mouse model (Zhang et al. 2014). Using 3, 5- diethoxycarbonyl-1, 4-dihydrocollidine (DDC) to induce liver fibrosis and cirrhosis, Zhang and co-workers showed that E2F1-/- mice had decreased total serum and fecal Bas. This raises the possibility that E2F1 is required for BA synthesis and biliary cholesterol excretion. Consistent with this, the authors showed that in primary hepatocytes of E2F1-/- mice, there was a reduction in transcript levels of CYP7A1 and CYP8B1, two essential enzymes for BA synthesis. Along these lines, we also observed a reduction in the hepatic expression of BA synthesis genes, including CYP7B1 in HCD-fed E2F1-/- mice. In addition to CYP7B1, the expression of the LXR and ABCG8 were also lower

in E2F1-/- as compared to E2F1+/+ mice. Given that ABCG8 is a downstream target of LXR, it is likely that LXR activity is reduced in E2F1-/- mice. Since major oxysterols derived from intermediates of the BA synthetic pathways serve as ligands for LXR activation, reduced LXR activity may indicate defects in BA synthesis. Therefore, it will be interesting to study the impact of E2F1 in BAs efflux and synthesis. For example, performing an NMR-based metabolic flux analysis will provide information that will help us to understand how E2F1 is implicated in BAs efflux or/and synthesis pathways.

4. Implication of E2F1 in liver fibrosis

PCSK9 inhibition reduces plasma LDL, increases LDLR and improves LDL clearance from the circulation. Hence, PCSK9 inhibitors are effective against hyperdyslipidemia and an alternative for patients who are intolerant to statins. The similar metabolic phenotypes between E2F1 and PCSK9 inhibition led us to consider E2F1 deletion as an alternative to PCSK9 inhibitors in hyperdyslipidemia prevention. Surprisingly, E2F1 deletion failed to prevent hypercholesterolemia. Instead, E2F1-/- mice had signs of liver fibrosis when fed a HCD. In HCD-fed E2F1-/- mice, hepatic protein expression of LDLR is upregulated and a fatty liver phenotype (high lipid content) develops. Histological analysis of the liver sections of HCD-fed E2F1-/- mice showed early signs of fibrosis (ballooning hepatocytes and trichrome stained). Fibrosis genes (α-collagen and α-SMA) expression were also higher in the livers of HCD-fed E2F1-/- mice as compared to HCD-fed E2F1+/+ mice. Thus uptake of LDL in the liver must be compensated with improved excretion to avoid accumulation of cholesterol in the liver. However, Zhang and co-workers (discussed previously), had reported that E2F1-/- mice were protected from liver fibrosis induced by DDC treatment. This was due to a reduction in the inflammatory response in E2F1-/- mice (Zhang et al. 2014). In view of our results, it is likely that fibrosis in their DDC-induced model is dependent on bile acid accumulation, toxicity, and inflammation, but not lipid accumulation. In our previous studies, we also showed that E2F1 deletion in db/db mouse model protects against hepatic steatosis by reducing lipogenic processes. In this project, we used a Paigen diet

to induce NAFLD in E2F1-/- mice which explain the discrepancies in our observations. Moreover, we quantified the level of hepatic triglycerides of E2F1-/- mice on a Paigen diet and showed that there were no significant changes between wild-type and E2F1-/- mice (appendix, figure 3). Altogether, these results suggest that the E2F1 transcription factor impinges on multiple metabolic pathways. The different forms of NAFLD induction result in a different functional role of E2F1 as a regulator of bile acid and lipid metabolism. Therefore, the effects of E2F1 deletion is highly context dependent.

Additionally, hepatomized PCSK9-/- mice, which is expected to have enhanced E2F1 activity had reduced fat droplet deposition in the liver as compared to hepatectomized PCSK9+/+ mice livers (Zaid et al. 2008). Moreover, loss of function of PCSK9 in humans is associated with hypocholesterolemia and is susceptible to familial heterozygous hypobetalipoproteinemia (FHBL), an autosomal dominant disease characterized by low plasma levels of total cholesterol (Tarugi et al. 2007). FHBL patients have a greater risk of developing NAFLD, due to an imbalance of lipid synthesis and export (Tanoli et al. 2004). Hepatic E2F1 expression analysis presented in this thesis have demonstrated that patients who are obese, as well as individuals with steatosis, have significantly higher E2F1 levels. The level of E2F1 protein expression was also found to be highly elevated in liver samples derived from human patients suffering from NASH cirrhotic liver (Zhang et al. 2014). Taken together our results indicate that a functional E2F1-PCSK9 axis prevents hepatic lipid accumulation. More importantly, routine diagnostic tests for liver injury should be implemented for patients using a PCSK9 inhibitor to prevent NAFLD. To date, there is no effective treatment for NAFLD. Attempts to use anti-diabetics, lipid lowering or anti-hypertensive drugs for NAFLD treatment had failed (Machado et al. 2014). Therefore, understanding the role of E2F1 in NASH development will provide new insights and targets for therapeutic intervention against NASH.

Figure. 11 Cell cycle regulators control both cell cycle and metabolic responses.

E2F1/
Cdk4/Rb

Metabolism

Cell cycle

Liver

Glucose, triglycerides, cholesterol
homeostasis

Cell proliferation

Metabolic and
Cardiovascular
diseases

Regeneration,
cancer development
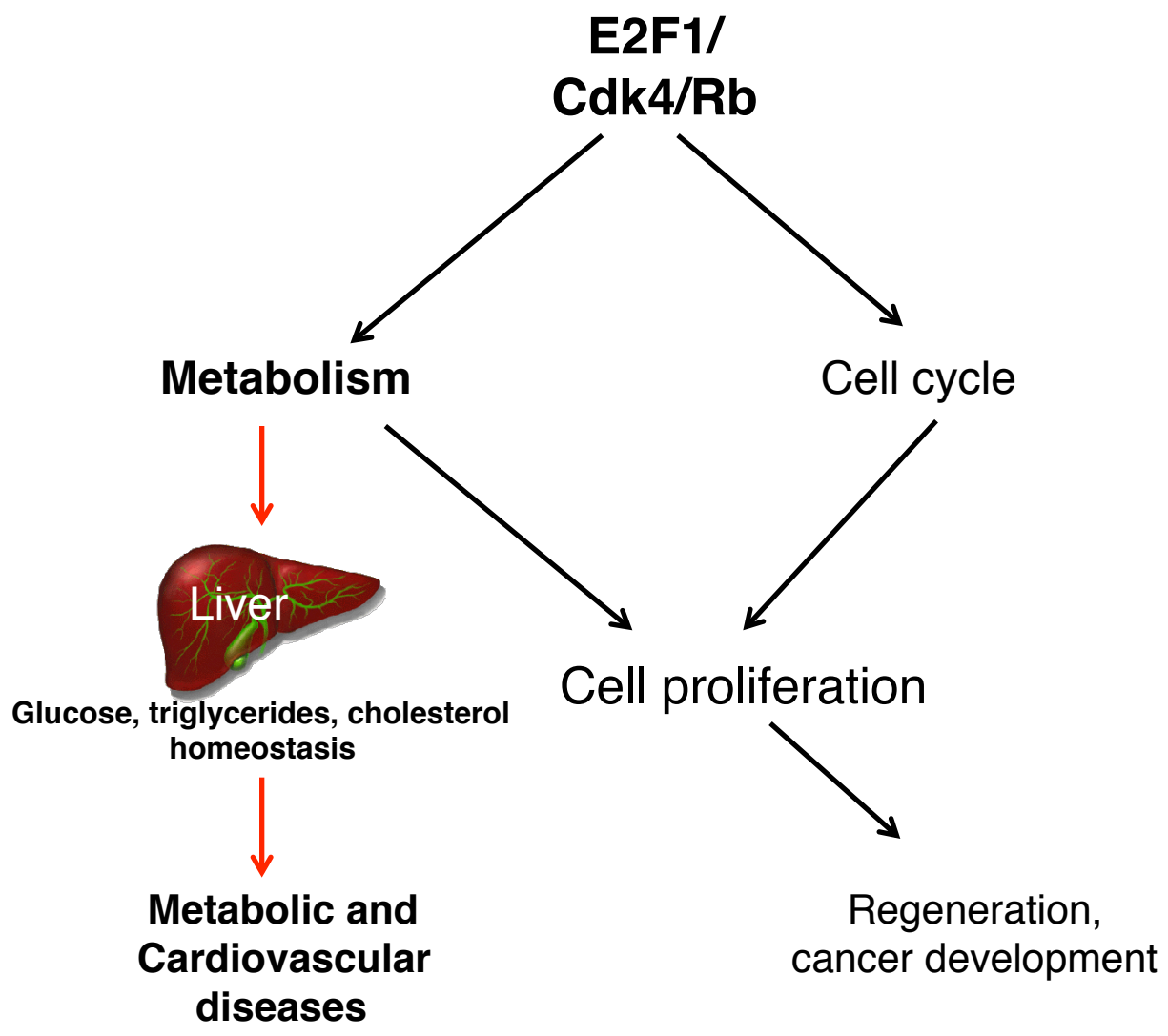
Cell regulators such as E2F1, CDK4, Rb are key regulators that control cell cycle proliferation and metabolism. Deregulation of these cell cycle regulators may lead to cancer or metabolic disease development.

5. Future perspective: E2F1- a prominent factor that does more than cell cycling

Most of the studies on E2F1 have focused on its role in cancer development and cell cycle regulation (Asano et al. 1996, Du et al. 1996, Dimova et al. 2003, Frolov et al. 2004). Studies from our laboratory as well as others have revealed novel E2F1 functions in the area of lipid synthesis, glycolysis, mitochondrial function, BAs, and cholesterol metabolism. These processes are crucial during metabolic homeostasis and contribute to cancer development and progression (figure 11).

In many human cancers, E2F1 activity is associated with cancer progression. During cancer development, E2F1 is highly expressed, permitting uncontrolled cell proliferation (Chen et al. 2009). Concurrently, the cancer cells undergo a metabolic switch to drive cell proliferation and survival. This metabolic switch encompasses increased in lipid synthesis, decreased in oxidation metabolism, and increased in glycolysis to support cell growth (Escote et al. 2015). In this context, E2F1 is likely to act as a master regulator, coordinating the metabolic support required for cancer cell proliferation. Therefore, the effects of an intervention aimed at E2F1 will be two-fold. First, cell cycle progression and proliferation will be halted. Second, the metabolic support that fuels cell proliferation will be disrupted. Currently, inhibiting kinases such as CDK4/6 located upstream of E2F1 has become an effective strategy to regulate E2F1 activity. Indeed, a CDK4/6 inhibitor is in phase 3 clinical trial for breast cancer treatment, with promising outcomes (Dukelow et al. 2015). Increasingly, studies have also shown that drugs usually used for the treatment of metabolic diseases such as metformin and statins have anti-tumor properties (Hindler et al. 2006, Chiang et al. 2007), suggesting that the metabolic response and cell proliferation are tightly linked. Therefore, identification of new roles for E2F1 in the regulation of metabolism will provide new insights for the development of combinatorial drug therapies for cancer and metabolic diseases.

Chapter 4: References

Chapter 4: References

Agellon, L. B., V. A. Drover, S. K. Cheema, G. F. Gbaguidi and A. Walsh (2002). "Dietary cholesterol fails to stimulate the human cholesterol 7alpha-hydroxylase gene (CYP7A1) in transgenic mice." J Biol Chem **277**(23): 20131-20134.

Annicotte, J. S., E. Blanchet, C. Chavey, I. Iankova, S. Costes, S. Assou, J. Teyssier, S. Dalle, C. Sardet and L. Fajas (2009). "The CDK4-pRB-E2F1 pathway controls insulin secretion." Nat Cell Biol **11**(8): 1017-1023.

Arguello, G., E. Balboa, M. Arrese and S. Zanlungo (2015). "Recent insights on the role of cholesterol in non-alcoholic fatty liver disease." Biochim Biophys Acta **1852**(9): 1765-1778.

Asano, M., J. R. Nevins and R. P. Wharton (1996). "Ectopic E2F expression induces S phase and apoptosis in Drosophila imaginal discs." Genes Dev **10**(11): 1422-1432.

Bagchi, S., R. Weinmann and P. Raychaudhuri (1991). "The retinoblastoma protein copurifies with E2F-I, an E1A-regulated inhibitor of the transcription factor E2F." Cell **65**(6): 1063-1072.

Biswas, A. K. and D. G. Johnson (2012). "Transcriptional and nontranscriptional functions of E2F1 in response to DNA damage." Cancer Res **72**(1): 13-17.

Blanchet, E., J. S. Annicotte, S. Lagarrigue, V. Aguilar, C. Clape, C. Chavey, V. Fritz, F. Casas, F. Apparailly, J. Auwerx and L. Fajas (2011). "E2F transcription factor-1 regulates oxidative metabolism." Nat Cell Biol **13**(9): 1146-1152.

Bou Malham, S. and A. C. Goldberg (2016). "Cardiovascular risk reduction: the future of cholesterol lowering drugs." Curr Opin Pharmacol **27**: 62-69.

Brown, A. J., L. Sun, J. D. Feramisco, M. S. Brown and J. L. Goldstein (2002). "Cholesterol addition to ER membranes alters conformation of SCAP, the SREBP escort protein that regulates cholesterol metabolism." Mol Cell **10**(2): 237-245.

Brown, M. S. and J. L. Goldstein (1986). "A receptor-mediated pathway for cholesterol homeostasis." Science **232**(4746): 34-47.

Brown, M. S., Y. K. Ho and J. L. Goldstein (1980). "The cholesteryl ester cycle in macrophage foam cells. Continual hydrolysis and re-esterification of cytoplasmic cholesteryl esters." J Biol Chem **255**(19): 9344-9352.

Chen, H. Z., S. Y. Tsai and G. Leone (2009). "Emerging roles of E2Fs in cancer: an exit from cell cycle control." Nat Rev Cancer **9**(11): 785-797.

Chiang, G. G. and R. T. Abraham (2007). "Targeting the mTOR signaling network in cancer." Trends Mol Med **13**(10): 433-442.

Cohen, D. E. (2008). "Balancing cholesterol synthesis and absorption in the gastrointestinal tract." J Clin Lipidol **2**(2): S1-3.

Cohen, J., A. Pertsemlidis, I. K. Kotowski, R. Graham, C. K. Garcia and H. H. Hobbs (2005). "Low LDL cholesterol in individuals of African descent resulting from frequent nonsense mutations in PCSK9." Nat Genet **37**(2): 161-165.

Cohen, J. C., E. Boerwinkle, T. H. Mosley, Jr. and H. H. Hobbs (2006). "Sequence variations in PCSK9, low LDL, and protection against coronary heart disease." N Engl J Med **354**(12): 1264-1272.

Costet, P., B. Cariou, G. Lambert, F. Lalanne, B. Lardeux, A. L. Jarnoux, A. Grefhorst, B. Staels and M. Krempf (2006). "Hepatic PCSK9 expression is regulated by nutritional status via insulin and sterol regulatory element-binding protein 1c." J Biol Chem **281**(10): 6211-6218.

de Almeida, E. R., E. M. Reiche, A. P. Kallaur, T. Flauzino and M. A. Watanabe (2013). "The roles of genetic polymorphisms and human immunodeficiency virus infection in lipid metabolism." Biomed Res Int **2013**: 836790.

DeGregori, J. (2002). "The genetics of the E2F family of transcription factors: shared functions and unique roles." Biochim Biophys Acta **1602**(2): 131-150.

DeGregori, J., G. Leone, A. Miron, L. Jakoi and J. R. Nevins (1997). "Distinct roles for E2F proteins in cell growth control and apoptosis." Proc Natl Acad Sci U S A **94**(14): 7245-7250.

Denechaud, P. D., I. C. Lopez-Mejia, A. Giralt, Q. Lai, E. Blanchet, B. Delacuisine, B. N. Nicolay, N. J. Dyson, C. Bonner, F. Pattou, J. S. Annicotte and L. Fajas (2016). "E2F1 mediates sustained lipogenesis and contributes to hepatic steatosis." J Clin Invest **126**(1): 137-150.

Dikkers, A., J. F. de Boer, A. K. Groen and U. J. Tietge (2015). "Hepatic ABCG5/G8 overexpression substantially increases biliary cholesterol secretion but does not impact in vivo macrophage-to-feces RCT." Atherosclerosis **243**(2): 402-406.

Dimova, D. K., O. Stevaux, M. V. Frolov and N. J. Dyson (2003). "Cell cycle-dependent and cell cycle-independent control of transcription by the Drosophila E2F/RB pathway." Genes Dev **17**(18): 2308-2320.

Dimri, G. P., K. Itahana, M. Acosta and J. Campisi (2000). "Regulation of a senescence checkpoint response by the E2F1 transcription factor and p14(ARF) tumor suppressor." Mol Cell Biol **20**(1): 273-285.

Du, W., J. E. Xie and N. Dyson (1996). "Ectopic expression of dE2F and dDP induces cell proliferation and death in the Drosophila eye." EMBO J **15**(14): 3684-3692.

Dukelow, T., D. Kishan, M. Khasraw and C. G. Murphy (2015). "CDK4/6 inhibitors in breast cancer." Anticancer Drugs **26**(8): 797-806.

Dyson, N. (1998). "The regulation of E2F by pRB-family proteins." Genes Dev **12**(15): 2245-2262.

Eguchi, A., A. Wree and A. E. Feldstein (2014). "Biomarkers of liver cell death." J Hepatol **60**(5): 1063-1074.

Escote, X. and L. Fajas (2015). "Metabolic adaptation to cancer growth: from the cell to the organism." Cancer Lett **356**(2 Pt A): 171-175.

Fajas, L., V. Egler, R. Reiter, J. Hansen, K. Kristiansen, M. B. Debril, S. Miard and J. Auwerx (2002). "The retinoblastoma-histone deacetylase 3 complex inhibits PPARgamma and adipocyte differentiation." Dev Cell **3**(6): 903-910.

Fajas, L., R. L. Landsberg, Y. Huss-Garcia, C. Sardet, J. A. Lees and J. Auwerx (2002). "E2Fs regulate adipocyte differentiation." Dev Cell **3**(1): 39-49.

Feingold, K. R. and C. Grunfeld (2000). Introduction to Lipids and Lipoproteins. Endotext. L. J. De Groot, P. Beck-Peccoz, G. Chrousos et al. South Dartmouth (MA).

Ferns, G., V. Keti and B. Griffin (2008). "Investigation and management of hypertriglyceridaemia." J Clin Pathol **61**(11): 1174-1183.

Ferrebee, C. B. and P. A. Dawson (2015). "Metabolic effects of intestinal absorption and enterohepatic cycling of bile acids." <u>Acta Pharm Sin B</u> **5**(2): 129-134.

Fon Tacer, K. and D. Rozman (2011). "Nonalcoholic Fatty liver disease: focus on lipoprotein and lipid deregulation." <u>J Lipids</u> **2011**: 783976.

Frolov, M. V. and N. J. Dyson (2004). "Molecular mechanisms of E2F-dependent activation and pRB-mediated repression." <u>J Cell Sci</u> **117**(Pt 11): 2173-2181.

Goldstein, J. L., R. A. DeBose-Boyd and M. S. Brown (2006). "Protein sensors for membrane sterols." <u>Cell</u> **124**(1): 35-46.

Hallman, D. M., S. R. Srinivasan, W. Chen, E. Boerwinkle and G. S. Berenson (2007). "Relation of PCSK9 mutations to serum low-density lipoprotein cholesterol in childhood and adulthood (from The Bogalusa Heart Study)." <u>Am J Cardiol</u> **100**(1): 69-72.

Hegele, R. A. (2009). "Plasma lipoproteins: genetic influences and clinical implications." <u>Nat Rev Genet</u> **10**(2): 109-121.

Hindler, K., C. S. Cleeland, E. Rivera and C. D. Collard (2006). "The role of statins in cancer therapy." <u>Oncologist</u> **11**(3): 306-315.

Hirano, Y., S. Murata, K. Tanaka, M. Shimizu and R. Sato (2003). "Sterol regulatory element-binding proteins are negatively regulated through SUMO-1 modification independent of the ubiquitin/26 S proteasome pathway." <u>J Biol Chem</u> **278**(19): 16809-16819.

Holtta-Vuori, M., K. Tanhuanpaa, W. Mobius, P. Somerharju and E. Ikonen (2002). "Modulation of cellular cholesterol transport and homeostasis by Rab11." <u>Mol Biol Cell</u> **13**(9): 3107-3122.

Horton, J. D., J. L. Goldstein and M. S. Brown (2002). "SREBPs: activators of the complete program of cholesterol and fatty acid synthesis in the liver." <u>J Clin Invest</u> **109**(9): 1125-1131.

Horton, J. D. and I. Shimomura (1999). "Sterol regulatory element-binding proteins: activators of cholesterol and fatty acid biosynthesis." <u>Curr Opin Lipidol</u> **10**(2): 143-150.

Hsieh, M. C., D. Das, N. Sambandam, M. Q. Zhang and Z. Nahle (2008). "Regulation of the PDK4 isozyme by the Rb-E2F1 complex." <u>J Biol Chem</u> **283**(41): 27410-27417.

Ioannou, G. N. (2016). "The Role of Cholesterol in the Pathogenesis of NASH." <u>Trends Endocrinol Metab</u> **27**(2): 84-95.

Janowski, B. A., M. J. Grogan, S. A. Jones, G. B. Wisely, S. A. Kliewer, E. J. Corey and D. J. Mangelsdorf (1999). "Structural requirements of ligands for the oxysterol liver X receptors LXRalpha and LXRbeta." <u>Proc Natl Acad Sci U S A</u> **96**(1): 266-271.

Kastelein, J. J., H. N. Ginsberg, G. Langslet, G. K. Hovingh, R. Ceska, R. Dufour, D. Blom, F. Civeira, M. Krempf, C. Lorenzato, J. Zhao, R. Pordy, M. T. Baccara-Dinet, D. A. Gipe, M. J. Geiger and M. Farnier (2015). "ODYSSEY FH I and FH II: 78 week results with alirocumab treatment in 735 patients with heterozygous familial hypercholesterolaemia." <u>Eur Heart J</u> **36**(43): 2996-3003.

Kovesdi, I., R. Reichel and J. R. Nevins (1986). "Identification of a cellular transcription factor involved in E1A trans-activation." <u>Cell</u> **45**(2): 219-228.

Lagarrigue, S., I. C. Lopez-Mejia, P. D. Denechaud, X. Escote, J. Castillo-Armengol, V. Jimenez, C. Chavey, A. Giralt, Q. Lai, L. Zhang, L. Martinez-Carreres, B. Delacuisine, J. S. Annicotte, E. Blanchet, S. Hure, A. Abella, F. J. Tinahones, J. Vendrell, P. Dubus, F. Bosch, C. R. Kahn and L. Fajas (2016). "CDK4 is an essential insulin effector in adipocytes." J Clin Invest **126**(1): 335-348.

Li, H., B. Dong, S. W. Park, H. S. Lee, W. Chen and J. Liu (2009). "Hepatocyte nuclear factor 1alpha plays a critical role in PCSK9 gene transcription and regulation by the natural hypocholesterolemic compound berberine." J Biol Chem **284**(42): 28885-28895.

Lu, T. T., J. J. Repa and D. J. Mangelsdorf (2001). "Orphan nuclear receptors as eLiXiRs and FiXeRs of sterol metabolism." J Biol Chem **276**(41): 37735-37738.

Luo, Y., C. P. Liang and A. R. Tall (2001). "The orphan nuclear receptor LRH-1 potentiates the sterol-mediated induction of the human CETP gene by liver X receptor." J Biol Chem **276**(27): 24767-24773.

Machado, M. V. and H. Cortez-Pinto (2014). "Non-alcoholic fatty liver disease: what the clinician needs to know." World J Gastroenterol **20**(36): 12956-12980.

Marotti, K. R., C. K. Castle, T. P. Boyle, A. H. Lin, R. W. Murray and G. W. Melchior (1993). "Severe atherosclerosis in transgenic mice expressing simian cholesteryl ester transfer protein." Nature **364**(6432): 73-75.

Miki, T., K. Nagashima and S. Seino (1999). "The structure and function of the ATP-sensitive K+ channel in insulin-secreting pancreatic beta-cells." J Mol Endocrinol **22**(2): 113-123.

Musso, G., R. Gambino and M. Cassader (2013). "Cholesterol metabolism and the pathogenesis of non-alcoholic steatohepatitis." Prog Lipid Res **52**(1): 175-191.

Nwokoro, N. A., C. A. Wassif and F. D. Porter (2001). "Genetic disorders of cholesterol biosynthesis in mice and humans." Mol Genet Metab **74**(1-2): 105-119.

Oram, J. F. and R. M. Lawn (2001). "ABCA1. The gatekeeper for eliminating excess tissue cholesterol." J Lipid Res **42**(8): 1173-1179.

Peet, D. J., S. D. Turley, W. Ma, B. A. Janowski, J. M. Lobaccaro, R. E. Hammer and D. J. Mangelsdorf (1998). "Cholesterol and bile acid metabolism are impaired in mice lacking the nuclear oxysterol receptor LXR alpha." Cell **93**(5): 693-704.

Peterson, A. S., L. G. Fong and S. G. Young (2008). "PCSK9 function and physiology." J Lipid Res **49**(6): 1152-1156.

Pirillo, A., A. L. Catapano and G. D. Norata (2016). "Niemann-Pick C1-Like 1 (NPC1L1) Inhibition and Cardiovascular Diseases." Curr Med Chem **23**(10): 983-999.

Rashid, S., D. E. Curtis, R. Garuti, N. N. Anderson, Y. Bashmakov, Y. K. Ho, R. E. Hammer, Y. A. Moon and J. D. Horton (2005). "Decreased plasma cholesterol and hypersensitivity to statins in mice lacking Pcsk9." Proc Natl Acad Sci U S A **102**(15): 5374-5379.

Richon, V. M. and G. Venta-Perez (1996). "Changes in E2F DNA-binding activity during induced erythroid differentiation." Cell Growth Differ **7**(1): 31-42.

Seidah, N. G., S. Benjannet, L. Wickham, J. Marcinkiewicz, S. B. Jasmin, S. Stifani, A. Basak, A. Prat and M. Chretien (2003). "The secretory proprotein convertase neural apoptosis-regulated convertase 1 (NARC-1): liver regeneration and neuronal differentiation." Proc Natl Acad Sci U S A **100**(3): 928-933.

Sinal, C. J., M. Tohkin, M. Miyata, J. M. Ward, G. Lambert and F. J. Gonzalez (2000). "Targeted disruption of the nuclear receptor FXR/BAR impairs bile acid and lipid homeostasis." Cell **102**(6): 731-744.

Song, B. L., N. B. Javitt and R. A. DeBose-Boyd (2005). "Insig-mediated degradation of HMG CoA reductase stimulated by lanosterol, an intermediate in the synthesis of cholesterol." Cell Metab **1**(3): 179-189.

Spinelli, V., O. Chavez-Talavera, A. Tailleux and B. Staels (2016). "Metabolic effects of bile acid sequestration: impact on cardiovascular risk factors." Curr Opin Endocrinol Diabetes Obes **23**(2): 138-144.

Stevens, C. and N. B. La Thangue (2004). "The emerging role of E2F-1 in the DNA damage response and checkpoint control." DNA Repair (Amst) **3**(8-9): 1071-1079.

Tanoli, T., P. Yue, D. Yablonskiy and G. Schonfeld (2004). "Fatty liver in familial hypobetalipoproteinemia: roles of the APOB defects, intra-abdominal adipose tissue, and insulin sensitivity." J Lipid Res **45**(5): 941-947.

Tarangelo, A., N. Lo, R. Teng, E. Kim, L. Le, D. Watson, E. E. Furth, P. Raman, U. Ehmer and P. Viatour (2015). "Recruitment of Pontin/Reptin by E2f1 amplifies E2f transcriptional response during cancer progression." Nat Commun **6**: 10028.

Tarugi, P., M. Averna, E. Di Leo, A. B. Cefalu, D. Noto, L. Magnolo, L. Cattin, S. Bertolini and S. Calandra (2007). "Molecular diagnosis of hypobetalipoproteinemia: an ENID review." Atherosclerosis **195**(2): e19-27.

Thompson, P. D., G. Panza, A. Zaleski and B. Taylor (2016). "Statin-Associated Side Effects." J Am Coll Cardiol **67**(20): 2395-2410.

van der Wulp, M. Y., H. J. Verkade and A. K. Groen (2013). "Regulation of cholesterol homeostasis." Mol Cell Endocrinol **368**(1-2): 1-16.

Wallace, M. C., S. L. Friedman and D. A. Mann (2015). "Emerging and disease-specific mechanisms of hepatic stellate cell activation." Semin Liver Dis **35**(2): 107-118.

Wu, X. and A. J. Levine (1994). "p53 and E2F-1 cooperate to mediate apoptosis." Proc Natl Acad Sci U S A **91**(9): 3602-3606.

Yabe, D., M. S. Brown and J. L. Goldstein (2002). "Insig-2, a second endoplasmic reticulum protein that binds SCAP and blocks export of sterol regulatory element-binding proteins." Proc Natl Acad Sci U S A **99**(20): 12753-12758.

Yamasaki, L., T. Jacks, R. Bronson, E. Goillot, E. Harlow and N. J. Dyson (1996). "Tumor induction and tissue atrophy in mice lacking E2F-1." Cell **85**(4): 537-548.

Yamauchi, Y., S. Yokoyama and T. Y. Chang (2016). "ABCA1-dependent sterol release: sterol molecule specificity and potential membrane domain for HDL biogenesis." J Lipid Res **57**(1): 77-88.

Yang, T., P. J. Espenshade, M. E. Wright, D. Yabe, Y. Gong, R. Aebersold, J. L. Goldstein and M. S. Brown (2002). "Crucial step in cholesterol homeostasis: sterols promote binding of SCAP to INSIG-1, a membrane protein that facilitates retention of SREBPs in ER." Cell **110**(4): 489-500.

Yu, L., R. E. Hammer, J. Li-Hawkins, K. Von Bergmann, D. Lutjohann, J. C. Cohen and H. H. Hobbs (2002). "Disruption of Abcg5 and Abcg8 in mice reveals their crucial role in biliary cholesterol secretion." Proc Natl Acad Sci U S A **99**(25): 16237-16242.

Zhang, D. W., T. A. Lagace, R. Garuti, Z. Zhao, M. McDonald, J. D. Horton, J. C. Cohen and H. H. Hobbs (2007). "Binding of proprotein convertase subtilisin/kexin type 9 to epidermal growth factor-like repeat A of low density lipoprotein receptor decreases receptor recycling and increases degradation." J Biol Chem **282**(25): 18602-18612.

Zhang, Y., N. Xu, J. Xu, B. Kong, B. Copple, G. L. Guo and L. Wang (2014). "E2F1 is a novel fibrogenic gene that regulates cholestatic liver fibrosis through the Egr-1/SHP/EID1 network." Hepatology **60**(3): 919-930.

Chapter 5: Appendix

Appendix, Figure 1
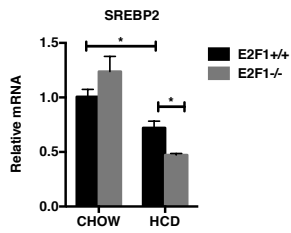
Figure 1: SREBP2 expression in the livers of E2F1+/+ and E2F1-/- mice fed a chow or HCD.
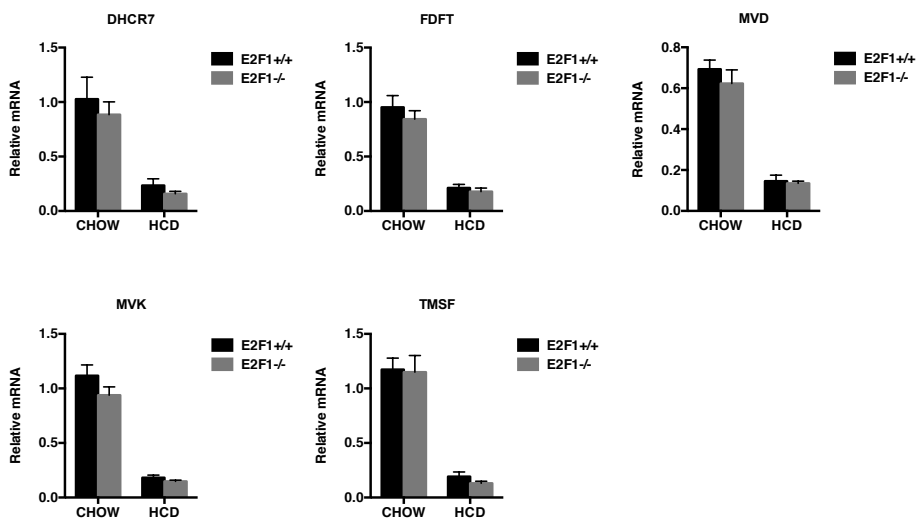
Appendix, Figure 2

Figure 2: Cholesterol biosynthesis genes expression in the livers of E2F1+/+ and E2F1-/- mice
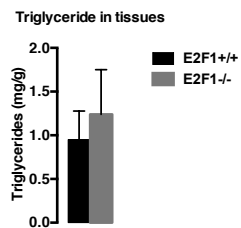fed a chow or HCD.

Appendix, Figure 3

Figure 3: Hepatic triglyceride level in E2F1+/+ and E2F1-/- mice fed a HCD.

52

Chapter 6: Articles

1. Article 1 : E2F1 mediates sustained lipogenesis and contributes to hepatic steatosis

E2F1 mediates sustained lipogenesis and contributes to hepatic steatosis

Pierre-Damien Denechaud,[1] Isabel C. Lopez-Mejia,[1] Albert Giralt,[1] Qiuwen Lai,[1] Emilie Blanchet,[2] Brigitte Delacuisine,[1] Brandon N. Nicolay,[3] Nicholas J. Dyson,[3] Caroline Bonner,[4,5,6] François Pattou,[4,5,6] Jean-Sébastien Annicotte,[2,7,] and Lluis Fajas[1]

[1]Department of Physiology, Université de Lausanne (UNIL), Lausanne, Switzerland. [2]Institut de Génétique Moléculaire de Montpellier, Université de Montpellier, Montpellier, France. [3]Laboratory of Molecular Oncology, Massachusetts General Hospital Cancer Center, Harvard Medical School, Charlestown, Massachusetts, USA. [4]European Genomic Institute for Diabetes, Lille, France. [5]INSERM UMR 1190, Lille, France. [6]Centre Hospitalier Régional Universitaire, Lille, France. [7]European Genomic Institute for Diabetes, Université Lille Nord de France, UMR 8199 CNRS, Lille, France.

E2F transcription factors are known regulators of the cell cycle, proliferation, apoptosis, and differentiation. Here, we reveal that E2F1 plays an essential role in liver physiopathology through the regulation of glycolysis and lipogenesis. We demonstrate that E2F1 deficiency leads to a decrease in glycolysis and de novo synthesis of fatty acids in hepatocytes. We further demonstrate that E2F1 directly binds to the promoters of key lipogenic genes, including *Fasn*, but does not bind directly to genes encoding glycolysis pathway components, suggesting an indirect effect. In murine models, E2F1 expression and activity increased in response to feeding and upon insulin stimulation through canonical activation of the CDK4/pRB pathway. Moreover, E2F1 expression was increased in liver biopsies from obese, glucose-intolerant humans compared with biopsies from lean subjects. Finally, *E2f1* deletion completely abrogated hepatic steatosis in different murine models of nonalcoholic fatty liver disease (NAFLD). In conclusion, our data demonstrate that E2F1 regulates lipid synthesis and glycolysis and thus contributes to the development of liver pathology.

Introduction

E2F transcription factors are the ultimate effectors of distinct signaling cascades that regulate the expression of genes involved in cellular homeostasis. E2Fs exist either as heterodimers associated with dimerization partner (DP) proteins or with larger complexes including members of the retinoblastoma family of proteins (pRBs) that includes RB1, RBL1, and RBL2 (1). In general, the association of E2Fs with pRB family members induces the repression of target genes. When phosphorylated by active cyclin–cyclin-dependent kinase (CDK) complexes, pRBs are released, enabling E2Fs to drive transcriptional regulation. In proliferating cells, E2F target genes include effectors of DNA replication, mitosis, DNA repair, and apoptosis (1).

Of particular interest is the observation that E2F1, the first-described and most-studied member of the E2F family, has important metabolic functions beyond the control of the cell cycle in nonproliferating cells. Indeed, we recently demonstrated, both in vitro and in vivo, that E2F1 directly regulates the expression of Kir6.2, a key component of the KATP channel that is involved in the regulation of glucose-induced insulin secretion in nonproliferating pancreatic β cells (2). E2F1 was also implicated in the regulation of adipose tissue metabolism through transcriptional regulation of the master adipogenic factor PPARγ during early stages of adipogenesis (3). E2F1 is also involved in metabolic functions in other tissues, such as muscle and brown adipose tissue, in which E2F1 modulates oxidative metabolism (4). Likewise, other studies have implicated E2F1 in the control of glucose homeostasis. For example, E2F1

directly regulates the gene encoding pyruvate dehydrogenase kinase 4 (PDK4), a key nutrient sensor and modulator of glucose oxidation, with the net result of restricting mitochondrial glucose oxidation (5). Moreover, 6-phosphofructo-2-kinase/fructose-2,6-bisphosphatase, the glycolytic enzyme involved in cell proliferation, was identified as an E2F target gene (6).

Overall, the above studies suggest that E2F1 contributes to whole-body metabolic homeostasis via distinct roles in different metabolic tissues. Studies concerning the retinoblastoma protein RB1 further support a major role of E2F1 in metabolism (7–9).

Although the liver plays a central role in whole-body glucose and lipid homeostasis, studies of the role of E2F1 in this tissue are limited to its participation in proliferation and oncogenesis (10, 11). Therefore, the function of E2F1 in liver metabolism remains to be explored. During fasting, the liver sustains a constant energy substrate supply for the organism by producing glucose from glycogenolysis and gluconeogenesis. In contrast, during the fed state, glucose enters the liver and is rapidly metabolized to replenish glycogen stores. Excess glucose is then converted into triglycerides (TG) via de novo lipogenic pathways (12).

In some metabolic disorders, including obesity, the liver exhibits increased glycolysis and lipid synthesis, resulting in the typical accumulation of fat in the liver (hepatic steatosis) (12). Genes involved in liver glycolysis and lipogenesis are regulated at the transcriptional level in response to insulin and glucose through the transcription factor sterol regulatory element–binding protein 1c (SREBP1c) and carbohydrate-responsive element–binding protein (CHREBP), respectively. Insulin, by activating SREBP1c, induces glucokinase (GCK) expression, which is the rate-limiting enzyme of glycolysis in the liver, thus controlling the glucose flux (13, 14). CHREBP, similar to SREBP1c, triggers the expression of genes such as acetyl-CoA
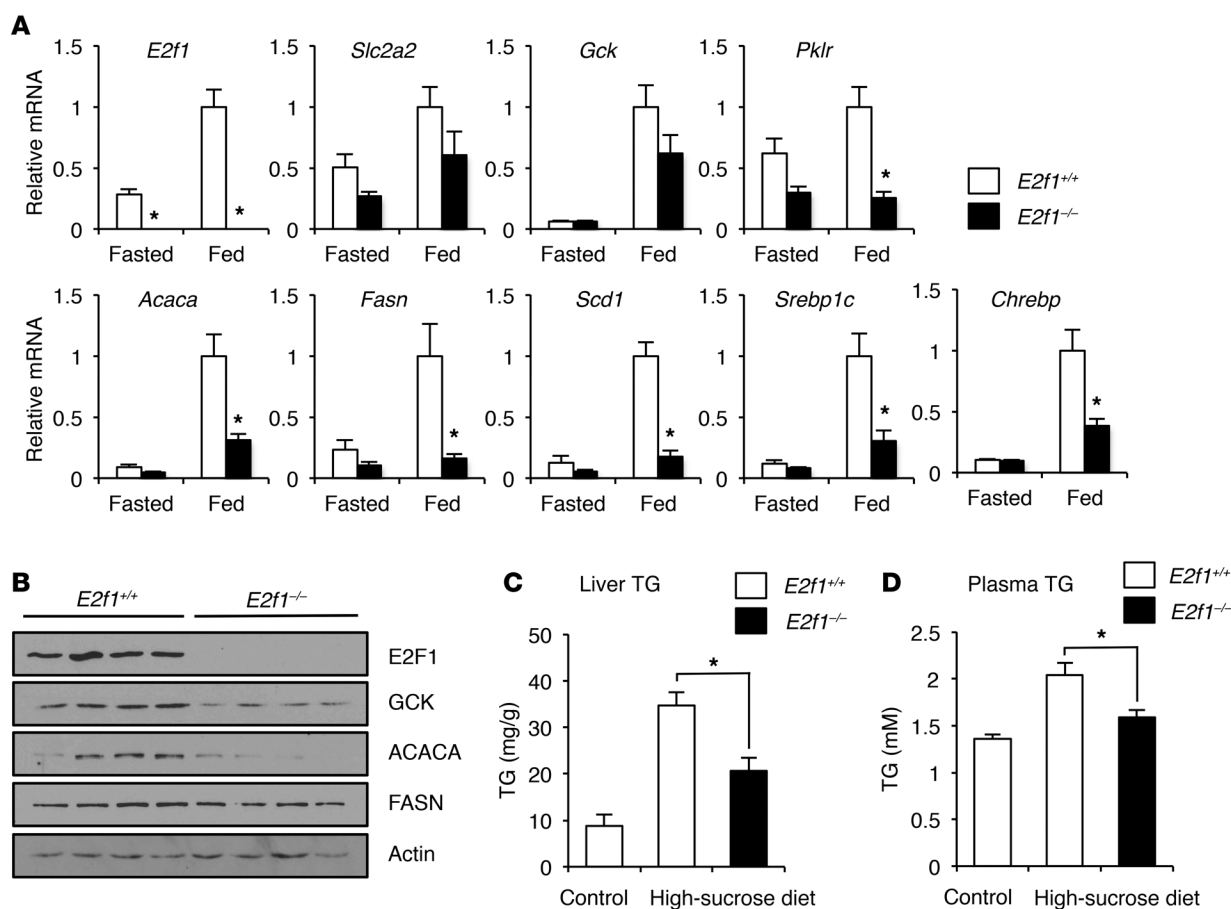
Figure 1. *E2f1⁻/⁻* mice show a decrease in liver glucose and lipid metabolism. (**A**) Relative mRNA levels of *E2f1* and relevant glycolytic and lipogenic genes in the livers of *E2f1⁺/⁺* versus *E2f1⁻/⁻* mice (*n* = 5 per group) under fed conditions. HFruct, high-fructose. (**B**) Western blot analyses of the expression of the indicated proteins in *E2f1⁺/⁺* and *E2f1⁻/⁻* mice. (**C**) Liver glycogen content, liver TG content, and plasma TG levels in fed *E2f1⁺/⁺* and *E2f1⁻/⁻* mice. (**C**) Liver TG content in *E2f1⁺/⁺* and *E2f1⁻/⁻* mice subjected to a 9-week high-sucrose diet (6 mice per group). (**D**) Plasma TG levels after overnight fasting of *E2f1⁺/⁺* and *E2f1⁻/⁻* mice subjected to a 9-week high-sucrose diet (6 mice per group). *$P < 0.05$, by 2-tailed, unpaired *t* test.

carboxylase (*ACACA*), fatty acid synthase (*FASN*), and stearoyl CoA desaturase (*SCD1*), which drive lipogenesis in the liver (15).

In this study, we demonstrate that E2F1 is essential for metabolic homeostasis in the liver through the control of glycogenic and lipogenic pathways. In particular, we show that E2F1 deficiency protects against obesity- and diabetes-induced liver steatosis in mouse models. Furthermore, we show that E2F1 expression is substantially increased in the liver of obese human subjects.

Results

E2F1 deficiency results in impaired glucose and lipid metabolism in the liver. To investigate the role of E2F1 in liver metabolism, we initially analyzed changes in glucose and lipid homeostasis in the livers of *E2f1⁻/⁻* mice. No major differences were observed in glucose or insulin levels in the plasma of *E2f1⁻/⁻* compared with that of *E2f1⁺/⁺* mice in the fed state (Supplemental Figure 1, A and B; supplemental material available online with this article; doi:10.1172/JCI81542DS1). Gene expression analyses indicated, however, that liver glycolytic pyruvate kinase (*Pklr*) and lipogenic *Acaca*, *Fasn*, and *Scd1* mRNA levels were decreased in *E2f1⁻/⁻* compared with levels in *E2F1⁺/⁺* mice (Figure 1A). Moreover, decreased mRNA levels correlated with reduced ACACA, FASN, and GCK protein

expression in the livers of these mice (Figure 1B). The glucose/ lipid pathway is transcriptionally regulated by multiple transcription factors, including SREPB1c and CHREBP, which function as insulin and glucose sensors, respectively. Interestingly, *Srebp1c* and *Chrebp* mRNA expression levels were strongly decreased in *E2f1⁻/⁻* mice compared with levels in *E2f1⁺/⁺* mice (Figure 1A). Surprisingly, no major differences were observed in E2F1-deficient mice fed a normal chow diet in terms of GCK activity, glycogen phosphorylase activity, or glycogen and TG content in the liver (Supplemental Figure 1, C–G). In the fasted state, we did not observe a significant reduction in the expression of glycolytic or lipogenic genes (Figure 1A).

Lipid homeostasis was also compromised by E2F1 deficiency. *E2f1⁺/⁺* and *E2f1⁻/⁻* mice were subjected to a high-sucrose dietary regime. The typical accumulation of TG observed in the liver in these conditions was reduced by 40% in *E2f1⁻/⁻* mice compared with the content found in their WT littermates (Figure 1C). We also observed a modest yet significant decrease in circulating TG levels in *E2f1⁻/⁻* mice in response to a high-sucrose diet (Figure 1D). These results were independent of any significant difference in body weight (BW), glycemia, insulinemia, or plasma free fatty acid (FFA) levels (Supplemental Figure 1,

H–K), suggesting that the observed effects in the absence of E2F1 were liver cell autonomous.

To demonstrate that the effects of *E2f1* deletion observed in the liver were effectively tissue autonomous, we generated *E2f1*-floxed mice on a C57BL/6 background. *E2f1*-floxed mice were crossed with *Alb-Cre* mice to delete *E2f1* specifically in the liver (*Alb-Cre E2f1^fl/fl^*, herein referred to as E2F1 LKO mice). We observed no differences in glycolytic or lipogenic gene expression in mice on a chow diet (Figure 2A); therefore, we decided to challenge these mice with a high-fructose diet to stimulate lipogenesis (16). Like *E2f1^-/-^* mice, E2F1 LKO mice showed a significant reduction in expression levels of glucose transporter 2 (*Slc2a2*), *Gck*, *Pklr*, *Acaca*, *Fasn*, *Scd1*, and *Srebp1c* genes in liver (Figure 2A). Subsequently, liver weight, liver TG content, and plasma TG levels were reduced in E2F1 LKO mice compared with *E2f1^fl/fl^* mice (Figure 2B).

E2F1 regulates glycolysis and lipogenesis in hepatocytes. To identify the molecular mechanisms involved in glucose and lipid homeostasis regulation by E2F1, we decided to use the model of primary cultures from mouse hepatocytes. As expected, the expression of *Slc2a2*, *Gck*, *Pklr*, *Acaca*, *Fasn*, *Scd1*, *Srebp1c*, and *Chrebp* mRNAs was increased in response to glucose and insulin in *E2f1^+/+^* hepatocytes (Figure 3A). This effect mimicked the observed changes in the liver under fed conditions (Figure 1A). In contrast, mRNA expression of these genes was not properly induced in response to glucose and insulin in *E2f1^-/-^* hepatocytes (Figure 3A). In addition, similar to the previous observation in liver (Figure 1B), GCK, ACACA, and FASN protein levels were also decreased in *E2f1^-/-^* compared with those in *E2f1^+/+^* cells (Figure 3B). These results suggested that E2F1 regulates the glycolytic and lipogenic gene expression programs in hepatocytes. Furthermore, in comparison with *E2f1^+/+^* cells, we found that decreased mRNA expression of key glycolytic genes correlated with decreased glycolysis in primary *E2f1^-/-^* hepatocytes, as measured by the extracellular acidification rate (ECAR) upon glucose injection into a Seahorse analyzer (Figure 4A). Consequently, there was a decrease in lactate concentration in the culture medium (Supplemental Figure 2A). Because E2F1 activity has previously been implicated in increased glucose oxidation in the heart (5), we verified that the reduced glycolysis observed in *E2f1^-/-^* hepatocytes was not the result of increased glucose oxidation and/or PDH activity. No differences in PDH activity were observed (Supplemental Figure 2, B and C), suggesting that impaired glycolysis, due in part to diminished GCK expression (and activity), contributed to a robust reduction of glycogen content in *E2f1^-/-^* hepatocytes after glucose-insulin stimulation (Figure 4B). This decrease in glycogen content could also be correlated with reduced expression levels of glycogen synthase and glycogen phosphorylase in *E2f1^-/-^* hepatocytes (Supplemental Figure 2, D and E). De novo lipid synthesis, which is typically observed when glucose levels are high, was also decreased in both basal and glucose-insulin–stimulated *E2f1^-/-^* hepatocytes (Figure 4C). Hence, we observed less lipid accumulation, as measured by Oil Red O staining, in *E2f1^-/-^* compared with *E2f1^+/+^* hepatocytes (Figure 4D). Taken together, these results suggested that the impaired glycolysis and lipid synthesis that we observed in the livers of *E2f1^-/-^* mice were due to the specific function of E2F1 in hepatocytes.

Table 1. E2F1 ChIP-seq data analysis

Enrichment of genes bound by E2F1

Biological processes	*P* value
Cellular metabolic process	2.5×10^{-87}
Primary metabolic process	3.5×10^{-68}
Macromolecule metabolic process	1.3×10^{-65}
Nitrogen compound metabolic process	1.0×10^{-54}
Organelle organization	2.6×10^{-37}
Cell cycle	1.3×10^{-36}
Biosynthetic process	9.9×10^{-30}
Cell-cycle process	9.8×10^{-25}
Cell division	2.9×10^{-23}
Cellular response to stimulus	1.8×10^{-22}
Regulation of metabolic process	3.1×10^{-16}

Enrichment of genes associated with E2F1 DNA binding using Gene Ontology Biological Processes (GOTERM_BP2) analysis.

E2F1 regulates global lipogenic and glycolytic gene expression programs in the liver. Our results indicated that E2F1 plays an important role in supporting glucose and lipid metabolism in the liver. The major function of E2F1 is to regulate gene transcription. Thus, to elucidate the mechanism underlying the effects of E2F1 depletion in the liver, we performed ChIP high-throughput DNA sequencing (ChIP-seq) in a primary culture of mouse hepatocytes infected with adenovirus-E2F1 (Ad-E2F1) using a validated anti-E2F1 Ab (Supplemental Figure 3, A and B) to identify E2F1 target genes. Experimental replicates were validated as described in Methods (Supplemental Figure 3, C and D). Sequencing alignment to the Ensembl Mouse Assembly NCBIM37 (mm9), peak detection, and peak assignment to genes was performed using the High-throughput Sequencing Data Analysis portal of the HTSstation (17). As expected, E2F1 target cell–cycle genes, including *Ccne1*, *Ccna2*, *Rb1*, *Rbl1*, *Cdkn2a*, *Tk1*, and *Dhfr* were found (Supplemental Figure 4). Consistent with previous studies (18), we found that E2F1 preferentially binds to promoter regions and that the major E2F1 motif enrichment is GCGCGC (Supplemental Figure 5, A–C). We used the Database for Annotation, Visualization, and Integrated Discovery (DAVID) to build a cluster of genes bound by E2F1 with the Gene Ontology Biological Processes (GOTERM_BP2) (http://www.geneontology.org) database. As expected, the cluster of genes bound by E2F1 that were involved in the cell cycle, cell division, and cell-cycle processes was well represented (Table 1).

Most interesting was the finding that the most significant cluster of genes was related to cellular metabolic processes (Table 1). This supported our hypothesis that E2F1 may be an important regulator not only of the cell cycle but also of cellular metabolism. Lipogenesis and glycolysis are major metabolic processes that take place in the liver, and our statistical analysis focusing on liver-specific genes also showed that the cluster of genes involved in fatty acid metabolism were significantly represented in the GOTERM_BP2 and KEGG_Pathway (Kyoto Encyclopedia of Genes and Genomes) (http://www.genome.jp/kegg/pathway.html) databases (Supplemental Figure 6). In a more precise analysis of the E2F1 ChIP-seq data, E2F1 was found to be bound to the
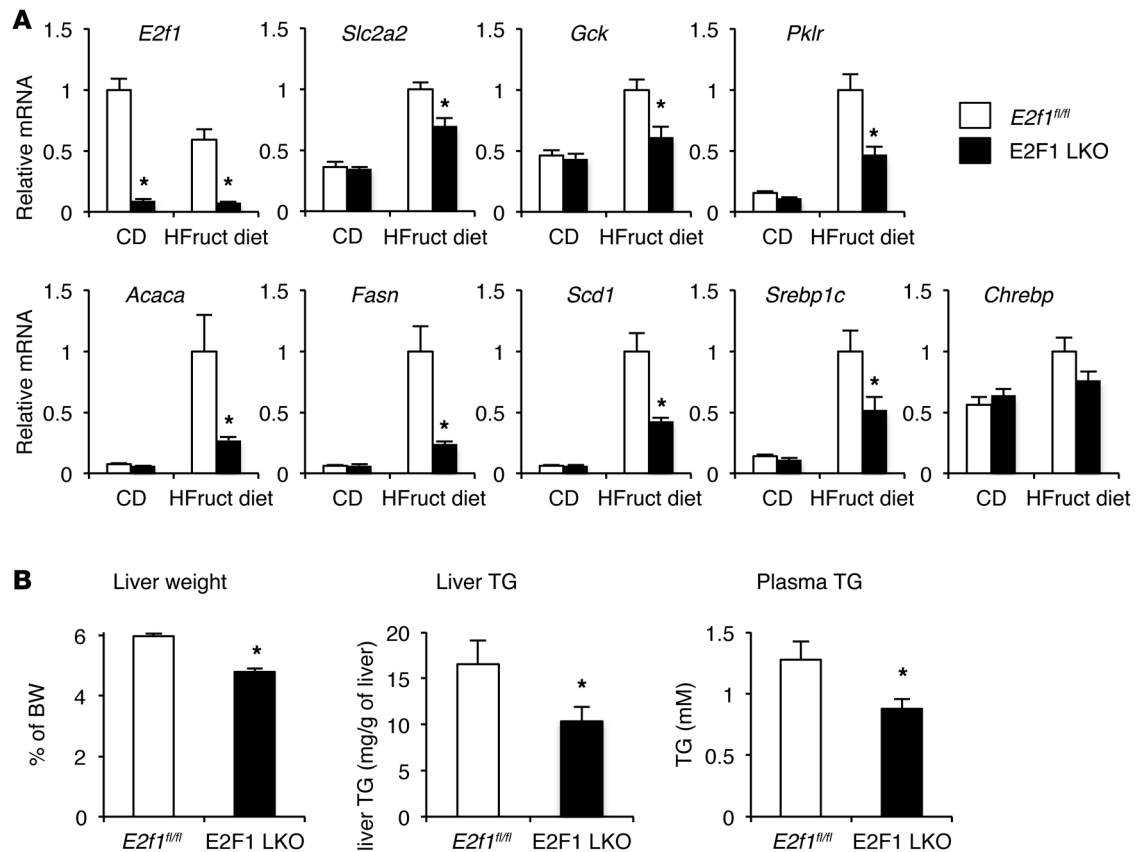
Figure 2. Liver-specific deletion of *E2f1* leads to decreased glycolytic and lipogenic programs. (**A**) Relative mRNA levels of *E2f1* and relevant glycolytic and lipogenic genes in the livers *E2f1^fl/fl* versus E2F1 LKO mice on a chow diet or after a 2-week high-fructose diet (*n* = 5 per group). (**B**) Liver weight, liver TG content, and plasma TG levels of *E2f1^fl/fl* versus E2F1 LKO mice after 2 weeks on a high-fructose diet (*n* = 5 per group). *$P < 0.05$, by 2-tailed, unpaired *t* test.

promoters of *Fasn*, *Chrebp*, and *Srebp1c* (Supplemental Figure 4). In addition, ChIP-quantitative PCR (ChIP-qPCR) experiments showed that E2F1 directly binds the promoters of the lipogenic *Acaca* and *Scd1* genes and confirmed that E2F1 binds the promoters of *Fasn* and of the transcription factors *Srebp1c* and *Chrebp* (Figure 5A). In contrast, we did not detect any significant chromatin enrichment in the promoters of the glycolytic genes *Slc2a2*, *Gck*, or *Pklr* (Figure 5A). The same pattern of DNA binding was observed in HepG2 human hepatoma cells lines when we performed ChIP on endogenous E2F1 (Supplemental Figure 7A). E2F1 overexpression in hepatocytes was able to induce *Acaca*, *Fasn*, and *Srebp1c* gene expression (Supplemental Figure 7B). In contrast, other genes we identified in the E2F1 ChIP analysis were not induced by E2F1 overexpression, suggesting that other E2F1 partners are required. The functional occupancy of E2F1 in these genes was assessed using luciferase-based reporter studies. E2F1 induced luciferase activity for the *Fasn*, *Scd1*, *Srebp1c*, and *Chrebp* promoters, but not for the *Slc2a2* or *Gck* promoters (Figure 5B). This suggested that E2F1 regulates the transcriptional activity of key genes including, but not limited to, *Fasn*, *Scd1*, *Chrebp*, and *Srebp1c*. In addition, through the regulation of *Srebp1c* and *Chrebp* transcription, E2F1 also indirectly regulated glycolysis (SLC2A2, GCK, PKLR) and lipogenesis (ACACA, FASN, SCD1) (Figure 5C).

To further characterize the action of E2F1 on the transcription of lipogenic genes, we decided to focus on the *Fasn* gene, which

encodes for the enzyme that catalyzes the rate-limiting reaction in fatty acid synthesis. Sequential deletions of the murine *Fasn* promoter determined the location of the E2F responsive element (E2FRE). Deletion of this responsive element abrogated the response to E2F1 (Supplemental Figure 8, A–C). It is still possible, however, that removal of the E2FRE in the *Fasn* promoter also abrogates the SREBP-mediated regulation of the promoter, since the E2FRE is located close to the sterol regulatory element (SRE) in this gene.

The transcription factor upstream stimulatory factor 1 (USF1) typically regulates the transcription of lipogenic genes in response to feeding and insulin signaling and cooperates with SREBP1c to induce *Fasn* gene transcription (19). We did not observe a synergistic effect of E2F1 on SREBP1 transactivation of the murine *Fasn* promoter luciferase reporter, suggesting that SREBP1 and E2F1 independently regulate this promoter (Supplemental Figure 9A). Interestingly, USF1 synergized with E2F1 to regulate the activity of the E2F1 synthetic target gene promoter (Figure 5D) and also of the *Fasn* promoter (Figure 5E). Co-IP experiments showed that USF1 and its heteropartner USF2 were associated with E2F1 (Figure 5F and Supplemental Figure 9B). These results suggest that, similar to other lipogenic transcription factors, E2F1 activity is also regulated by interactions with USF1. These results also demonstrate that E2F1 is a true and direct regulator of the transcription of key genes that participate in lipogenic pathways in the liver (Figure 5C).
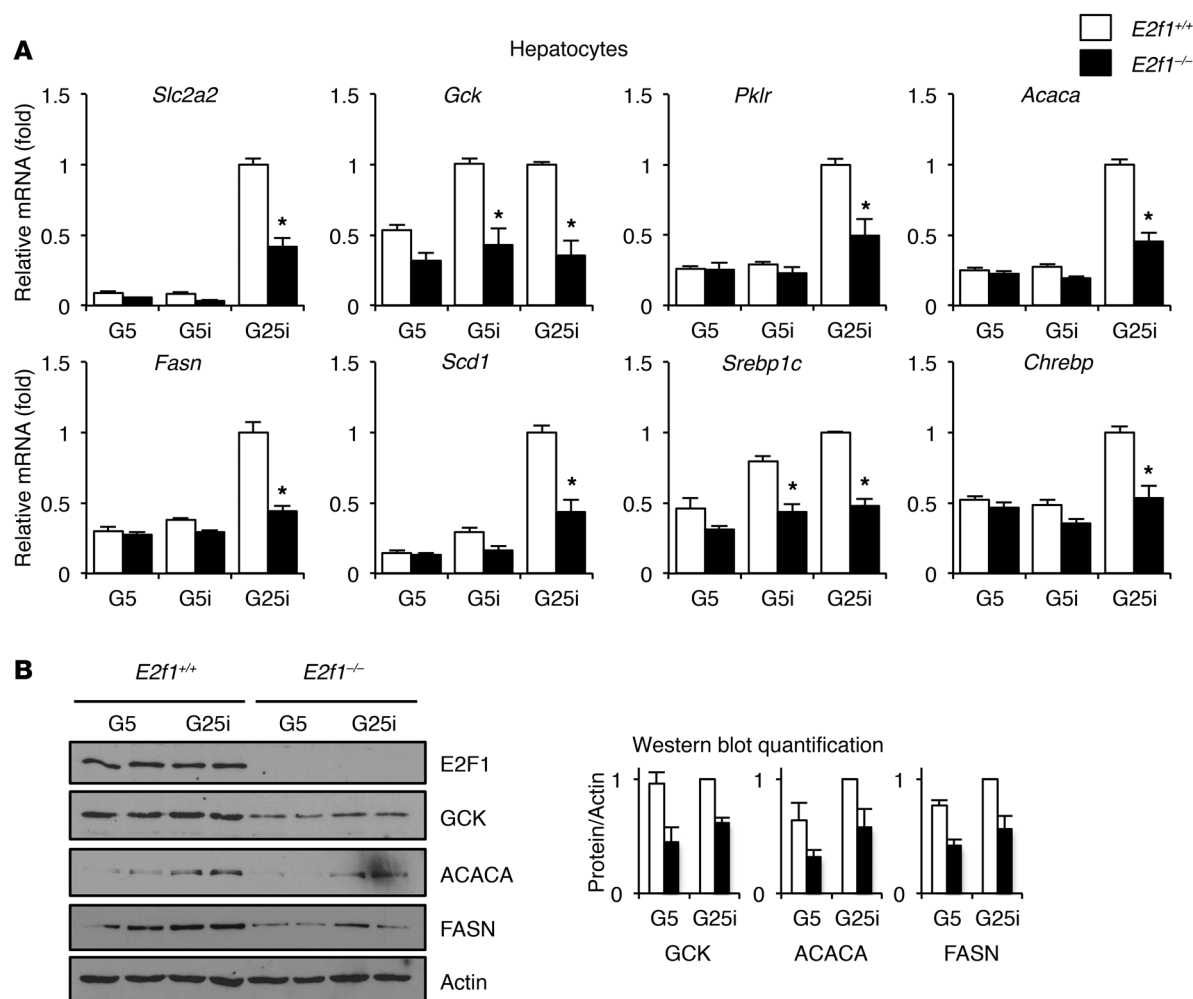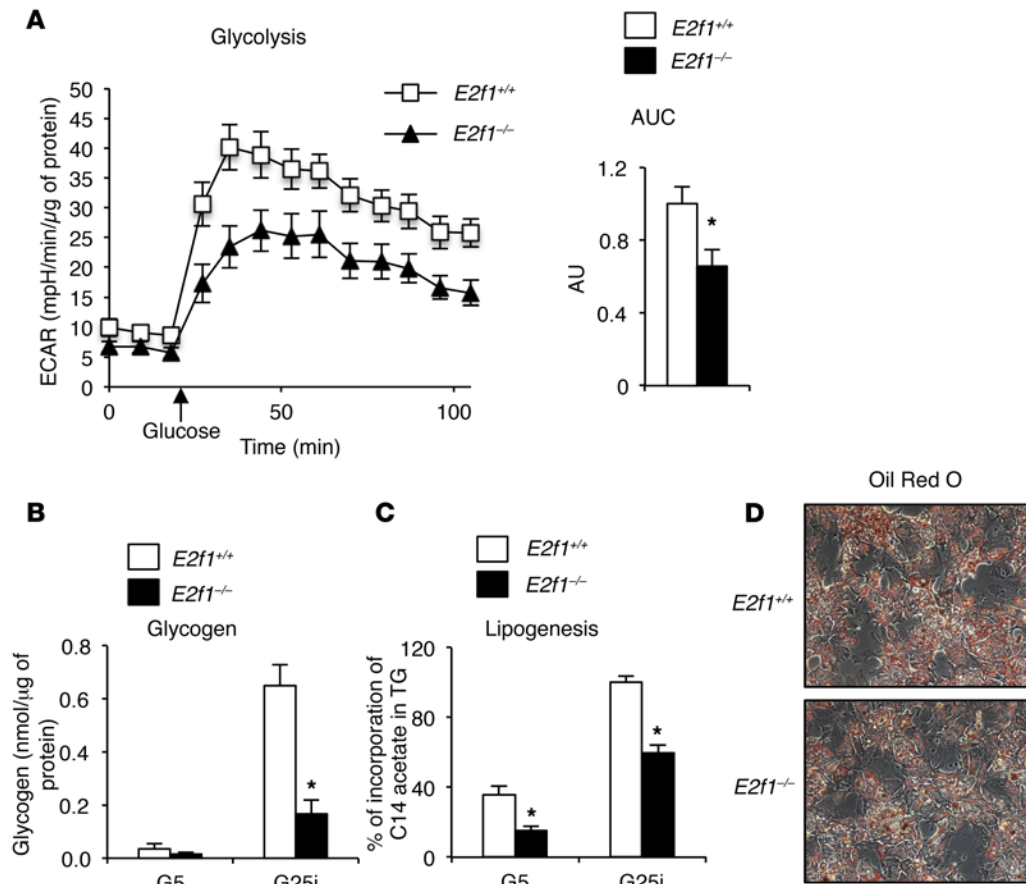
Figure 3. Expression of glycolytic and lipogenic genes is impaired in *E2f1⁻/⁻* hepatocytes. (**A**) Relative mRNA expression of relevant glycolytic and lipogenic genes in primary hepatocytes from *E2f1⁺/⁺* and *E2f1⁻/⁻* mice treated for 24 hours with 5 mM low glucose alone (G5); 5 mM low glucose and 100 nM insulin (G5i); or 25 mM high glucose and 100 nM insulin (G25i). (**B**) Western blot analysis shows expression levels of the indicated proteins in *E2f1⁺/⁺* and *E2f1⁻/⁻* hepatocytes treated for 24 hours with G5 or G25i. All experiments represent the average of 3 independent experiments. *$P < 0.05$ compared with control, by 2-tailed, unpaired *t* test.

The CDK4/RB/E2F1 pathway is regulated by insulin in hepatocytes. The expression of lipogenic and glycolytic genes in the liver is glucose and insulin sensitive. Interestingly, we found that *E2f1* mRNA and protein expression levels in mouse livers were increased in response to refeeding conditions, suggesting that E2F1 regulates lipogenic gene expression in response to glucose and insulin in this tissue (Figure 6, A and B). Indeed, our data showed that insulin induced mRNA and protein expression of E2F1 in primary mouse hepatocytes (Supplemental Figure 10, A and B). Moreover, E2F1 transcriptional activity was also increased in response to insulin, as measured by promoter-reporter luciferase-based assays (Figure 6C). E2F1 transcriptional activity is modulated by nonphosphorylated RB1, which binds to and represses E2F1 activity. Upon phosphorylation, RB1 is released from E2F1 complexes, thereby eliciting the transcription of E2F1 target genes. Similar to canonical E2F1 target genes, *Fasn* transcription was regulated in an RB1-dependent manner: E2F1 transcriptional activation of the *Fasn* promoter was blunted by RB1, suggesting that FASN is a bona fide

E2F1 target (Figure 6D). Moreover, RB1 had no effect on the basal activity of the *Fasn* promoter in the absence of E2F1 (Figure 6D and Supplemental Figure 10C). Furthermore, RB1 protein was phosphorylated in response to refeeding or insulin stimulation in liver and hepatocytes, respectively (Figure 6, E and F), and this result was consistent with increased E2F1 activity in response to insulin in these cells (Figure 6C). Furthermore, IP experiments in HepG2 hepatocytes showed that RB1 dissociated from E2F1 upon insulin stimulation in hepatocytes (Figure 6G).

RB1 dissociates from E2F1 when it is phosphorylated by members of the CDK family. We have previously shown that CDK4 kinase activity is induced by insulin in pancreatic β cells (2), suggesting that insulin could also regulate CDK4 activity in hepatocytes, leading to induction of E2F1 activity in these cells. Indeed, inhibition of CDK4 by shRNA in hepatocytes blocked RB1 Ser780 phosphorylation (Supplemental Figure 10D) and resulted in the attenuation of glucose and insulin effects on ACACA and FASN mRNA and protein expression levels (Figure 6, H and I). These

Figure 4. Glucose and lipid metabolism is impaired in *E2f1*⁻/⁻ hepatocytes. (**A**) ECAR of *E2f1*⁺/⁺ and *E2f1*⁻/⁻ hepatocytes after glucose treatment using a Seahorse analyzer (2 independent experiments, each with 8 technical replicates). (**B**) Glycogen content in *E2f1* ⁺/⁺ and *E2f1* ⁻/⁻ hepatocytes treated for 24 hours with G5 or G25i. (**C**) Quantification of the incorporation of C14-labeled acetate in the TG fraction in hepatocytes treated for 24 hours with G5 or G25i from the indicated genotypes, as a measure of lipogenesis. (**D**) Representative Oil Red O staining of *E2f1*⁺/⁺ versus *E2f1*⁻/⁻ hepatocytes (original magnification, ×200). Unless otherwise specified, all experiments represent the average of 3 independent experiments. *$P < 0.05$ compared with control, by 2-tailed, unpaired *t* test.

results suggested that CDK4, likely through E2F1 activation, regulates the expression of lipogenic genes.

E2F1 expression is increased in obese mice and humans. Increased glycolysis and de novo lipogenesis are typically observed during hepatic steatosis and hypertriglyceridemia development. Our results indicate that E2F1 regulates liver glucose and lipid metabolism, and we were therefore interested in elucidating the putative participation of E2F1 in liver pathology. Fatty liver is the first step in nonalcoholic fatty liver disease (NAFLD) and represents a risk factor for nonalcoholic steatohepatitis (NASH), fibrosis, cirrhosis, and hepatocellular carcinoma (20). Interestingly, in mice fed a high-fat diet and in *db/db* mice, which constitute two models of hepatic steatosis, the mRNA expression levels of *E2f1* were markedly increased compared with those in control animals (Figure 7, A and B). In addition, hepatic RB1 protein was hyperphosphorylated at Ser780 (Figure 7C). These results are consistent with increased E2F1 activity in these mouse models of fatty liver disease. In order to translate the findings obtained in mouse models to human pathology, we quantified the levels of *E2F1* gene expression in liver biopsies from 10 lean patients versus levels in 10 obese, glucose-intolerant patients. The metabolic parameters for these patients are presented in Supplemental Table 1. A significant increase in *E2F1* mRNA levels was observed in the liver of obese, glucose-intolerant patients compared with levels detected in the lean subjects, supporting our findings in mice (Figure 7D).

E2F1 deficiency protects against hepatic steatosis. To further demonstrate the participation of E2F1 in liver steatosis, we generated *db/db E2f1*⁻/⁻ mice. Deletion of *E2f1* in the *db/db* model led to lower plasma insulin levels and BW (Figure 8A and Supplemental Figure 11A). No major differences in plasma glucose, FFA, or adiposity (fat mass content) were observed between *db/db E2f1*⁺/⁺ and *db/db E2f1*⁻/⁻ mice, suggesting that *E2f1* deletion on the *db/db* genetic background does not protect against diabetes or obesity, despite the misleading reduction in BW of these mice (Supplemental Figure 11, B and C). Indeed, *db/db E2f1*⁻/⁻ mice have the classical features of obese *db/db* mice, as they are hyperphagic, polydipsic, move less, and their respiratory exchange ratio (RER) is also reduced compared with *db/+ E2f1*⁺/⁺ mice (Supplemental Figure 11, D and E). However, we observed no differences in insulin sensitivity, as measured by an insulin tolerance test (ITT) (Supplemental Figure 11F), nor in the levels of AKT phosphorylation under basal conditions (Figure 8B) or after insulin stimulation (Supplemental Figure 11G). In contrast, *E2f1* deletion on the *db/db* background resulted in decreased hepatic expression of lipogenic and glycolytic genes as well as decreased expression of SREBP1c and CHREBP at both the mRNA (Figure 8C) and protein (Figure 8D) levels compared with *db/db E2f1*⁺/⁺ mice. This suggested that E2F1 participates in the regulation of lipogenic genes in the development of NAFLD in the *db/db* model. Most important was the finding that *E2f1* deletion reversed the fatty liver phenotype in *db/db* mice. Indeed, the livers of *db/db E2f1*⁻/⁻ mice showed a normal macroscopic appearance compared with the pale and increased size of the livers of *db/db E2f1*⁺/⁺ mice (Figure 9A). Moreover, *db/db E2f1*⁻/⁻ livers had decreased weight compared with *db/db E2f1*⁺/⁺ livers (Figure 9B)
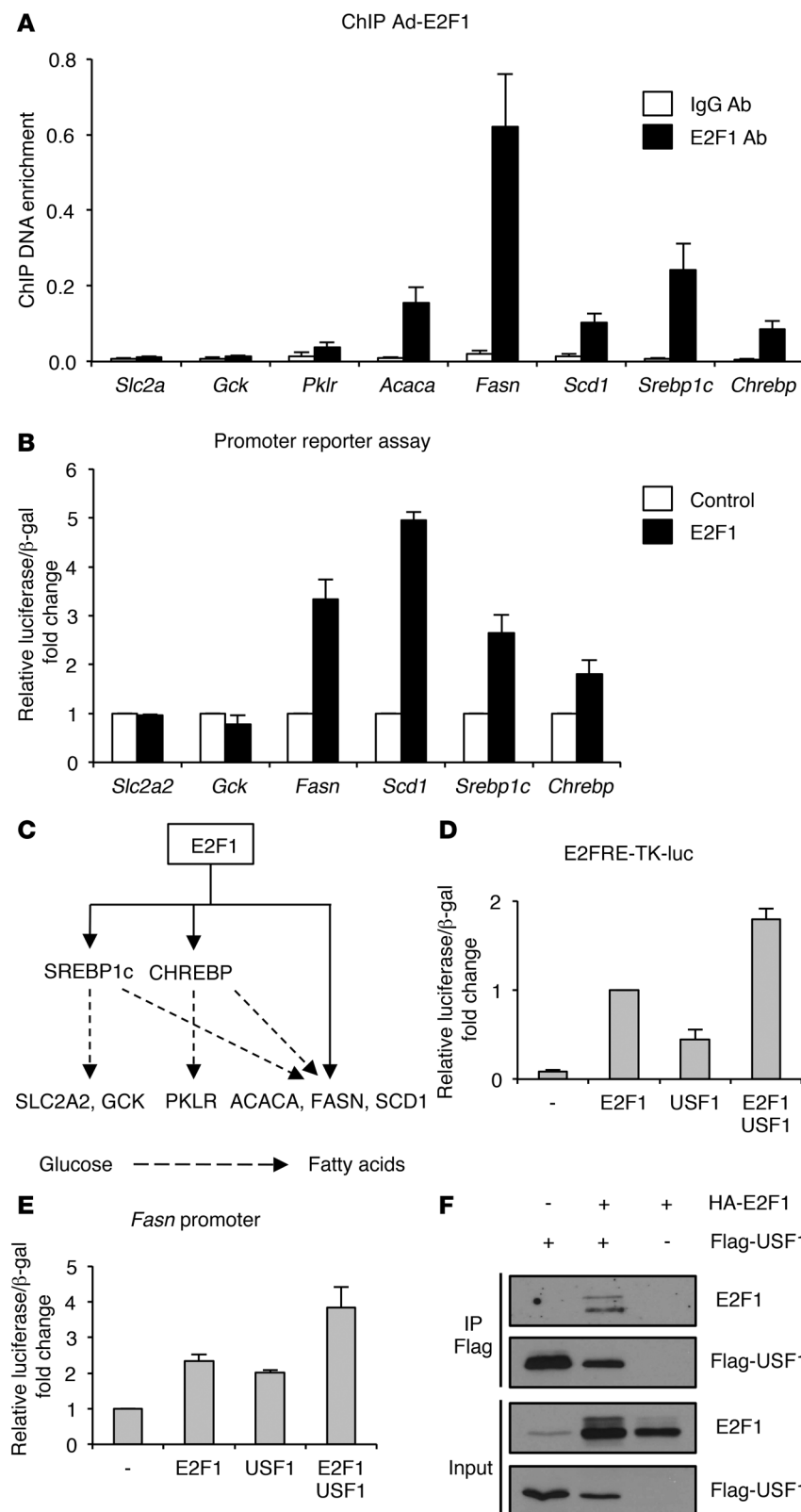
Figure 5. Lipogenic genes are bona fide E2F1 targets. (**A**) E2F1 ChIP on hepatocytes expressing Ad-E2F1 demonstrated E2F1 binding to the *Acaca*, *Fasn*, *Scd1*, *Srebp1c*, and *Chrebp* promoters, but not the *Slc2a2* or *Gck* promoter (*n* = 5). (**B**) Luciferase-based reporter activity of the indicated promoters in HepG2 cells transfected with empty vector or the E2F1-HA expression vector. (**C**) Representative role of E2F1 in the transcriptional control of glycolysis and lipogenesis. E2F1 directly controlled *Srebp1c*, *Chrebp*, *Acaca*, *Fasn*, and *Scd1* gene expression and indirectly controlled *Slc2a2*, *Gck*, and *Pklr* via SREBP1c and CHREBP. SREBP1c and CHREBP also participated in the control of *Acaca*, *Fasn*, and *Scd1* gene expression. (**D**) E2F-TK-luc reporter activity in HepG2 hepatocytes transfected with empty vector, E2F1, or USF1. (**E**) Mouse *Fasn* promoter activity in hepatocytes transfected with empty vector, E2F1 or USF1. (**F**) Co-IP experiment on E2F1 and USF1 in HepG2 hepatocytes. Cells were transfected with E2F1-HA and Flag-USF1 as indicated, and protein was immunoprecipitated with a Flag Ab.

observed when lipogenesis is reduced. Finally, microscopic analysis indicated that E2F1 deficiency prevented hepatic steatosis (NAFLD) and the accumulation of intravesicular lipid droplets, which was observed with Oil Red O staining in hepatic steatosis (Figure 9F). These results suggest that E2F1 is an important factor facilitating the development of NAFLD.

Finally, to demonstrate that the observed effects were not the result of decreased insulin levels on the $E2f1^{-/-}$ background, we decided to also characterize obese $db/db\ E2f1^{+/-}$ mice. These mice were similar to $db/db\ E2f1^{+/+}$ mice in terms of BW, plasma insulin levels, hyperphagia, water consumption, ambulatory movement, and RER (Supplemental Figure 12, A–D), whereas they were more glucose tolerant and insulin sensitive compared with $db/db\ E2f1^{+/+}$ mice (Supplemental Figure 12, E and F). This suggested that the effects of E2F1 are not secondary to decreased insulin levels or decreased weight. Furthermore, $db/db\ E2f1^{+/-}$ mice had decreased hepatic steatosis, as illustrated by a lower liver TG content compared with that detected in $db/db\ E2f1^{+/+}$ mice (Supplemental Figure 13B), but to a lesser extent than in $db/db\ E2f1^{-/-}$ mice (Figure 9C). These results were fully consistent with a reduction of the majority of glycolytic and lipogenic gene expression levels in the livers of $db/db\ E2f1^{+/-}$ mice (Supplemental Figure 13A).

and consistently showed a decrease in TG content (Figure 9C). Liver lipidomic analysis further demonstrated a strong decrease in palmitate and oleate fatty acids (Figure 9D). Consequently, the desaturation index of $db/db\ E2f1^{-/-}$ livers was also decreased compared with that of $db/db\ E2f1^{+/+}$ livers (Figure 9E), which is typically

Discussion

We show here that E2F1 is participates in hepatic glycolysis and de novo lipid synthesis through global transcriptional regulation of these pathways. Furthermore, we identify what we believe to be a
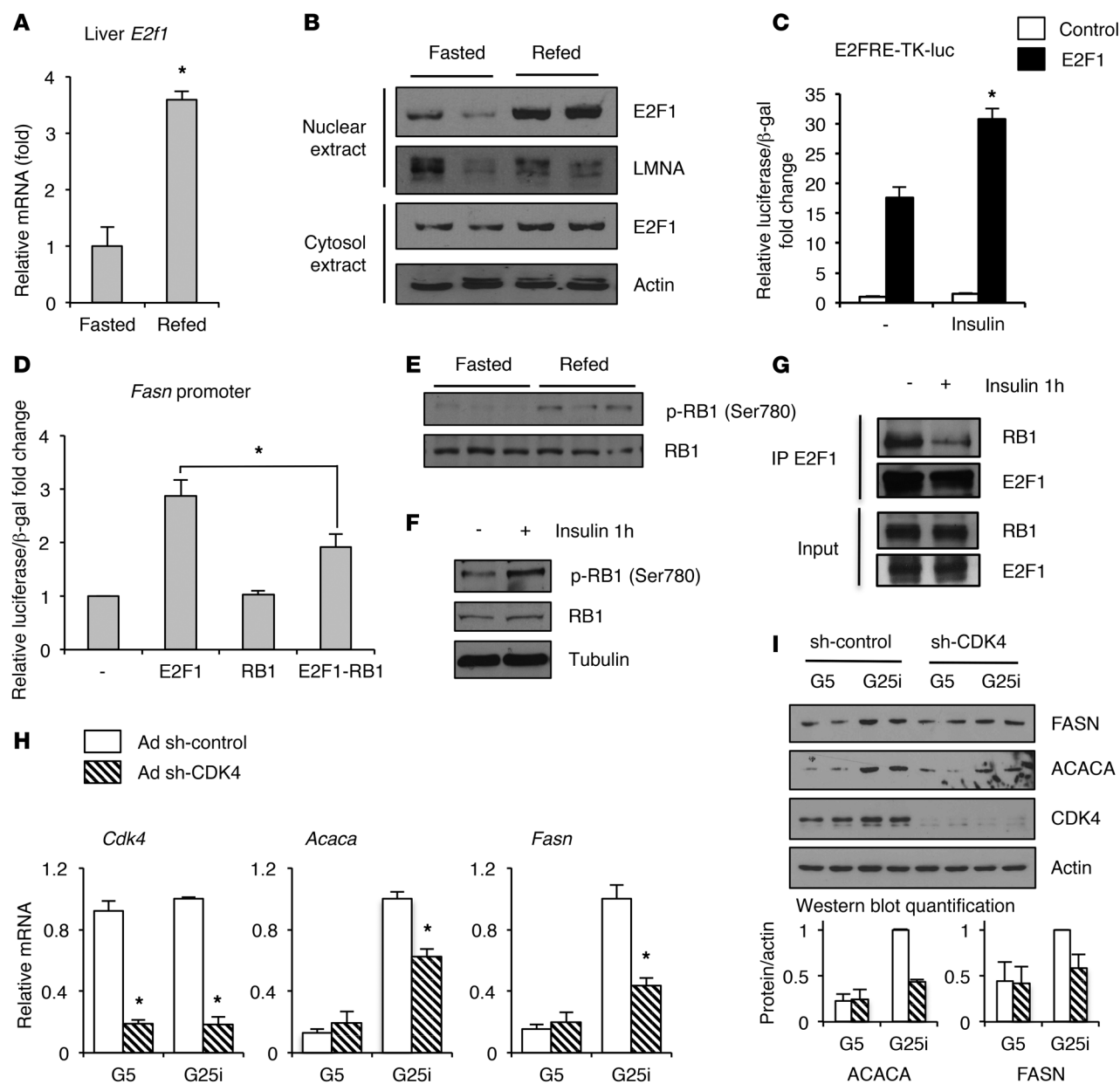
Figure 6. Insulin regulates E2F1 activity through RB1 and CDK4. (**A**) Relative *E2f1* mRNA expression levels in the livers of mice after a 24-hour fast, followed by an 18-hour refeeding. (**B**) Protein expression analyses of the indicated cellular fractions in the livers of mice under the same conditions as in **A**. (**C**) E2F reporter activity (E2FRE-TK-luc) in response to insulin in HEK293T cells. (**D**) Mouse *Fasn* promoter activity in HepG2 cells transfected with empty vector, E2F1, or RB1. (**E**) Ser780 phosphorylation of RB1 in the livers of fasted and refed mice. (**F**) Ser780 phosphorylation of RB1 in hepatocytes after 1 hour of insulin stimulation. (**G**) RB1 co-IP with E2F1 after 1 hour of insulin stimulation in HepG2 hepatocytes. (**H**) Relative mRNA expression of the indicated genes in hepatocytes treated with adenovirus expressing sh-control or sh-CDK4 and stimulated for 24 hours with G5 or G25i. (**I**) Protein levels of ACACA, FASN, and CDK4 in hepatocytes treated with adenovirus expressing sh-control or sh-CDK4 and stimulated for 24 hours with G5 or G25i. The experiments were performed at least 3 times. *$P < 0.05$, by 2-tailed, unpaired t test.

new class of E2F1 targets that include ACACA, FASN, SCD1, SRE-BP1c, and CHREBP, which are not directly involved in control of the cell cycle, proliferation, or apoptosis but rather are major regulators of metabolic pathways. Other genes such as those encoding the SLC2A2 transporter and GCK and PKLR glycolytic enzymes are also indirectly regulated by E2F1 through the SREBP1c and CHREBP transcription factors. These two transcription factors also participate in the E2F1-mediated control of *Acaca*, *Fasn*, and

Scd1 gene expression. Interestingly, E2F1 expression and activity were increased in response to feeding and insulin levels in mouse livers and hepatocytes, respectively (Figure 6 and Supplemental Figure 9, A and B). This qualifies E2F1 as a major regulator of liver glucose and lipid metabolism (Figure 5C). To our knowledge, only one additional transcription factor, LXRα, has been shown to regulate the same transcriptional program in the liver (15). This novel function of E2F1 was initially observed using a total KO. By using
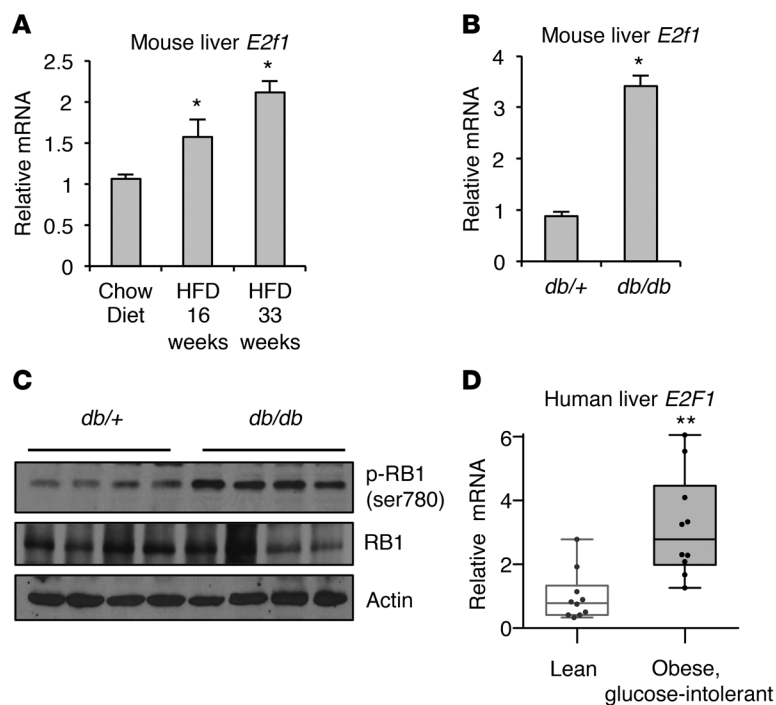
Figure 7. *E2F1* gene expression is increased in obese mice and humans. (**A**) Relative expression of *E2f1* mRNA in the livers of mice after 16 or 33 weeks on a high-fat diet. (**B**) *E2f1* mRNA expression in the livers of control *db/+* and *db/db* mice. (**C**) Ser780 phosphorylation of RB1 in the livers of *db/db* mice. (**D**) Relative expression of *E2F1* mRNA in livers of lean subjects and obese, glucose-intolerant patients. * $P < 0.05$ and ** $P < 0.002$ compared with control, by 2-tailed, unpaired t test.

tion in the *db/db* mouse model of NAFLD, or in mice fed a high-sucrose diet, protected against lipid accumulation in the liver. However, decreased hepatic steatosis did not prevent marked hyperglycemia in *db/db E2f1^{-/-}* mice, which is in contrast to the current knowledge that a reduction in hepatic TG levels correlates with improved insulin sensitivity (22, 23).

SREBP1c and CHREBP are essential activators of lipogenesis (12). In the context of NAFLD, it was reported that liver-specific KO of the gene encoding SCAP, which is necessary to promote SREBP1c nuclear activity, eliminates fatty liver in ob/ob diabetic mice (24). The same observations were reported for CHREBP downregulation in ob/ob mice using an adenoviral strategy (22). Since we show that E2F1 regulates the expression of SREBP1c and CHREBP, the abrogation of fatty liver in *db/db E2f1^{-/-}* mice could be at least partly due to the decreased expression of these transcription factors in the absence of E2F1.

Similar to our results, other studies have shown that liver steatosis can be regulated independently of insulin resistance. Liver-specific *Irs1^{-/-}* mice, when fed a high-fat diet, were insulin resistant despite being protected from liver steatosis (25). Most interestingly, these mice showed near-normal liver histology and exhibited decreased nodular lesions compared with control mice and were protected from liver tumorigenesis (26). Other examples include the liver-specific phosphoinositide 3-kinase (PI3K) *p110a*-KO mice, which, similar to our findings in *E2f1^{-/-}* mice, were protected from hepatic steatosis without augmented plasma glucose and insulin levels when fed a high-fat diet (27). Conversely, insulin sensitization does not require amelioration of liver steatosis, as shown in CHREBP-overexpressing mice fed a high-fat diet, which were protected against insulin resistance despite increased lipid accumulation in the liver (28). Liver-specific *Pten*-KO mice also showed improved insulin sensitivity despite having liver steatosis (29). Indeed, insulin resistance is associated with increased lipid synthesis but also with increased glucose production in the liver. This indicates that lipogenesis could remain sensitive to insulin in the liver, whereas gluconeogenesis becomes resistant to inhibition by insulin according to a selective insulin resistance pathway, as suggested by Brown and Goldstein (30). It was demonstrated, however, that despite hyperglycemia and hyperinsulinemia, liver insulin receptor–KO (LIRKO) mice exhibit low plasma TG levels and no elevation of hepatic TG, suggesting that the divergent signaling pathway that controls lipid and glucose synthesis is downstream of the insulin receptor (31). Other studies in human subjects have also provided evidence to suggest that defects in insulin action in diabetic patients occur at the post-receptor level (32).

The paradox of "selective" insulin resistance raises the question of where the insulin-signaling regulatory pathway diverges from the gluconeogenic and lipogenic pathways. Elevated gluconeogenesis is explained by the lack of insulin repression due to an insulin-resistant state. However, there is a missing link between insulin resistance and the high rate of lipogenesis. It has been proposed that ER stress and inflammation could be

this model, we could not exclude the possibility that some of the effects observed in the absence of E2F1 were secondary, at least in part, to the role of E2F1 in insulin secretion (2). However, we demonstrated that this function was liver cell autonomous by using primary hepatocytes and E2F1 LKO mice fed a high-fructose diet. Even with residual liver E2F1 expression (Figure 2A), these mice clearly showed a decrease in glycolytic and lipogenic gene expression, leading to a reduction of hepatic steatosis.

De novo lipogenesis is a key regulatory pathway in liver and adipose tissue that facilitates the storage of excess energy in the form of lipids, typically as a result of increased glucose uptake. Fatty acid synthesis contributes, however poorly, to lipid content in the liver under normal physiological conditions (21), which is consistent with our observation that the effects of E2F1 on lipid synthesis in normal physiology are mild. Excess fat accumulation in the liver, such as that typically observed in obese, type 2 diabetic patients, can originate from increased fatty acid uptake, intensified fatty acid synthesis, reduced fatty acid oxidation, or decreased lipid export and transport. Nearly 30% of the TG content in the livers of NAFLD patients originates from de novo lipid synthesis (21). Interestingly, we found that E2F1 expression was significantly increased in the livers of obese, glucose-intolerant human subjects compared with that observed in normal-weight subjects (Figure 7D). Similar results were obtained in mouse models of fatty liver disease, in which E2F1 expression and activity were greatly increased, contributing to the augmentation of lipid content in the liver. Accordingly, our results showed that *E2f1* dele-
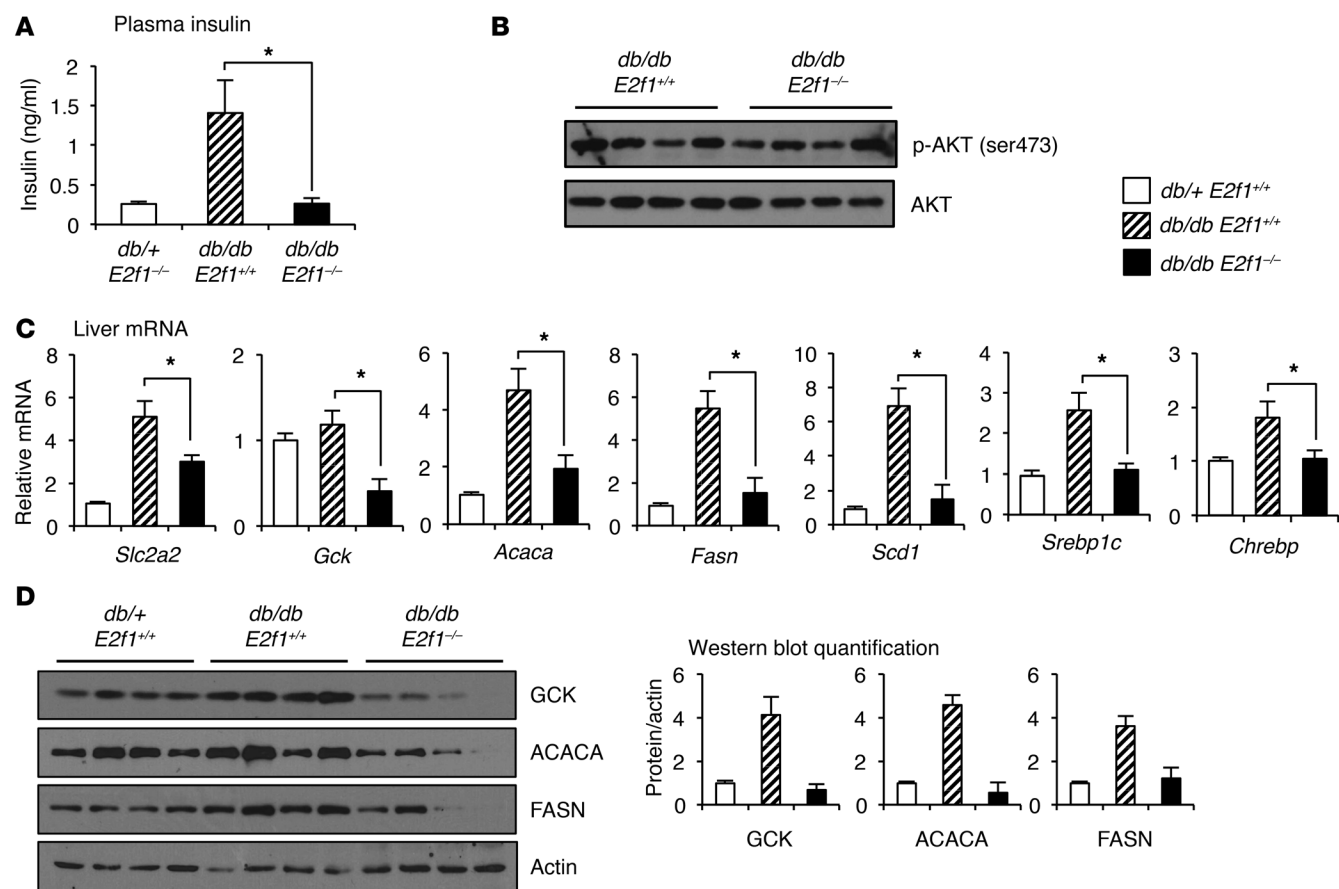
Figure 8. E2f1 deletion in db/db mouse model decreases glycolytic and lipogenic programs. (**A**) Plasma insulin levels in db/+ E2f1+/+, db/db E2f1+/+, and db/db E2f1-/- mice (n = 5–9). (**B**) Ser473 phosphorylation of AKT in the livers of db/db E2f1+/+ and db/db E2f1-/- mice. (**C**) Relative liver mRNA expression levels of the indicated genes in the annotated mouse genotypes (n = 4–6). (**D**) Western blot analyses of the expression of the indicated proteins in the livers of db/+ E2f1+/+, db/db E2f1+/+, and db/db E2f1-/- mice. *$P < 0.05$, by 2-tailed, unpaired t test.

involved in this abnormal regulation of liver function (33–35). ER stress has been reported to contribute to hepatic steatosis by supporting high lipogenic gene expression via SREBP1c and CHREBP activation (36). In our study, we demonstrate that liver E2F1 expression and activity were robustly increased in insulin-resistant db/db mice and in obese, glucose-intolerant patients (Figure 7) and thus participates in liver steatosis. In this context, E2F1 could be activated by ER stress and, together with SREBP1c and CHREBP, maintain high lipogenesis.

E2F1 activity is increased in cancer cells, as this factor is essential for the transactivation of genes such as c-Myc and cyclin E, which regulate S-phase onset, DNA replication, and mitosis. Strikingly, de novo fatty acid biosynthesis is essential for dividing cells to synthesize new membranes. Lipogenesis also participates in the generation of signaling molecules, such as phosphatidylinositol, phosphatidylserine, and phosphatidylcholine, which are important in the activation of proliferative and survival pathways. Interestingly, it was shown that E2F1 participates in the control of lipid synthesis concomitantly with the regulation of proliferation in cancer cells (37). This was further demonstrated by the recent finding showing that fatty acid synthesis is coordinated with cell-cycle progression in proliferating cells (38). Moreover, a biphasic model of lipid accumulation, in which cycling cells show higher levels of

lipids at the G1/S and G2/M transitions, was proposed (10, 38). The symmetrical effects of E2F1 on metabolic and proliferative pathways highlight the potential role of this cell-cycle regulator as a key mediator of the adapted metabolic response to proliferative stimuli, such as those observed during cancer cell transformation. Furthermore, our finding that E2F1 expression is increased in mouse models of diabetes and obesity could explain the increased cancer risk among obese and diabetic patients. Likewise, protection from E2F1-dependent hepatic steatosis may also protect against hepatic fibrosis and carcinogenesis (10, 11).

In summary, our results show that E2F1 mediates a metabolic switch that is notably increased to trigger lipid synthesis, most specifically under physiopathological conditions such as fatty liver disease.

Methods

Abs and biochemistry. The following Abs were obtained from Cell Signaling Technology: FASN (no. 3180); ACACA (no. 3662); lamin A/C (no. 2032); and phosphorylated RB (Ser780) (no. 8180). The following Abs were obtained from Santa Cruz Biotechnology Inc.: E2F1 (C-20; catalog sc-193); RB (C-15; catalog sc-50); RB (C-2; catalog sc-74562); CDK4 (C-22; catalog sc-260); and normal IgG rabbit (catalog sc-2027). The following Abs were obtained from Sigma-Aldrich:
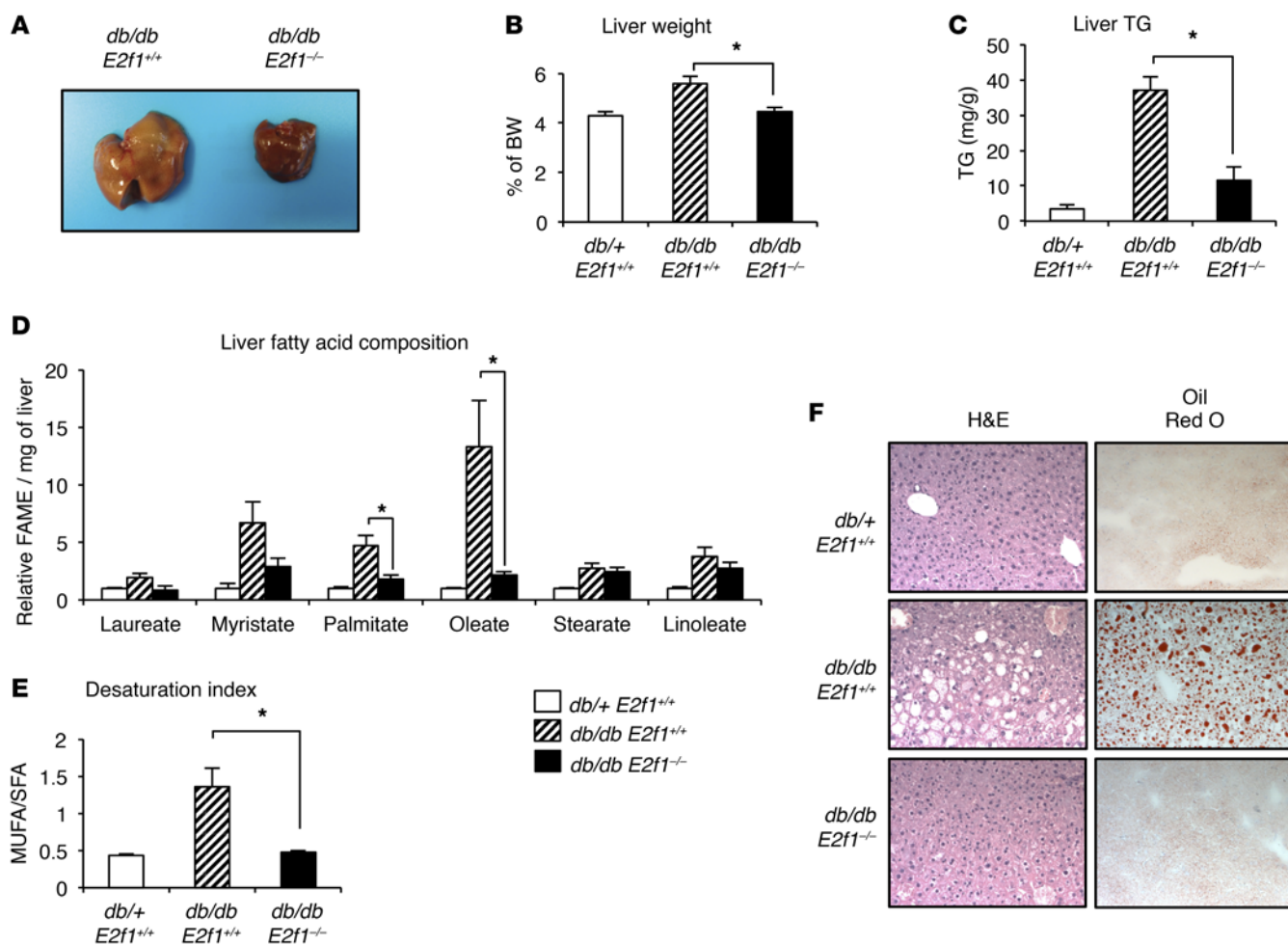
Figure 9. *E2f1* deletion in the *db/db* mouse model protects against hepatic steatosis. (**A**) Images of *db/db E2f1⁻/⁻* compared with *db/db E2F1⁺/⁺* mouse livers. (**B**) Liver weight expressed as a percentage of the total mass for the indicated genotypes (*n* = 5–9). (**C**) Quantification of liver TG in the indicated genotypes (*n* = 5–9). (**D**) Liver FAME analysis of *db/+ E2f1⁺/⁺*, *db/db E2f1⁺/⁺*, and *db/db E2f1⁻/⁻* mice (*n* = 4–7). (**E**) Desaturation index corresponded to the ratio of monounsaturated fatty acid:oleate C18:1/saturated fatty acid:palmitate C16 plus stearate C18 (MUFA/SFA) ratio. (**F**) Representative H&E and Oil red O staining of liver sections from *db/+ E2f1⁺/⁺*, *db/db E2f1⁺/⁺*, and *db/db E2f1⁻/⁻* mice (original magnification, ×200). *$P < 0.05$, by 2-tailed, unpaired *t* test.

β-actin (catalog A2066); tubulin (catalog T6199); and Flag-M2 (catalog F3165). The anti-GCK Ab was previously described (15). USF1 and USF2 Abs were a gift of B. Viollet (Institut Cochin, Paris, France) (39). Protein A agarose (Life Technologies) and anti-Flag M2 affinity gel (Sigma-Aldrich) were used for co-IP experiments. For subcellular fractionation, liquid N2 ground liver or cell pellets were washed in cold PBS and lysed using an NE-PER cell fractionation kit (Pierce, Thermo Scientific). Total protein extract and immunoblot analyses were performed as previously described (28).

DNA constructs and adenovirus. E2F1, RB, DP-1, E2FRE-TK-luc, and CMV–β-gal have been previously described (2). The mouse *Gck* and *Slc2a2* promoters were a gift of K. Schoonjans (Ecole Polytechnique Fédérale de Lausanne [EPFL], Lausanne, Switzerland) and Y.H. Ahn (Yonsei University College of Medicine, Seoul, South Korea), respectively (40, 41). USF1 and USF2 plasmids were a gift of B. Viollet (Institut Cochin, Paris, France) (39). The human *FASN* promoter, human *SCD1* promoter, human *SREBP1c* promoter, and human *CHREBP* promoter were obtained from SwitchGear Genomics. The mouse *Fasn* promoter was cloned in pGL3-basic by PCR from C57B6/J

DNA. The primer sequences were as follows: GAAGATCTTCCT-GTCTGGGCTCTGGAGGCAGACGACAAGC (forward) and CCGAGCGTCGGAGGAATTTAAAGGGAGGGAGGAGAGGGT (reverse). *E2F1* cDNA and *CDK4* cDNA were inserted into the pAd-C-MV-DEST-V5 adenoviral vector (Life Technologies). GFP adenovirus was a gift of J.R. Nevins (Duke University, Durham, North Carolina, USA), and sh-*Cdk4* and sh-control adenoviruses were obtained from Vector BioLabs.

Cell culture and transfection. HEK293T and HepG2 cells were obtained from the American Type Culture Collection (ATCC) and respectively transfected using Lipofectamine 2000 reagent (Life Technologies) and X-tremeGENE (Roche). Primary hepatocytes were isolated as previously described (28). For experiments showing *E2f1⁺/⁺* and *E2f1⁻/⁻* hepatocytes, cells were isolated from *E2f1⁺/⁺* and *E2f1⁻/⁻* mice. For other experiment using hepatocytes, cells were isolated from C57Bl6 mice. C57Bl6 hepatocytes were not used as controls for *E2f1⁻/⁻* hepatocytes. Primary hepatocytes were obtained from C57Bl6J *E2f1⁺/⁺* and *E2f1⁻/⁻* mice. Mouse hepatocytes were harvested, cultured, and infected with adenoviruses as previously described (28).

Hepatocyte glycolysis and lipogenesis. Glycolysis experiments were performed as previously described (40). Briefly, hepatocytes were seeded onto Seahorse XF24 plates (Seahorse Bioscience) and then glucose starved overnight. Cells were then washed and placed in an unbuffered DMEM–based medium containing 2 mM glutamine for 1.5 hours. After ECAR, an indirect measurement of glycolysis was done with the Seahorse analyzer, and glucose (25 mM) was injected into the cells directly with the Seahorse apparatus. For the lipogenesis experiment, hepatocytes were treated for 24 hours with low-glucose (G5) or high-glucose insulin (G25i). C14 acetate (0.5 μCi) was added for the last 2 hours. Incorporation of C14 into TG was measured by chromatography after lipid extraction and separation, following normalization for protein quantity.

ChIP and ChIP-seq experiments. Primary hepatocytes were infected with Ad-E2F1 after 36 hours, and cells were fixed for 10 minutes in 1% formaldehyde. Nuclear extracts were sonicated and precleared with protein A agarose/salmon sperm DNA. Chromatin was immunoprecipitated with anti–E2F1 c-20 Ab (catalog sc-193) or normal rabbit IgG (catalog sc-2027) (both from Santa Cruz Biotechnology Inc.). The full Western blot of E2F1 Ab is shown in Supplemental Figure 2, A and B. Immunoprecipitated chromatin was washed, reverse cross-linked, and purified with MinElute columns (QIAGEN). Quantification of E2F1 binding on a specific promoter was determined by qPCR (oligonucleotide sequences are listed in in Supplemental Table 1). Recoveries were calculated as a percentage of the input. For ChIP-seq, we performed two independent experimental replicates. Each replicate was the combination of two independent ChIP experiments. The Lausanne Genomic Technologies Facility (GTF) of UNIL generated the library and performed the sequencing (Illumina HiSeq 2500) of input and E2F1 ChIP (10 ng DNA). Sequencing alignment to the Ensembl Mouse Assembly NCBIM37 (mm9), peak detection, and peak assignment to genes were performed using the High-Throughput Sequencing portal HTSstation (17) developed at the Bioinformatics and Biostatistics Core Facility (BBCF) of the EPFL School of Life Sciences. The pipeline is available at http://htsstation.epfl.ch.

To assess the quality of the replicates and the reproducibility of the experiment, signals for both replicates were compared prior to combination (Supplemental Figure 2, C and D). Browser shots of input and E2F1 ChIP alignment are provided in Supplemental Figure 3. ChIP-seq peaks were determined using MACS software. A novel deconvolution algorithm was provided, which evaluates the shape of peaks within enriched regions found by MACS. This approach provides a more accurate estimation of binding-site locations and a lower number of false-positives (17). Using the DAVID website (http://david.abcc.ncifcrf.gov), we clustered E2F1 target genes with the general GOTERM_BP2 database. Data generated from ChIP-seq experiments are publicly available in the NCBI's Gene Expression Omnibus (GEO) database (GEO GSE74006).

Animal experiments and procedures. $E2f1^{+/+}$ and $E2f1^{-/-}$ (B6;129S4-E2f1tm1 Meg/J) mice were purchased from The Jackson Laboratory. C57BL/6J mice were obtained from Janvier Labs and were not used as controls for $E2f1^{-/-}$ mice. $E2f1^{-/-}$ mice and $db/+$ mice (Janvier Labs) were crossed to obtain $E2f1\ db$ mice. For the high-sucrose experiment, 30% sucrose (for 6 weeks), followed by 60% sucrose (for 3 weeks), was added to the drinking water, and the mice were euthanized after 4 hours of refeeding. $E2f1^{fl/fl}$ mice were generated by Tac-

onicArtemis ($E2f1^{tm3110Arte}$). The construct was designed to flank LoxP sites between $E2f1$ exons 2 and 3 and to insert a positive selection marker (puromycin resistance) flanked by FRT sites in intron 1 as described in Supplemental Figure 14. After transfection into the TaconicArtemis C57BL/6N Tac ES cell line, homologous recombinant clones were isolated using positive (PuroR) and negative (TK) selection and expanded. After microinjection into BALB/c blastocysts, blastocysts were transferred into the uterine horn of 2.5-day postcoitum, pseudopregnant NMRI female mice. Highly chimeric mice were bred with females of the C57BL/6 strain. The $E2f1$-floxed allele was obtained after FLP-mediated removal of the selection marker. $E2f1$ liver-specific–KO (E2F1 LKO) mice were obtained after crossing $E2f1$-floxed mice with *Alb-Cre* mice, thus driving recombination in liver. Unless otherwise indicated in the figure legends, mice were sacrificed during the dark phase (fed condition).

Analytical procedures. TG serum concentrations were measured with a Hitachi robot (Roche) according to the manufacturer's instructions. Liver glycogen levels and TG content were determined as previously described (28)

Lipid analysis. Snap-frozen pieces of mouse liver were homogenized over dry ice in 50% aqueous methanol (–20°C). Samples were snap-frozen and then thawed, and this was repeated 3 times. Samples were then centrifuged at 21,000 g for 10 minutes at 4°C. Clarified supernatants were then transferred to fresh tubes on ice and were subjected to an addition of 2 volumes of amylene-stabilized chloroform at –20°C, vortexed, and then centrifuged at 21,000 g for 10 minutes at 4°C. The chloroform phase was lyophilized and then used for fatty acid analysis. Fatty acid methyl esters (FAMEs) were generated by resuspending the lyophilized chloroform phase in 2% H_2SO_4/methanol and allowing transesterification to occur at 60°C for 4 hours. FAMEs were then isolated by adding 1 volume of hexane (ACS grade), vortexing, adding a one-tenth volume of saturated NaCl, vortexing, and finally centrifuging the samples at room temperature at 21,000 g for 1 minute. The hexane phase was isolated and then lyophilized. Lyophilized FAMEs were resuspended in 50 μl hexane and subjected to gas chromatography–mass spectrometric (GC-MS) analysis. The GC temperature was maintained at 100°C for 5 minutes after the injection of 1 μl; the temperature was increased to 200°C by raising the temperature 15°C per minute, then the temperature was increased to 250°C by raising the temperature 5°C per minute, and finally, the temperature was increased to 300°C by raising the temperature 15°C per minute. The MS source and quadrupole tandem were held at 230°C and 150°C. The detector ran in full-scan mode while recording ion abundances in the 100−650 m/z range.

Histology. Livers were fixed in 4% neutral buffered formalin and embedded in paraffin. Then, liver sections were cut and stained with H&E. For the detection of neutral lipids, liver cryosections were stained using the Oil Red O technique.

mRNA analysis. mRNAs from liver and primary hepatocytes were isolated using an RNeasy Kit (QIAGEN) and then reverse transcribed. qPCR analysis was performed using a 7900HT Fast Real-Time PCR System (Applied Biosystems) and SYBR Green detection of the amplified products. The relative quantification for a given gene was corrected to the cyclophilin B and RS9 mRNA values (oligonucleotide sequences are provided in Supplemental Table 1).

Humans samples. All obese patients included in this study were from the Atlas Biologique de l'Obésité Sévère (ABOS) study. This

The Journal of Clinical Investigation

study also includes a group of lean and normoglycemic control patients who had surgery for benign and noninflammatory pathologies. Clinical data were collected at the Centre Hospitalier Régional Universitaire de Lille. The obese patients were morbidly obese (BMI >40) and glucose intolerant. The metabolic parameters for the two groups are presented in Supplemental Table 1. Liver samples were collected during surgery within the first 15 minutes of the procedure, weighed, and snap-frozen in liquid nitrogen. Total RNA and protein were extracted from liver samples (10 mg) using the All-in-One Purification Kit (Norgen Biotek Corp.). First-strand cDNA synthesis was performed using 500 ng total RNA as a template and Superscript II reverse transcriptase (Life Technologies) primed with 50 pmol random hexamers (New England BioLabs). qPCR was performed using the Bio-Rad MyiQ Single-Color Real-Time PCR Detection System and Bio-Rad iQ SYBR Green Supermix (Bio-Rad). Gene expression was normalized to two housekeeping genes (*ACTB,* encoding eta-actin, or *RPS9,* encoding ribosomal protein S9). Relative mRNA fold changes between groups were calculated using the ΔCt method.

Statistics. Results are expressed as the mean ± SEM. Statistical significance was assessed with a 2-tailed, unpaired *t* test using Prism 6 software (GraphPad Software). Differences were considered statistically significant at $P < 0.05$. All experiments were performed on at least three independent occasions unless otherwise stated.

Study approval. All animal care and treatment procedures were performed in accordance with Swiss guidelines and were approved by the Canton of Vaud, Service de la Consommation et des Affaires Vétérinaires (SCAV) (authorization VD 2627.b). The protocol concerning the use of biopsies from human subjects was performed in agreement with French regulations and approved by the institutional ethics committees of the University of Lille and the Centre Hospitalier Régional Universitaire de Lille (Clinicaltrials.gov NCT01129297). All patients provided written informed consent to participate in this study.

Author contributions

PDD and LF conceptualized the study and designed the experiments. PDD, ICLM, AGC, QL, EB, BD, and JSA performed the experiments. BNN and NJD performed lipidomics analysis. CB and FP performed the human study.

Acknowledgments

Address correspondence to: Lluis Fajas, Department of Physiologie, Université de Lausanne. CH-1005 Lausanne, Switzerland. Phone: 41.21.692.55.10; E-mail: lluis.fajas@unil.ch.

Jean-Sébastien Annicotte's present address is: European Genomic Institute for Diabetes, Université Lille Nord de France, UMR 8199 CNRS, Lille, France.

1. Dimova DK, Dyson NJ. The E2F transcriptional network: old acquaintances with new faces. *Oncogene.* 2005;24(17):2810–2826.
2. Annicotte JS, et al. The CDK4-pRB-E2F1 pathway controls insulin secretion. *Nat Cell Biol.* 2009;11(8):1017–1023.
3. Fajas L, Landsberg RL, Huss-Garcia Y, Sardet C, Lees JA, Auwerx J. E2Fs regulate adipocyte differentiation. *Dev Cell.* 2002;3(1):39–49.
4. Blanchet E, et al. E2F transcription factor-1 regulates oxidative metabolism. *Nat Cell Biol.* 2011;13(9):1146–1152.
5. Hsieh MC, Das D, Sambandam N, Zhang MQ, Nahle Z. Regulation of the PDK4 isozyme by the Rb-E2F1 complex. *J Biol Chem.* 2008;283(41):27410–27417.
6. Fernandez de Mattos S, Lam EW, Tauler A. An E2F-binding site mediates the activation of the proliferative isoform of 6-phosphofructo-2-kinase/fructose-2,6-bisphosphatase by phosphatidylinositol 3-kinase. *Biochem J.* 2002;368(pt 1):283–291.
7. Dali-Youcef N, et al. Adipose tissue-specific inactivation of the retinoblastoma protein protects against diabesity because of increased energy expenditure. *Proc Natl Acad Sci U S A.* 2007;104(25):10703–10708.
8. Nicolay BN, et al. Loss of RBF1 changes glutamine catabolism. *Genes Dev.* 2013;27(2):182–196.
9. Lopez-Mejia IC, Fajas L. Cell cycle regulation of mitochondrial function. *Curr Opin Cell Biol.* 2015;33:19–25.
10. Conner EA, Lemmer ER, Omori M, Wirth PJ, Factor VM, Thorgeirsson SS. Dual functions of E2F-1 in a transgenic mouse model of liver carcinogenesis. *Oncogene.* 2000;19(44):5054–5062.
11. Zhang Y, et al. E2F1 is a novel fibrogenic gene that regulates cholestatic liver fibrosis through the Egr-1/SHP/EID1 network. *Hepatology.* 2014;60(3):919–930.
12. Postic C, Girard J. Contribution of de novo fatty acid synthesis to hepatic steatosis and insulin resistance: lessons from genetically engineered mice. *J Clin Invest.* 2008;118(3):829–838.
13. Brown MS, Goldstein JL. The SREBP pathway: regulation of cholesterol metabolism by proteolysis of a membrane-bound transcription factor. *Cell.* 1997;89(3):331–340.
14. Foretz M, Guichard C, Ferré P, Foufelle F. Sterol regulatory element binding protein 1c is a major mediator of insulin action on the hepatic expression of glucokinase and lipogenesis-related genes. *Proc Natl Acad Sci U S A.* 1999;96(22):12737–12742.
15. Denechaud PD, et al. ChREBP, but not LXRs, is required for the induction of glucose-regulated genes in mouse liver. *J Clin Invest.* 2008;118(3):956–964.
16. Chan SM, et al. Activation of PPARα ameliorates hepatic insulin resistance and steatosis in high fructose-fed mice despite increased endoplasmic reticulum stress. *Diabetes.* 2013;62(6):2095–2105.
17. David FP, et al. HTSstation: a web application and open-access libraries for high-throughput sequencing data analysis. *PLoS One.* 2014;9(1):e85879.
18. Cao AR, Rabinovich R, Xu M, Xu X, Jin VX, Farnham PJ. Genome-wide analysis of transcription factor E2F1 mutant proteins reveals that N- and C-terminal protein interaction domains do not participate in targeting E2F1 to the human genome. *J Biol Chem.* 2011;286(14):11985–11996.
19. Wong RH, Chang I, Hudak CS, Hyun S, Kwan HY, Sul HS. A role of DNA-PK for the metabolic gene regulation in response to insulin. *Cell.* 2009;136(6):1056–1072.
20. Yeh MM, Brunt EM. Pathological features of fatty liver disease. *Gastroenterology.* 2014;147(4):754–764.
21. Donnelly KL, Smith CI, Schwarzenberg SJ, Jessurun J, Boldt MD, Parks EJ. Sources of fatty acids stored in liver and secreted via lipoproteins in patients with nonalcoholic fatty liver disease. *J Clin Invest.* 2005;115(5):1343–1351.
22. Dentin R, et al. Liver-specific inhibition of ChREBP improves hepatic steatosis and insulin resistance in ob/ob mice. *Diabetes.* 2006;55(8):2159–2170.
23. Neschen S, et al. Prevention of hepatic steatosis and hepatic insulin resistance in mitochondrial acyl-CoA:glycerol-sn-3-phosphate acyltransferase 1 knockout mice. *Cell Metab.* 2005;2(1):55–65.

24. Moon YA, et al. The Scap/SREBP pathway is essential for developing diabetic fatty liver and carbohydrate-induced hypertriglyceridemia in animals. *Cell Metab*. 2012;15(2):240–246.

25. Guo S, et al. The Irs1 branch of the insulin signaling cascade plays a dominant role in hepatic nutrient homeostasis. *Mol Cell Biol*. 2009;29(18):5070–5083.

26. Nakamura A, et al. Protection from non-alcoholic steatohepatitis and liver tumourigenesis in high fat-fed insulin receptor substrate-1-knockout mice despite insulin resistance. *Diabetologia*. 2012;55(12):3382–3391.

27. Chattopadhyay M, Selinger ES, Ballou LM, Lin RZ. Ablation of PI3K p110-alpha prevents high-fat diet-induced liver steatosis. *Diabetes*. 2011;60(5):1483–1492.

28. Benhamed F, et al. The lipogenic transcription factor ChREBP dissociates hepatic steatosis from insulin resistance in mice and humans. *J Clin Invest*. 2012;122(6):2176–2194.

29. Horie Y, et al. Hepatocyte-specific Pten deficiency results in steatohepatitis and hepatocellular carcinomas. *J Clin Invest*. 2004;113(12):1774–1783.

30. Brown MS, Goldstein JL. Selective versus total insulin resistance: a pathogenic paradox. *Cell Metab*. 2008;7(2):95–96.

31. Biddinger SB, et al. Hepatic insulin resistance is sufficient to produce dyslipidemia and susceptibility to atherosclerosis. *Cell Metab*. 2008;7(2):125–134.

32. Semple RK, et al. Postreceptor insulin resistance contributes to human dyslipidemia and hepatic steatosis. *J Clin Invest*. 2009;119(2):315–322.

33. Wellen KE, Hotamisligil GS. Inflammation, stress, and diabetes. *J Clin Invest*. 2005;115(5):1111–1119.

34. Hotamisligil GS. Inflammation and metabolic disorders. *Nature*. 2006;444(7121):860–867.

35. Ozcan U, et al. Chemical chaperones reduce ER stress and restore glucose homeostasis in a mouse model of type 2 diabetes. *Science*. 2006;313(5790):1137–1140.

36. Kammoun HL, et al. GRP78 expression inhibits insulin and ER stress-induced SREBP-1c activation and reduces hepatic steatosis in mice. *J Clin Invest*. 2009;119(5):1201–1215.

37. Bhatia B, Hsieh M, Kenney AM, Nahle Z. Mitogenic Sonic hedgehog signaling drives E2F1-dependent lipogenesis in progenitor cells and medulloblastoma. *Oncogene*. 2011;30(4):410–422.

38. Scaglia N, Tyekucheva S, Zadra G, Photopoulos C, Loda M. De novo fatty acid synthesis at the mitotic exit is required to complete cellular division. *Cell Cycle*. 2014;13(5):859–868.

39. Viollet B, Lefrancois-Martinez AM, Henrion A, Kahn A, Raymondjean M, Martinez A. Immunochemical characterization and transacting properties of upstream stimulatory factor isoforms. *J Biol Chem*. 1996;271(3):1405–1415.

40. Oosterveer MH, et al. LRH-1-dependent glucose sensing determines intermediary metabolism in liver. *J Clin Invest*. 2012;122(8):2817–2826.

41. Im SS, et al. Glucose-stimulated upregulation of GLUT2 gene is mediated by sterol response element-binding protein-1c in the hepatocytes. *Diabetes*. 2005;54(6):1684–1691.

2. Article 2 : CDK4 is an essential insulin effector in adipocytes

CDK4 is an essential insulin effector in adipocytes

Sylviane Lagarrigue,[1,2] Isabel C. Lopez-Mejia,[1] Pierre-Damien Denechaud,[1] Xavier Escoté,[1] Judit Castillo-Armengol,[1]
Veronica Jimenez,[3] Carine Chavey,[2] Albert Giralt,[1] Qiuwen Lai,[1] Lianjun Zhang,[4] Laia Martinez-Carreres,[1]
Brigitte Delacuisine,[1] Jean-Sébastien Annicotte,[2,5] Emilie Blanchet,[2] Sébastien Huré,[1,2] Anna Abella,[6]
Francisco J. Tinahones,[7,8] Joan Vendrell,[9] Pierre Dubus,[10] Fatima Bosch,[3] C. Ronald Kahn,[11] and Lluis Fajas[1,2]

[1]Department of Physiology, Université de Lausanne, Lausanne, Switzerland. [2]Institut de Génétique Moléculaire de Montpellier (IGMM), Université de Montpellier, Montpellier, France.
[3]Center of Animal Biotechnology and Gene Therapy and Department of Biochemistry and Molecular Biology, School of Veterinary Medicine, Universitat Autònoma de Barcelona, Bellaterra,
and Centro de Investigación Biomédica en Red de Diabetes y Enfermedades Metabólicas Asociadas, Barcelona, Spain. [4]Translational Tumor Immunology, Ludwig Center for Cancer Research,
Université de Lausanne, Epalinges, Switzerland. [5]European Genomic Institute for Diabetes, Université Lille Nord de France, UMR 8199 CNRS, Lille, France. [6]INSERM U834, Montpellier, France.
[7]Unidad de Gestión Clínica de Endocrinología y Nutrición, Hospital Universitario Virgen de la Victoria, Málaga, Spain. [8]Centro de Investigación Biomédica en Red-Fisiopatología de la Obesidad y la Nutrición
(CIBERobn CB06/003), Instituto de Salud Carlos III, Madrid, Spain. [9]CIBERDEM, Institut d'Investigació Pere Virgili, Universitat Rovira i Virgili, Hospital Universitari Joan XXIII, Tarragona, Spain.
[10]EA2406, Histologie et pathologie moléculaire des tumeurs, Université de Bordeaux, Bordeaux, France. [11]Section on Integrative Physiology and Metabolism, Joslin Diabetes Center,
Harvard Medical School, Boston, Massachusetts, USA.

Insulin resistance is a fundamental pathogenic factor that characterizes various metabolic disorders, including obesity and type 2 diabetes. Adipose tissue contributes to the development of obesity-related insulin resistance through increased release of fatty acids, altered adipokine secretion, and/or macrophage infiltration and cytokine release. Here, we aimed to analyze the participation of the cyclin-dependent kinase 4 (CDK4) in adipose tissue biology. We determined that white adipose tissue (WAT) from CDK4-deficient mice exhibits impaired lipogenesis and increased lipolysis. Conversely, lipolysis was decreased and lipogenesis was increased in mice expressing a mutant hyperactive form of CDK4 (CDK4^{R24C}). A global kinome analysis of CDK4-deficient mice following insulin stimulation revealed that insulin signaling is impaired in these animals. We determined that insulin activates the CCND3-CDK4 complex, which in turn phosphorylates insulin receptor substrate 2 (IRS2) at serine 388, thereby creating a positive feedback loop that maintains adipocyte insulin signaling. Furthermore, we found that CCND3 expression and IRS2 serine 388 phosphorylation are increased in human obese subjects. Together, our results demonstrate that CDK4 is a major regulator of insulin signaling in WAT.

Introduction

Insulin signaling is a versatile system that coordinates growth, proliferation, and development of multiple tissues and organs by controlling metabolic processes that accommodate the energy needs of cellular function (1). Defects in insulin signaling contribute to insulin resistance, a common complication of obesity that occurs early in the pathogenesis of type 2 diabetes and cardiovascular disease (2, 3). Insulin response depends on tissue and cellular functions. In white adipose tissue (WAT), insulin signaling regulates lipid synthesis (1) and glucose transport (4–6) and represses lipolysis (7). However, the exact mechanism by which insulin signaling coordinates regulated cellular functions is not fully understood. Cyclin-dependent kinase 4 (CDK4) plays an important role in the G$_1$/S transition of the cell cycle. Its kinase activity is regulated through interaction with the D-type cyclins (CCND1, CCND2, and CCND3) (8). The resulting cyclin D–CDK4 complexes catalyze the phosphorylation of the members of the retinoblastoma (RB) protein family (RB1, RBL1, and RBL2). Phosphorylation of RB1 by cyclin D–CDK4 releases the E2F

transcription factors, thereby ensuring the expression of genes required for cell-cycle progression (9). Conversely, members of the family of CDK inhibitors (INK and CIP/KIP) block CDK activity in response to quiescence stimuli. Many studies have assessed the roles of CDK4 in cell growth, proliferation, and cancer (10), but the role of CDK4 in adipose tissue function has never been explored. The most marked phenotypes of mice lacking CDK4 (*Cdk4$^{neo/neo}$*) are reduced body size and insulin-deficient diabetes due to a severe decrease in pancreatic β cell growth (11). β Cell–specific reexpression of the *Cdk4^{R24C}* allele renders CDK4 resistant to the inhibitory effects of INK4 proteins (12) and restores β cell proliferation and normoglycemic conditions (13). Interestingly, CDK4 reexpression in pancreatic β cells does not rescue body size reduction, suggesting that this phenotype is not due to endocrine defects secondary to decreased insulin levels. We previously demonstrated that CDK4 regulates adipogenesis, suggesting a role of CDK4 in WAT function (14).

Results

CDK4 activity is positively correlated with WAT mass. The first suggestion of a role of CDK4 in adipose tissue biology came from the finding that CDK4 and 2 D-type cyclins (CCND2 and CCND3) are highly expressed in epididymal WAT (eWAT) compared with the other tissues analyzed (Figure 1A). The high levels of expres-
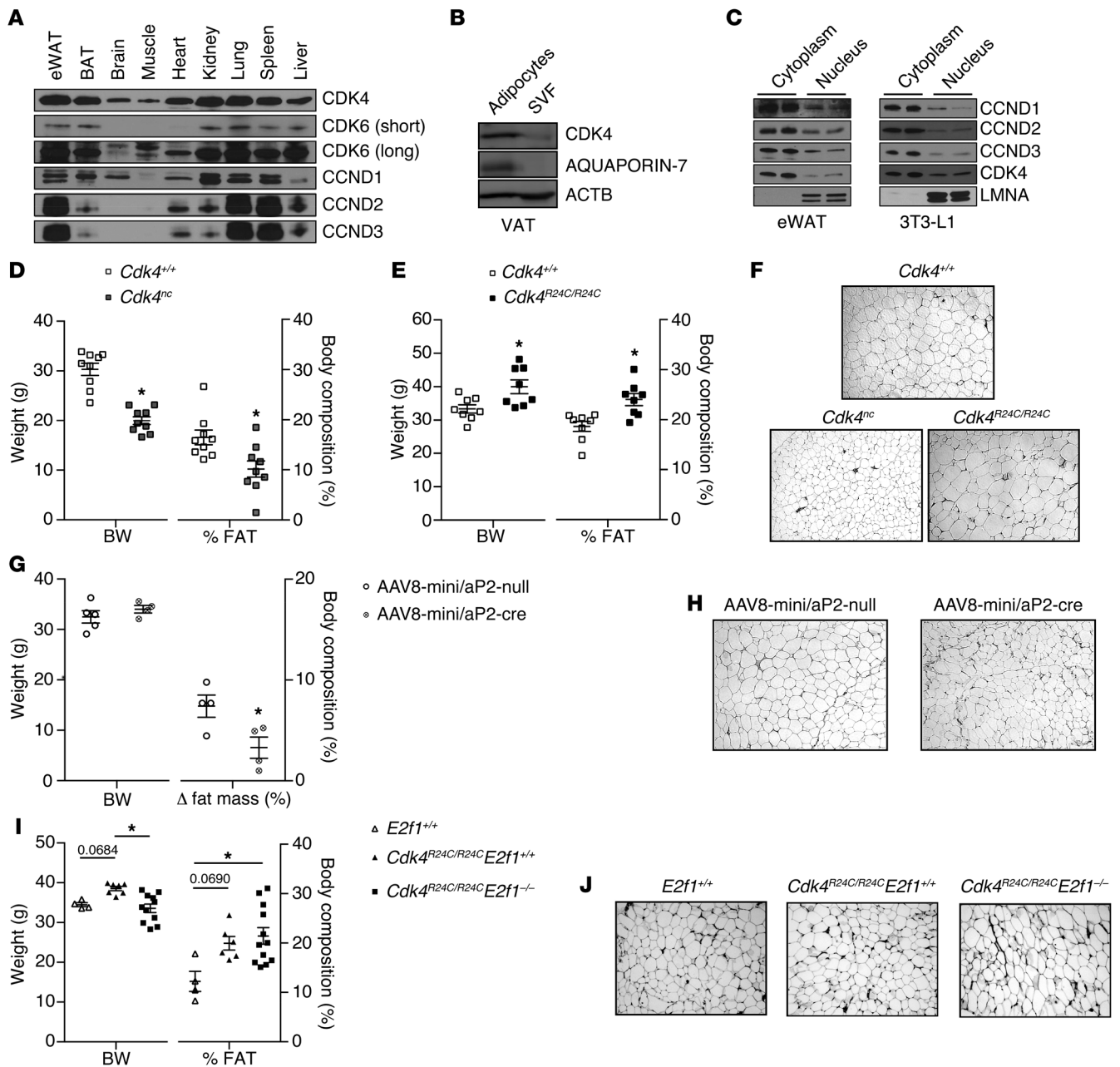
Figure 1. Positive correlation between CDK4 activity and WAT mass. (**A**) Expression levels of CCND1, CCND2, CCND3, CDK4, and CDK6 proteins in mouse eWAT, BAT, brain, muscle, heart, kidney, lung, spleen, and liver. Representative blot of several animals analyzed is shown. (**B**) CDK4 protein level in the SVF and mature adipocytes isolated from VAT. (**C**) Subcellular localization of CCND1, CCND2, CCND3, and CDK4 proteins in cytoplasm and nuclear fractions of eWAT and mature 3T3-L1 adipocytes. LMNA was used as a control for the nuclear fraction. (**B** and **C**) Representative blots out of 3 independent experiments are shown. (**D** and **E**) Body weight and percentage of fat mass of 20-week-old $Cdk4^{+/+}$ and $Cdk4^{nc}$ mice ($n = 9$) (**D**) and 30-week-old $Cdk4^{+/+}$ and $Cdk4^{R24C/R24C}$ mice ($n = 8$) (**E**) as obtained using EchoMRI technology. (**F**) H&E staining of eWAT sections from $Cdk4^{+/+}$, $Cdk4^{nc}$, and $Cdk4^{R24C/R24C}$ mice. (**G**) Body weight, Δ fat mass of 20-week-old $Cdk4^{flox/flox}$ mice infected with AAV8-mini/aP2-null ($n = 5$) or AAV8-mini/aP2-cre ($n = 4$) analyzed by EchoMRI technology (we show the difference between the percentage of fat before and the percentage of fat 3 weeks after infection). (**H**) H&E staining of eWAT sections from $Cdk4^{flox/flox}$ mice infected with AAV8-mini/aP2-null or AAV8-mini/aP2-cre. (**I**) Body weight and percentage of fat mass of 30-week-old $E2f1^{+/+}$ ($n = 4$), $Cdk4^{R24C/R24C} E2f1^{+/+}$ ($n = 6$), and $Cdk4^{R24C/R24C} E2f1^{-/-}$ mice ($n = 12$). (**J**) H&E staining of eWAT sections from $E2f1^{+/+}$, $Cdk4^{R24C/R24C} E2f1^{+/+}$, and $Cdk4^{R24C/R24C} E2f1^{-/-}$ mice. Statistically significant differences were determined with unpaired 2-tailed Student's t tests (**D**, **E**, and **G**) or 1-way ANOVA followed by Tukey's multiple comparisons test (**I**). *$P < 0.05$. Original magnification, ×100.

sion of CCND3 in eWAT (Figure 1A and Supplemental Figure 1, A and B; supplemental material available online with this article; doi:10.1172/JCI81480DS1) are consistent with previous findings showing increased CCND3 expression during adipogenesis (15).

Protein expression analysis in visceral adipose tissue (VAT) cellular fractions showed that CDK4 was better expressed in mature adipocytes compared with the stromal vascular fraction (SVF) (Figure 1B and Supplemental Figure 1C). Furthermore, CDK4 expression
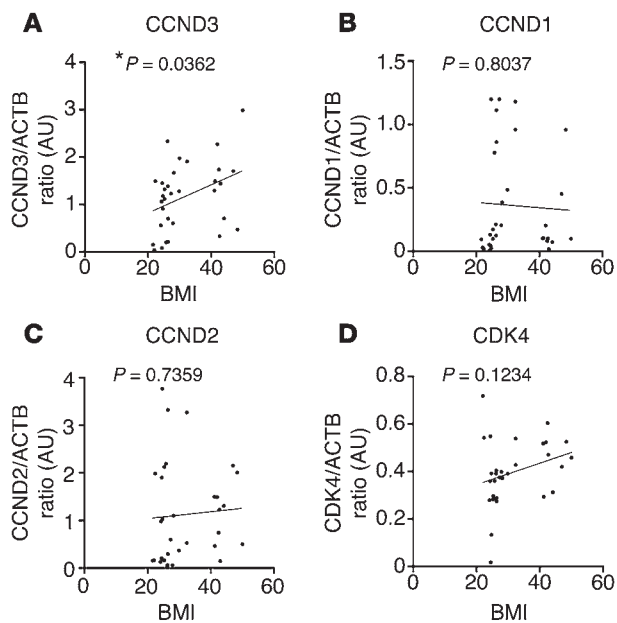
Figure 2. Positive correlation between CCND3 expression and human VAT mass. (**A**–**D**) Correlation between the CCND3/ACTB ratio ($n = 32$, Pearson's $r = 0.3717$, $P < 0.05$) (**A**), the CCND1/ACTB ratio ($n = 32$, Pearson's $r = -0.04574$, $P < 0.05$) (**B**), the CCND2/ACTB ratio ($n = 32$, Pearson's $r = 0.06203$, $P < 0.05$) (**C**), and the CDK4/ACTB ratio ($n = 30$, Pearson's $r = 0.2875$, $P < 0.05$) (**D**) and BMI in VAT of human subjects. Data are normalized to ACTB. *$P < 0.05$.

was also higher in differentiated 3T3-L1 adipocytes compared with nondifferentiated 3T3-L1 preadipocytes (Supplemental Figure 1C). Interestingly, the subcellular localization of CDK4 and CCND3 as well as of the other D-type cyclins revealed that these proteins are not only found in the nucleus; rather, they are mainly localized in the cytoplasm of adipocytes (Figure 1C and Supplemental Figure 1D), suggesting a role for CDK4 that is independent of the RB/E2F pathway in these cells. Moreover, since the duplication rate in mature adipocytes is low (16), these results suggested a novel cell-cycle independent role for CDK4. In order to analyze the participation of CDK4 in adipose tissue biology, we set to determine the phenotype of CDK4 mutant mice. The previously generated *Cdk4^neo/neo* mice are diabetic and have impaired pancreatic β cell development and decreased insulin levels (11). Analysis of adipose tissue function in these mice would be confusing, since any observed effect could be secondary to insulin deficiency. We therefore used *Cdk4^neo/neo Rip-Cre* (*Cdk4^neo/neo;cre/cre*; herein referred to as *Cdk4^nc*) mice that reexpress *Cdk4* in β cells and thus have normal insulin levels (13). We also used a mouse model of CDK4 hyperactivation, the R24C model. *Cdk4^R24C/R24C* mice express a mutant CDK4 protein that is not sensitive to INK4a inhibitors (11) and is consequently more active. A first analysis showed that *Cdk4^nc* mice had decreased body weight, whereas *Cdk4^R24C/R24C* mice exhibited increased body weight compared with *Cdk4^+/+* mice (Figure 1, D and E). Significant changes in WAT mass accounted for body weight variation. *Cdk4^nc* and *Cdk4^R24C/R24C* mice had decreased and increased WAT mass, respectively, as measured by EchoMRI (Figure 1, D and E, and Supplemental Figure 1, E and F). Changes in fat mass were consistent with variation in adipocyte size (Figure 1F and Supplemental Figure 1G). Overall, severe atrophy could be observed in fat pads from *Cdk4^nc* mice, whereas *Cdk4^R24C/R24C* mice developed adipose tissue hypertrophy (Supplemental Figure 1H).

To demonstrate that the effects of Cdk4 deletion in adipose tissue were cell autonomous, we used an approach involving systemic administration of adeno-associated viral vectors of serotype 8 (AAV8), which has been previously reported as leading to genetic

engineering of white and brown adipocytes in adult mice and has very poor tropism for macrophages (17). We infected *Cdk4^flox/flox* mice (Supplemental Figure 1I) with AAV8 vectors expressing the Cre recombinase under the control of the mini/aP2 adipose tissue–specific promoter (AAV8-mini/aP2-cre) or with the control vector (AAV8-mini/aP2-null). First of all, we determined the tissues that were infected by assessing the presence of viral genome (vg) using Cre PCR. The vg was only present in brown adipose tissue (BAT), eWAT, s.c. WAT, and liver, whereas we could not detect it in pancreas and muscle (Supplemental Figure 1J). Quantitative reverse-transcription–PCR (RT-qPCR) analysis showed a significant decrease of *Cdk4* mRNA in eWAT and s.c. WAT, whereas no changes were observed in liver and BAT (Supplemental Figure 1K). After 3 weeks, the systemic administration of AAV8-mini/aP2-cre triggered a decrease in fat mass gain; indeed, AAV8-mini/aP2-cre–infected mice gained significantly less fat mass (Figure 1G) and experienced a reduction in adipocyte size (Figure 1H). However, no differences were found in body weight and lean mass in *Cdk4^flox/flox* mice infected with AAV8-mini/aP2-cre vector (Figure 1G and Supplemental Figure 1L). The use of this adipose tissue–specific *Cdk4* depletion model supports a cell-autonomous contribution for CDK4 in adipose tissue. Overall, these 3 models (*Cdk4^nc*, *Cdk4^R24C/R24C*, and *Cdk4^flox/flox* mice infected with AAV8 mini/aP2-cre) clearly demonstrate a positive correlation between CDK4 activity and WAT mass/size.

E2F1, a known proproliferative downstream effector of CDK4, was previously shown to promote adipogenesis (16). Therefore, in order to determine whether adipocyte proliferation was not affected with the modulation of CDK4 activity, we generated *Cdk4^R24C/R24C E2f1^-/-* mice. No significant changes were observed in adiposity, adipocyte size, lean mass, or adipocyte proliferation as measured by Ki67 expression in *Cdk4^R24C/R24C E2f1^-/-* compared with *Cdk4^R24C/R24C E2f1^+/+* mice (Figure 1, I and J, and Supplemental Figure 1, M and N). These results demonstrate that when CDK4 is hyperactive, the deletion of E2f1 does not affect fat mass, mature adipocyte size, and proliferation. Because *Cdk4^R24C/R24C* mice develop a wide spectrum of tumors (18, 19), we investigated to determine whether the WAT phenotype observed in these mice could be secondary to tumor development. We could not find any correlation between fat mass and tumor development. Indeed, all mice used in this study were tumor free (Supplemental Figure 1O). Moreover, tumor development was negatively correlated with fat mass in 60-week-old *Cdk4^R24C/R24C* mice, proving that the increased WAT mass in these mice was not secondary to tumor formation (Supplemental Figure 1P).

CCND3 is positively correlated with WAT mass in human subjects. Our data suggesting the involvement of CCND3-CDK4 in adipose tissue was further supported by the positive correlation between CCND3 protein expression in visceral WAT samples from human subjects and their BMI (Figure 2A and Supplemental Figure 1, Q
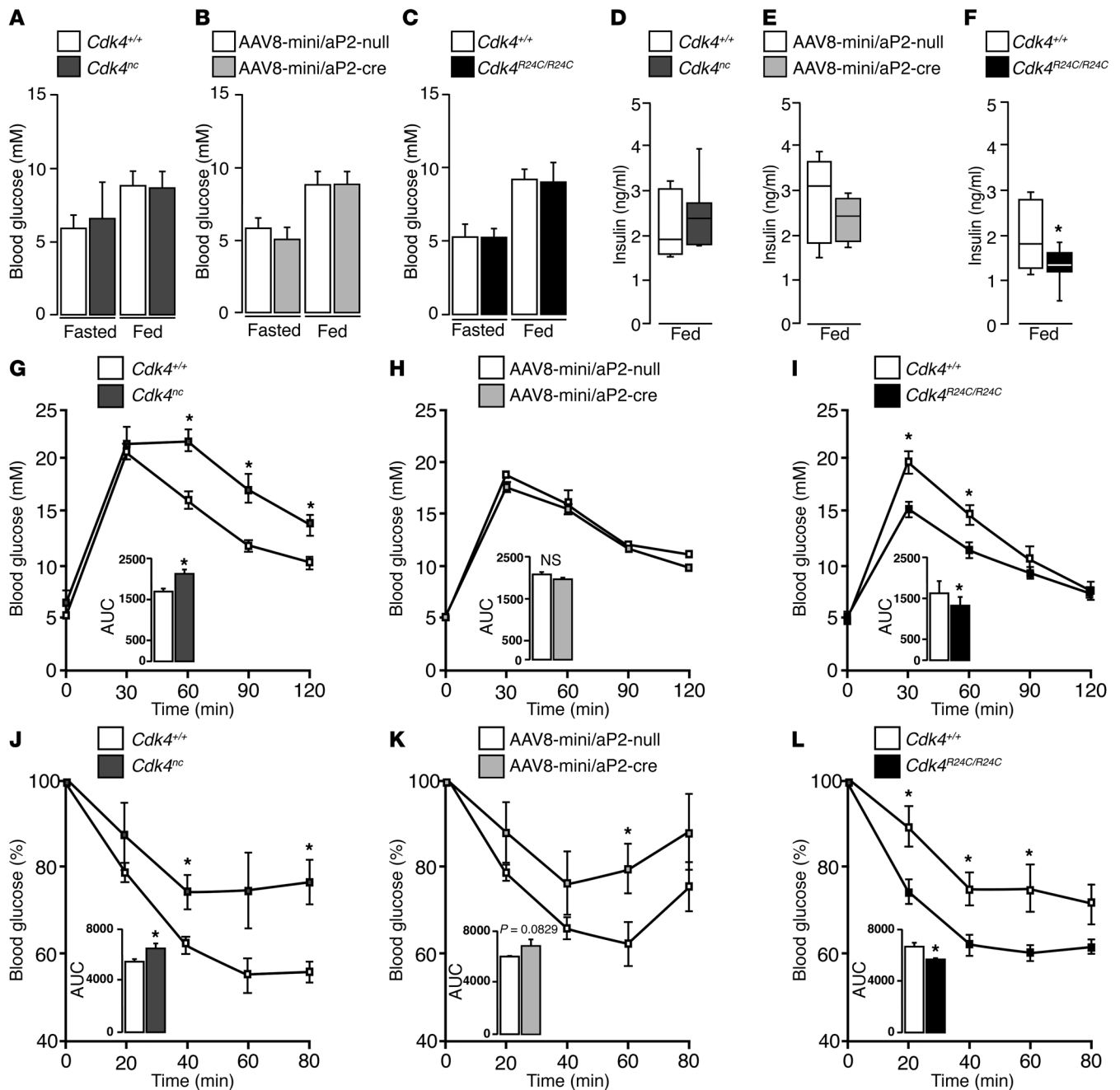
Figure 3. CDK4 promotes insulin sensitivity in vivo. (**A–C**) Fasting glycemia in *Cdk4+/+* and *Cdk4nc* (*n* = 8) mice (**A**), *Cdk4flox/flox* infected with AAV8-mini/aP2-null or AAV8-mini/aP2-cre vectors (*n* = 5–4) (**B**), and *Cdk4+/+* and *Cdk4R24C/R24C* (*n* = 12) mice (**C**). (**D–F**) Fed serum insulin in *Cdk4+/+* and *Cdk4nc* (*n* = 7) (**D**), *Cdk4flox/flox* infected with AAV8-mini/aP2-null or AAV8-mini/aP2-cre vectors (*n* = 5–4) (**E**), and *Cdk4+/+* and *Cdk4R24C/R24C* mice (*n* = 8) (**F**). (**G–I**) GTT in *Cdk4+/+* and *Cdk4nc* (*n* = 7) (**G**), *Cdk4flox/flox* infected with AAV8-mini/aP2-null or AAV8-mini/aP2-cre (*n* = 5–4) (**H**), and *Cdk4+/+* and *Cdk4R24C/R24C* (*n* = 6) mice (**I**). (**J–L**) ITT in *Cdk4+/+* and *Cdk4nc* (*n* = 5) (**J**), *Cdk4flox/flox* infected with AAV8-mini/aP2-null or AAV8-mini/aP2-cre vectors (*n* = 5–4) (**K**), and *Cdk4+/+* and *Cdk4R24C/R24C* (*n* = 12) mice (**L**). AUC for GTT and ITT was analyzed and is shown below the curves. Data were expressed as mean ± SEM. Statistically significant differences were determined with unpaired 2-tailed Student's *t* tests. *$P < 0.05$.

and R). No association was found for CCND1, CCND2, or CDK4 (Figure 2, B–D). These results confirmed a positive correlation between WAT mass and CCND3-CDK4 expression and activity and suggested that these proteins participate in WAT function.

CDK4 promotes insulin sensitivity in vivo. No differences in fasting and feeding glycemia were observed in *Cdk4nc* or *Cdk4flox/flox* infected with AAV8-mini/aP2-cre vector and *Cdk4R24C/R24C* mice

compared with their respective control mice (Figure 3, A–C). Insulin quantification in plasma showed, however, a significant decrease in *Cdk4R24C/R24C* mice, whereas no differences were observed in *Cdk4nc* or *Cdk4flox/flox* mice infected with AAV8-mini/aP2-cre vector in fed conditions (Figure 3, D–F). Decreased insulin levels are indicative of either better insulin sensitivity or of a defect in insulin secretion by pancreatic β cells. *Cdk4nc* mice were glucose intolerant (Figure 3G)
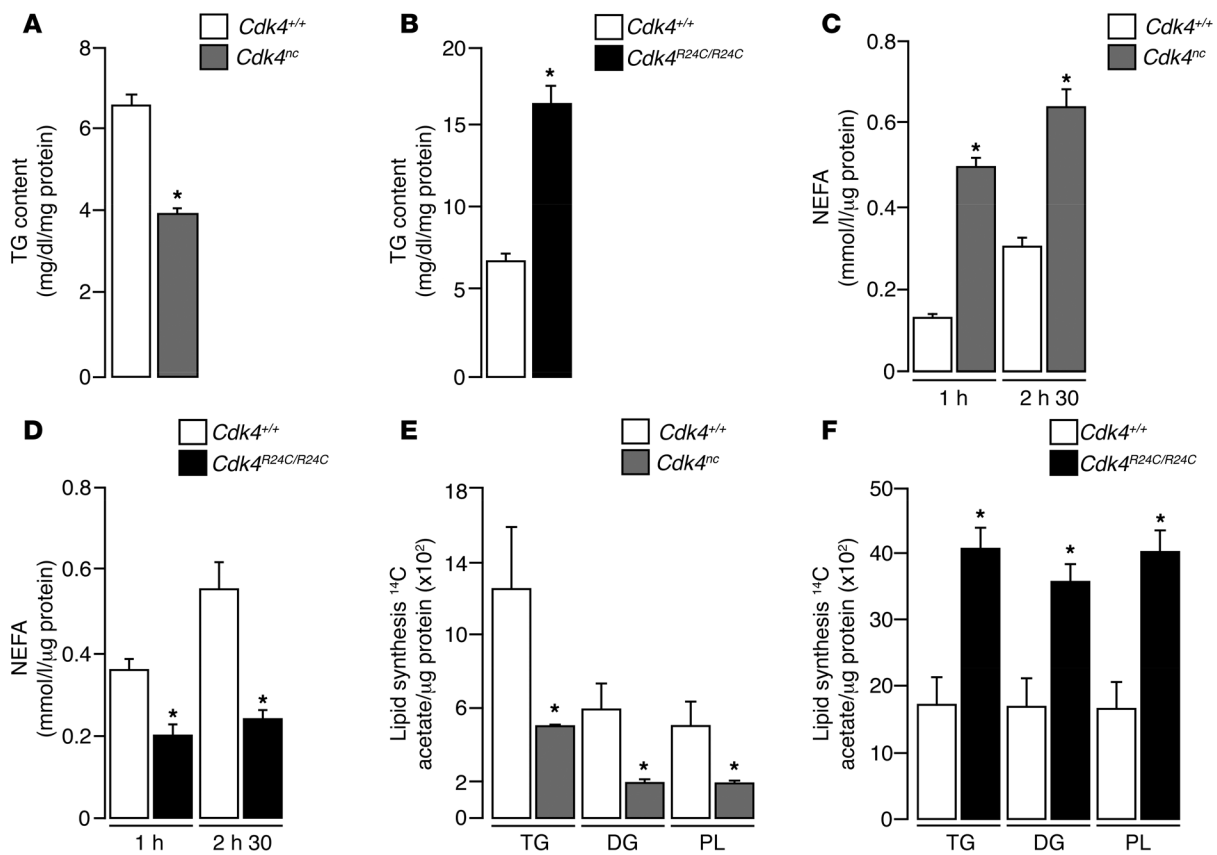
Figure 4. CDK4 represses lipolysis and is a positive modulator of lipogenesis. (**A**) Quantification of TG content of eWAT from $Cdk4^{+/+}$ and $Cdk4^{nc}$ mice (n = 3). (**B**) Quantification of TG content of eWAT of $Cdk4^{+/+}$ and $Cdk4^{R24C/R24C}$ mice (n = 3). (**C**) Rate of NEFA release in eWAT explants from fasting $Cdk4^{+/+}$ and $Cdk4^{nc}$ mice (n = 3). (**D**) Rate of NEFA release in eWAT explants from fasting $Cdk4^{+/+}$ and $Cdk4^{R24C/R24C}$ mice (n = 6). (**E**) Ex vivo lipogenesis experiments in eWAT explants using labeled ^{14}C-acetate incorporation to detect TG, DG, and PL synthesis in $Cdk4^{+/+}$ and $Cdk4^{nc}$ mice (n = 3). (**F**) Ex vivo lipogenesis experiments in eWAT explants from $Cdk4^{+/+}$ and $Cdk4^{R24C/R24C}$ mice. ^{14}C-acetate incorporation was used to detect TG, DG, and PL synthesis by TLC (n = 3). Data are expressed as mean ± SEM. Statistically significant differences were determined with unpaired 2-tailed Student's t tests. $*P < 0.05$.

and cleared glucose at a slower rate than $Cdk4^{+/+}$ mice, a characteristic of insulin resistance (Figure 3J). We did not observe any significant differences in glucose tolerance tests (GTTs) in $Cdk4^{flox/flox}$ mice infected with AAV8-mini/aP2-cre vector; however, these mice had a trend toward insulin resistance compared with $Cdk4^{flox/flox}$ mice infected with AAV8-mini/aP2-null vector (P = 0.0829) (Figure 3, H and K). In contrast, $Cdk4^{R24C/R24C}$ mice were more glucose tolerant and insulin sensitive than $Cdk4^{+/+}$ mice (Figure 3, I and L). Together, these results show that CDK4 activity is positively correlated with insulin sensitivity.

CDK4 represses lipolysis and stimulates lipogenesis. We previously showed the participation of CDK4 and CCND3 in adipogenesis. We proved that these proteins control the activity of the master regulator of adipocyte differentiation, PPARγ (14). In this study, we analyze the participation of CDK4 in the function of mature adipocytes. Lipids are mobilized from WAT through lipolysis, a breakdown of triglycerides (TG) into glycerol and free fatty acids (FFA) (20). As expected, changes in WAT mass were positively correlated with alterations in TG content in our mouse models: $Cdk4^{nc}$ and $Cdk4^{R24C/R24C}$ mice had less and more TG in eWAT, respectively (Figure 4, A and B). Decreased TG content in $Cdk4^{nc}$ eWAT was likely the result of an imbalanced lipogenesis/lipolysis ratio. Indeed, treatment of fully differentiated 3T3-L1

adipocytes with a chemical CDK4 inhibitor (PD0332991) (21) resulted in the delipidation of these adipocytes and in a 40% decrease in their TG content (Supplemental Figure 2, A and B). Lipolysis experiments in eWAT explants from mice revealed a 4-fold increase of nonesterified fatty acid (NEFA) release in $Cdk4^{nc}$ eWAT compared with $Cdk4^{+/+}$ eWAT (Figure 4C). Similarly, glycerol release was also increased in these mice (Supplemental Figure 2C). Conversely, $Cdk4^{R24C/R24C}$ eWAT showed significantly decreased NEFA (Figure 4D) and glycerol release (Supplemental Figure 2D), which suggested impaired lipolysis. Interestingly, eWAT explants from $Cdk4^{nc}$ mice, in addition to increased lipolysis, had reduced lipogenesis, as measured by acetate incorporation into the distinct TG, diacyclycerols (DG), and phospholipid (PL) lipid fractions (Figure 4E). On the other hand, eWAT explants from mice expressing the hyperactive $Cdk4^{R24C}$ allele showed increased lipogenesis (Figure 4F). However, we could not detect any differences in liver TG content in $Cdk4^{+/+}$, $Cdk4^{nc}$, and $Cdk4^{R24C/R24C}$ mice (Supplemental Figure 2, E and F). This validated a positive correlation between CDK4 activity and lipogenesis and a negative correlation between CDK4 activity and lipolysis. Strikingly, these are exactly the effects of insulin in adipocytes, suggesting that CDK4 could mediate the effects of insulin in adipose tissue.
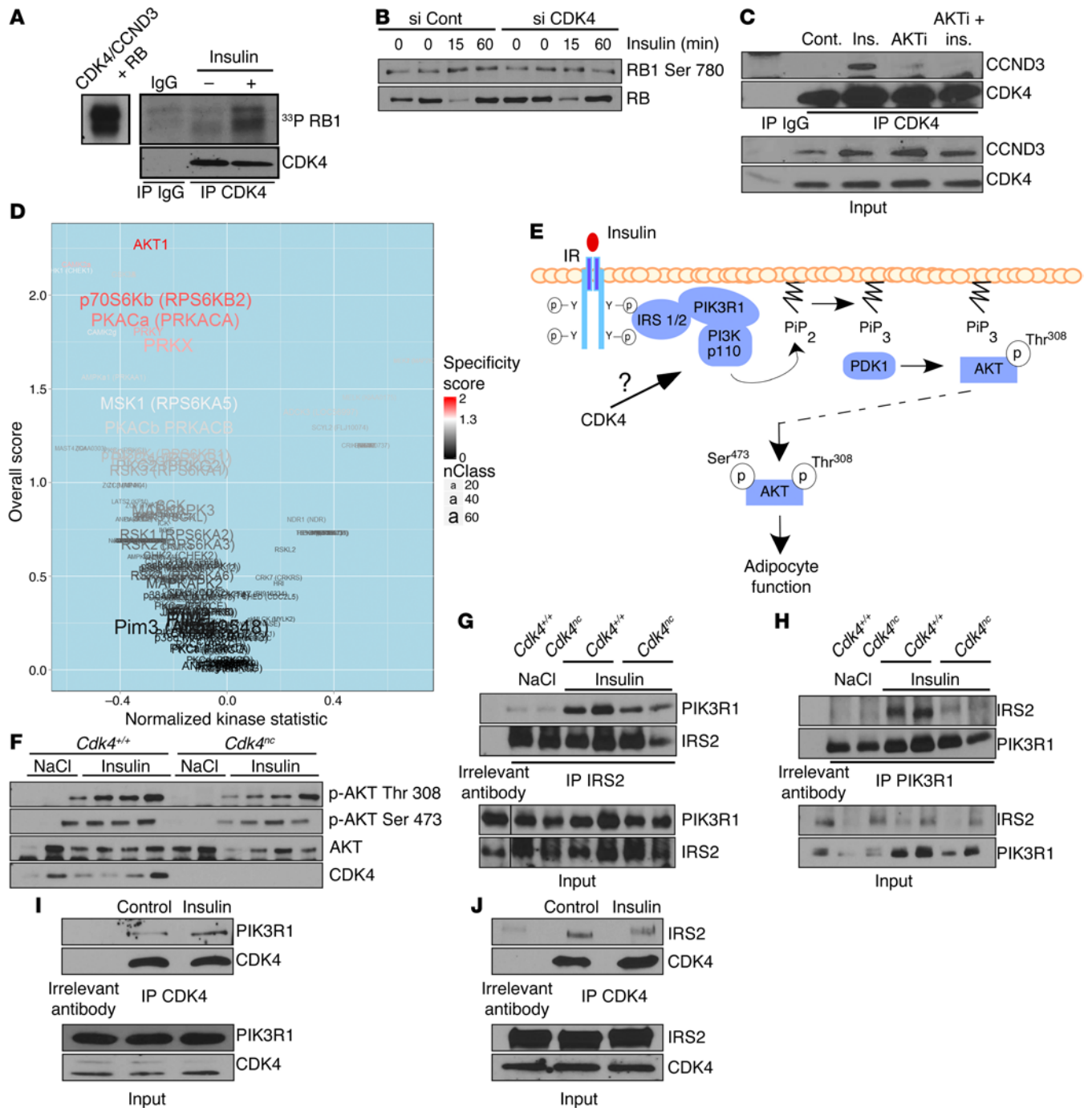
Figure 5. CDK4 is activated by insulin and translates insulin signaling in adipocytes. (**A**) CDK4 activity in vivo. SDS-PAGE autoradiography showing RB1 phosphorylation by CDK4 immunoprecipitated from 3T3-L1 mature adipocytes after insulin stimulation. The left panel shows RB1 phosphorylation by recombinant CDK4 used as a positive control. (**B**) Western blot analysis showing the inhibition of insulin-induced RB1 phosphorylation on Ser780 by CDK4 knockdown in mature 3T3-L1 adipocytes. (**C**) CCND3 and CDK4 association is increased upon insulin stimulation, but decreased upon cotreatment with insulin and AKT inhibitor in mature 3T3-L1 adipocytes. (**D**) Volcano plot showing differences in putative kinase activities between control and *Cdk4^{nc}* mice injected (portal vein) with insulin for 3 minutes (*n* = 4). Kinases with a positive kinase statistic show higher activity in *Cdk4^{nc}* samples compared with control samples, whereas kinases with negative kinase statistic show lower activity in *Cdk4^{nc}* samples compared with control samples. (**E**) Based on the upstream kinase activity (**D**) results and on the GeneGO analysis of the PamGene experiment, the putative role of CDK4 upstream of AKT in the insulin signaling pathway is represented. (**F**) Immunoblot showing AKT phosphorylation on Thr308 and Ser473 in response to insulin injection (3 minutes) in fasted control and *Cdk4^{nc}* mice (*n* = 2 for NaCl and *n* = 4 for insulin treatment). (**G** and **H**) Coimmunoprecipitation experiments showing the interaction between endogenous IRS2 and PIK3R1. IRS2 (**G**) and PIK3R1 (**H**) were immunoprecipitated and the presence of PIK3R1 (**G**) and IRS2 (**H**) was detected by Western blot analysis in *Cdk4$^{+/+}$* and *Cdk4^{nc}* mice treated with insulin for 3 minutes (*n* = 2 for NaCl and *n* = 3 for insulin treatment). (**I** and **J**) Coimmunoprecipitation experiments showing the interaction between endogenous PIK3R1 or IRS2 and CDK4. CDK4 was immunoprecipitated and the presence of PIK3R1 (*n* = 3) (**I**) and IRS2 (*n* = 1) (**J**) was detected by Western blot analysis in 3T3-L1 mature adipocytes treated with insulin. A representative Western blot is shown. Unless specified otherwise, all experiments are representative of 3 independent experiments.

Table 1. CDK consensus sites in mouse IRS1, IRS2, PDKP1, and PIK3R1

Protein	Site position	Sequence	CDK4 Interaction
PIK3R1	Thr86	TPKP	+
PDPK1	Thr357	TPPP	–
	Thr521	TPNP	
IRS1	Ser1209	SPRR	+
IRS2	Ser388	SPGP	+
	Thr576	TPAR	
	Ser980	SPKP	
	Ser1004	SPYP	
	Ser1226	SPMR	

CDK4 is activated by insulin and mediates insulin signaling in adipocytes. We wanted next to uncover the mechanisms of CDK4 activation following insulin stimulation in adipocytes. CDK4 activity was stimulated by insulin in differentiated 3T3-L1 cells, as suggested by increased phosphorylation of PIK3R1 by immunoprecipitated CDK4 (Figure 5A). Similar results were observed when eWAT from insulin-treated mice was used (Supplemental Figure 3A). Interestingly, CDK4 knockdown (Figure 5B) or treatment of 3T3-L1 adipocytes with PD0332991 (Supplemental Figure 3B) abrogated the effects of insulin on PIK3R1 phosphorylation. Furthermore, association of CDK4 with its regulatory subunit CCND3 was dependent on the insulin signaling pathway, since AKT inhibition abolished this association (Figure 5C).

Next, we addressed how CDK4 could participate in the insulin-signaling pathway in adipocytes. Since the insulin signaling cascade is dependent on the rapid activation of a series of tyrosine and serine/threonine protein kinases (STKs), we used a new technology developed by PamGene to determine differential global kinase activity in *Cdk4^nc* and control mice in response to insulin. We used arrays that consisted of 140 immobilized serine/threonine-containing peptides that are targets of most known kinases (STK PamChips) (22). These chips were incubated with lysates prepared from eWAT from *Cdk4^nc* or control mice injected with insulin. The same experiment was performed using lysates from cells treated with PD0332991 and stimulated with insulin. Peptides whose phosphorylation varied significantly between the control and *Cdk4^nc*-treated mice or between the control and PD0332991-treated samples (Supplemental Figure 3, C and D) were indicative of differential specific kinase activities. Putative upstream kinase analysis underscored significant differences in the AKT pathway (Figure 5D and Supplemental Figure 3, E and F). This suggested that CDK4 activity played a role upstream of AKT, as indicated in Figure 5E. Western blot analyses further proved that AKT activity, as measured by phosphorylation in Ser473 and Thr308, was decreased in *Cdk4^nc* mice in response to insulin (Figure 5F). Similarly, chemical inhibition of CDK4 also attenuated AKT signaling in 3T3-L1 adipocytes (Supplemental Figure 3G). This further supports the hypothesis that CDK4 regulates insulin signaling upstream of AKT. Upon insulin stimulation, the intrinsic tyrosine kinase domain of the insulin receptor leads to receptor

autophosphorylation at tyrosine residues. The subsequent recruitment and phosphorylation of insulin receptor substrate 1 (IRS1) and IRS2 are the pivotal events that, in turn, activate the downstream PI3K-PDK1-AKT axis to regulate lipogenesis and lipolysis in adipocytes (23). We therefore investigated whether CDK4 regulated the insulin-signaling pathway by facilitating the recruitment of IRS into PIK3R1, the PI3K subunit p85a. We found that *Cdk4* deletion greatly impaired the ability of IRS2 to bind with PIK3R1 in response to insulin stimulation (Figure 5, G and H). Furthermore, CDK4 was recruited to PIK3R1 (Figure 5I) and IRS2 (Figure 5J) complexes in adipocytes. However, we only detected an increase of interaction in response to insulin between PIK3R1 and CDK4.

IRS2 is a substrate of CDK4. Interestingly, in silico analysis highlighted the presence of CDK4 consensus phosphorylation sites in the p85A subunit of PI3K (PIK3R1), phosphoinositide-dependent kinase 1 (PDK1), IRS1, and IRS2 (Table 1). However, in vitro kinase assays showed no phosphorylation of PIK3R1, or PDPK1 by CDK4 (data not shown). In vitro kinase assays showed, however, that CDK4 could phosphorylate recombinant glutathione S–transferase–purified (GST-purified) IRS2 protein (Figure 6A). IRS2 contains 5 CDK4 consensus sites distributed along the protein (Ser388, Thr576, Ser980, Ser1004, and Ser1226) (Table 1 and Supplemental Figure 4A). Site-directed mutagenesis (serine to alanine) and protein truncation approaches helped us to map the CDK4 phosphorylation sites of IRS2 at Ser388 and Ser1226 (Figure 6, B and C). Interestingly, these 2 potential phosphorylation sites are highly conserved through evolution (Supplemental Figure 4B).

We next evaluated the functional relevance of IRS2^S388A and IRS2^S1226A mutants that cannot be phosphorylated by CDK4. Rescue of IRS2 activity in *Irs2^-/-* preadipocytes with ectopic expression of WT IRS2 resulted in the restoration of insulin signaling as assessed by immunofluorescence staining of AKT phosphorylation (Figure 6, D and E). In contrast, IRS2^S388A mutants, which cannot be phosphorylated by CDK4, could not restore insulin signaling in these cells (Figure 6, D and E). No significant phenotype was observed for IRS2^S1226A mutants (data not shown). Moreover, IRS2^S388A mutants were not recruited to PIK3R1 protein complexes upon insulin stimulation when ectopically expressed in 293T cells (Figure 6, F and G). This demonstrated that the phosphorylation of IRS2 on Ser388 by CDK4 is essential for its activity.

CDK4 regulates insulin signaling in vivo via IRS2^Ser388 phosphorylation. To determine the potential roles of CDK4 on IRS2 phosphorylation, we generated a phosphospecific antibody to Ser388 of IRS2 that we validated by in vitro CDK4 kinase assay (Supplemental Figure 5A). IRS2 Ser388 was highly phosphorylated in the adipose tissue of *Cdk4^+/+* mice after 50 minutes of insulin stimulation (Figure 7, A and B). This phosphorylation was almost abrogated in the adipose tissue of insulin-treated *Cdk4^nc* mice. Moreover, decreased IRS2 Ser388 phosphorylation resulted in impaired insulin signaling pathways, as demonstrated by reduced AKT phosphorylation (Figure 7, A and B). In sharp contrast, CDK4 hyperactivity, as observed in *Cdk4^R24C/R24C* mice, resulted in a robust increase in IRS2 Ser388 phosphorylation (Figure 7, C and D). Consequently, AKT phosphorylation was also increased (Figure 7, C and D). Chemical inhibition of CDK4 also resulted in the abrogation of both IRS2 Ser388 and AKT phosphorylations (Figure 7, E and F). From these results, we can conclude that this
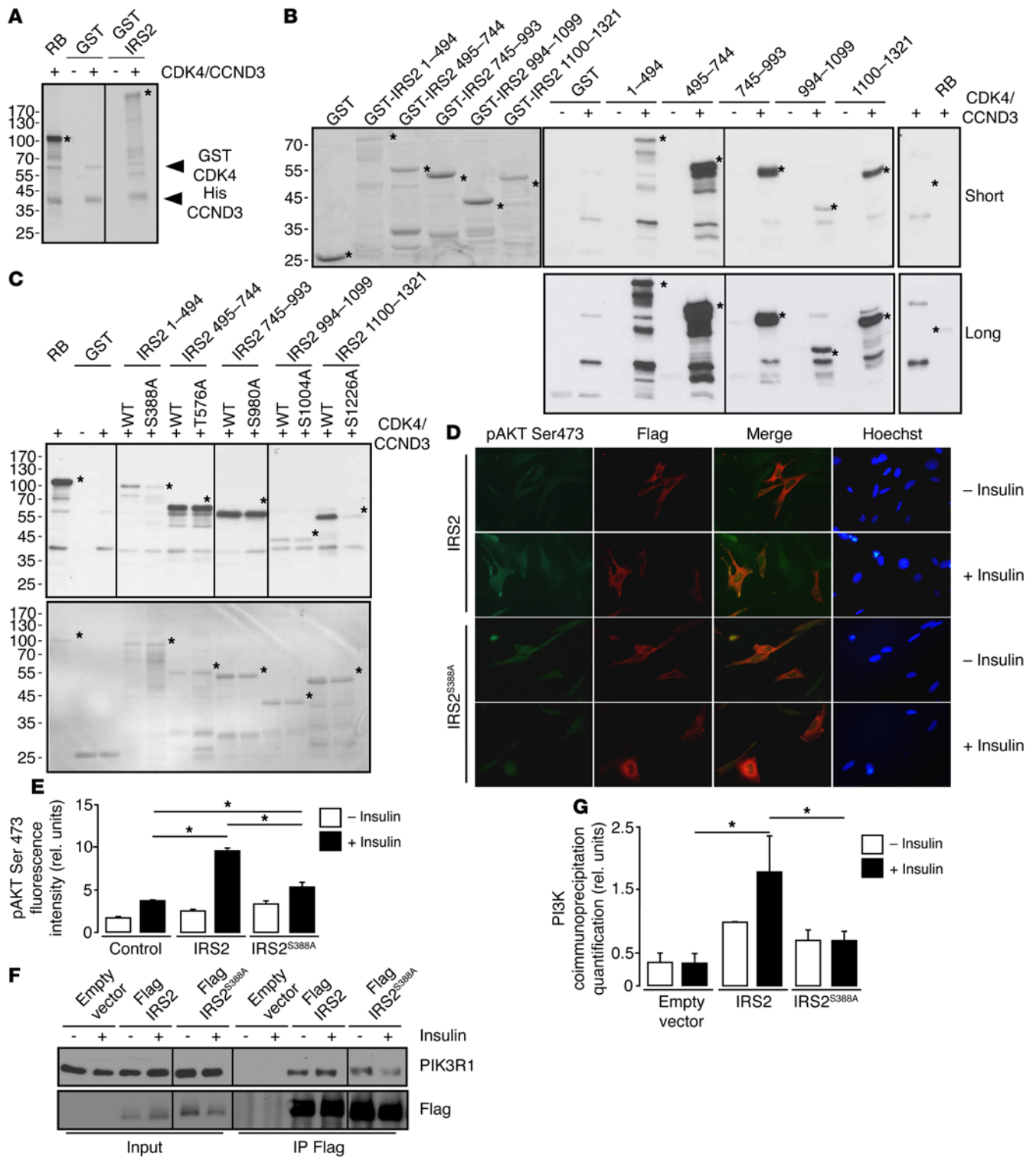
Figure 6. CDK4 phosphorylates IRS2. (**A**) CCND3-CDK4 complex directly phosphorylates full-length GST-IRS2 in vitro ($n = 3$). (**B**) In vitro phosphorylation of GST-IRS2 fragments (1–494aa, 495–744aa, 745–993aa, 994–1099aa, 1100–1321aa) by CCND3/CDK4. Left panel, SDS-PAGE stained with Coomassie blue for the loading control. Middle panels, autoradiography of the SDS-PAGE gels containing the different GST-IRS2 fragments, incubated with CCND3/CDK4. Right panel, RB1 recombinant protein was used as a positive control ($n = 3$). (**C**) Defective IRS2^S388A and IRS2^S1226A phosphorylation by CCND3-CDK4. Upper panel, autoradiography; lower panel, SDS-PAGE gel stained with Coomassie blue for the loading control. ($n = 2$). (**D**) Decrease in pAKT Ser473 phosphorylation in Flag-IRS2^S388A electroporated *Irs2^-/-* cells upon insulin stimulation, compared with the WT Flag-IRS2–transfected cells ($n = 3$). Original magnification, ×400. (**E**) Quantification of pAKT Ser473 fluorescence intensity for untransfected, Flag-IRS2–transfected, and Flag-IRS IRS2^S388A electroporated *Irs2^-/-* preadipocytes was performed with ImageJ software (http://imagej.nih.gov/ij/). At least 100 cells were quantified per condition. (**F**) Representative Western blot analysis showing impaired interaction between PIK3R1 and Flag-IRS2^S388A mutant after insulin stimulation compared with cells transfected with Flag-IRS2 in 293T cells. (**G**) Quantification of the blot shown in **F**. A representative Western blot is shown. Data are expressed as mean ± SEM. Statistically significant differences were determined with 2-way ANOVA followed by Tukey's multiple comparisons test (**E**–**G**). *$P < 0.05$.
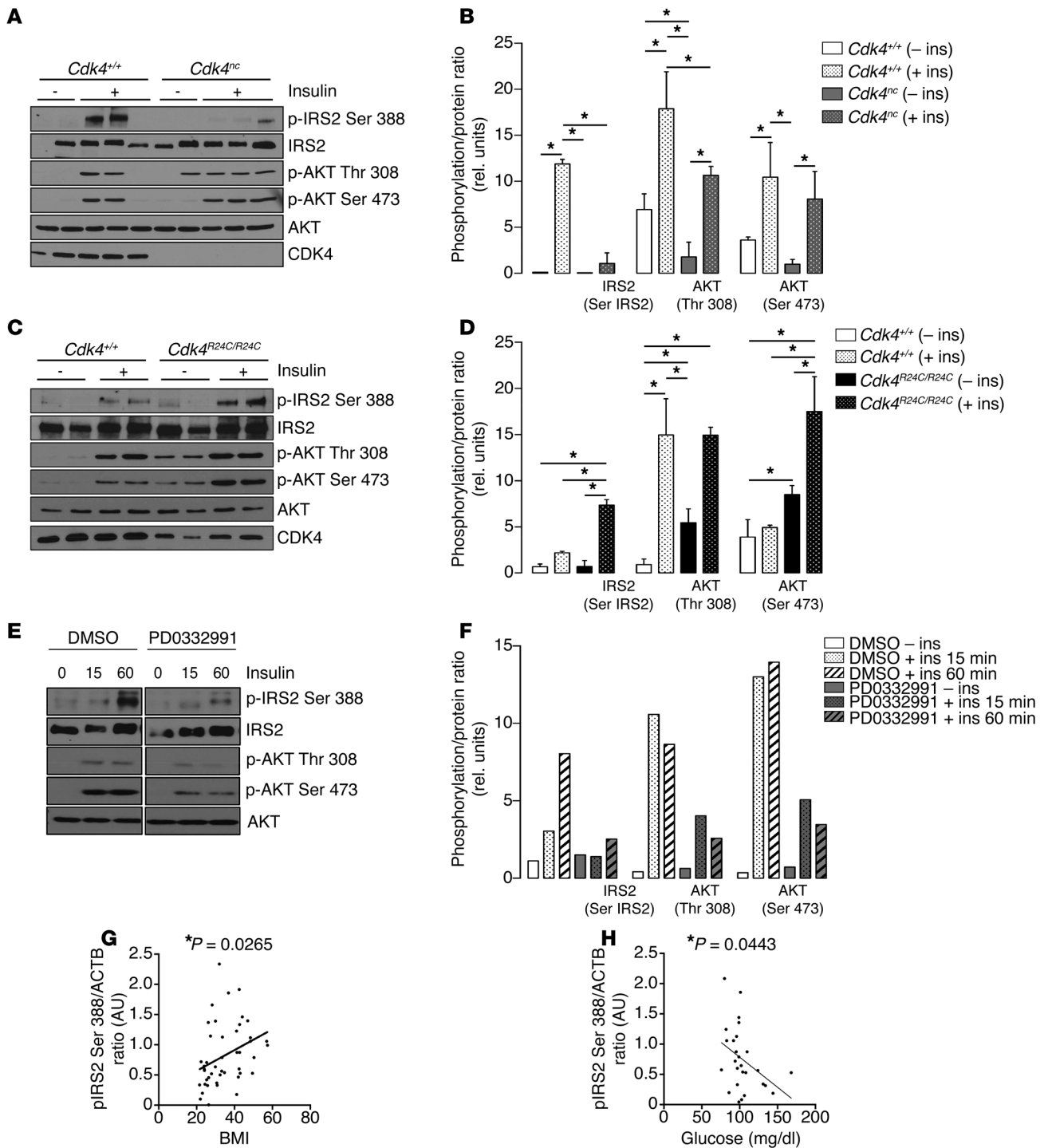
Figure 7. CDK4 phosphorylates in vivo the IRS2 protein at the Ser388. (**A**–**D**) Immunoblot analysis of IRS2 phosphorylation on Ser388 and AKT phosphorylation on Thr308 and Ser473 in control and $Cdk4^{nc}$ ($n = 2$ starved/5 insulin for $Cdk4^{+/+}$ and $n = 2$ starved/5 insulin for $Cdk4^{nc}$) mice (**A**). (**B**) Quantification of the blot shown in **A** using ImageJ software. $Cdk4^{R24C/R24C}$ ($n = 2$ starved/3 insulin for both $Cdk4^{+/+}$ and $Cdk^{R24C/R24C}$). (**C**) Mice were treated for 50 minutes with insulin. (**D**) Quantification of the blot shown in **C** using ImageJ software. (**E**) Immunoblot analysis of IRS2 phosphorylation on Ser388 and AKT phosphorylation on Thr308 and Ser473 in 3T3-L1 mature adipocytes during a time course insulin stimulation with or without PD0332991 ($n = 1$). (**F**) Quantification of the blot shown in **E** using ImageJ software. (**G**) Correlation between the pIRS2 Ser388/ACTB ratio in VAT and the BMI of the subjects ($n = 45$, Pearson's $r = 0.3307$, $P < 0.05$). (**H**) Correlation between the pIRS2 Ser388/ACTB ratio in VAT and the glycemia of the subjects ($n = 27$, Pearson's $r = -0.3900$, $P < 0.05$). Data are expressed as mean ± SEM. Statistically significant differences were determined with 2-way ANOVA followed by Tukey's multiple comparisons test (**B**–**D**). *$P < 0.05$.

newly identified site in IRS2, which is phosphorylated by CDK4, maintains the activation of the insulin signaling pathway. To further investigate the status of IRS2 Ser388 in type 2 diabetic mouse models, such as *db/db* mice, that are known to be hyperinsulinemic, we analyzed this phosphorylation in the basal state and upon insulin stimulation in adipose tissue. The *db/db* mice have a tendency toward an increased IRS2 Ser388 phosphorylation under basal conditions, compared with *db/+* mice ($P = 0.0511$) (Supplemental Figure 5B). However, insulin-resistant *db/db* mice did not show increased IRS2 Ser388 phosphorylation upon insulin stimulation (Supplemental Figure 5B). Most important was the finding that IRS2 Ser388 phosphorylation in human visceral WAT samples was positively correlated with the BMI of the subjects (Figure 7G and Supplemental Figure 5, C and D). Interestingly, we found a negative correlation between IRS2 Ser388 phosphorylation and fasting glucose in human subjects. This further advocates for a role of CDK4 in both adipose tissue biology and glucose homeostasis (Figure 7H and Supplemental Figure 5E).

Discussion

We showed throughout this study that the cell-cycle regulatory kinase CDK4 is a key regulator of adipocyte function. The participation of this kinase in the control of proliferation through the control of the activity of E2F transcription factors has been extensively studied (24). The results of our study provide 3 lines of evidence that CDK4 acts independently of E2F to regulate adipocyte function. First, we discovered a role of the cell-cycle kinase CDK4 in the control of the insulin-signaling pathway. CDK4, through phosphorylation of IRS2, maintains insulin action in adipocytes. This is consistent with the phenotypes of genetic CDK4 mouse models. Indeed, adipose tissue from *Cdk4^nc^* mice has decreased lipogenesis as well as increased lipolysis. In contrast, mice that express hyperactive CDK4^R24C^ exhibit decreased lipolysis and increased lipogenesis in WAT. These findings place CDK4 at the initiation of the insulin-triggered adipocyte-signaling pathway.

We show in this study a function of CDK4, that of a mediator of insulin signaling. Indeed, we show that the effects of CDK4 in adipocytes are independent of E2F activity and, therefore, most likely independent of the control of the cell cycle. E2F1 is the most studied member of the E2F family. E2F1 has numerous metabolic functions, such as the participation in adipose tissue metabolism through the transcriptional regulation of the master adipogenic factor PPARγ during early stages of adipogenesis (16). Here, we demonstrate, by generation of *Cdk4^R24C/R24^ E2f1^+/+^* and *Cdk4^R24C/R24C^ E2f1^-/-^* mice, that CDK4 has E2F1-independent functions in mature adipose tissue. Indeed, the genetic deletion of E2F1 in the R24C background does not affect adiposity or adipocyte proliferation (Figure 1, I and J, and Supplemental Figure 1N).

Based on our results, we propose that CDK4 is integrated in the insulin-signaling pathway as follows. In response to insulin, the canonical cascade of events is elicited. This includes the sequential activation of IR, IRS1-2, PI3K, PDPK1, and AKT. AKT then activates CDK4 (because inhibition of AKT blocks CDK4 activation), which then phosphorylates IRS2, creating a positive feedback loop. The activation of CDK4 by AKT is likely an indirect event. Several studies previously reported that AKT phosphorylates and inhibits p21 and p27, which are both CDK4 inhibitors (25, 26).

Interestingly, IRS proteins are also involved in the activation of several growth factor receptor pathways other than the insulin receptor pathway, such as the IGF 1 receptor (IGF1R) pathway (27). The prooncogenic activities of IGF1R (26) are mediated by its downstream effectors, IRS1 and IRS2. IRS proteins transduce mitogenic, antiapoptotic, and antidifferentiation signals to the cell, mainly through the PI3K–AKT module (28). Although antioncogenic synergistic effects have been observed using either CDK4 and IGF1R inhibitors or CDK4 and PI3K inhibitors, no crosstalk between both pathways has been described (29–32). The CDK4/CDK6 inhibitor (PD0332991, palbociclib) has been approved for the treatment of breast cancer (33). Two other CDK4/CDK6 inhibitors, LY-2835219 (also known as abemaciclib) and LEE011 (also known as ribociclib), are also currently in advanced stages of clinical trials (34). Interestingly, it has previously been reported that a major enzyme of de novo lipogenesis, the fatty acid synthase (FASN), is increased in numerous cancers, including breast cancer (35). The activity of FASN is known to be stimulated by insulin through the PI3K/AKT pathway, and here, we demonstrate that CDK4 is a key effector of insulin, thus promoting de novo lipid synthesis. Based on our findings, we can speculate that CDK4, through phosphorylation and regulation of IRS activity, could simultaneously sustain de novo lipid synthesis and the oncogenic activity of the aforementioned pathways in transformed cells.

The second major finding of our study is the discovery of a residue in IRS2 that is phosphorylated by CDK4 in response to insulin. A large number of publications previously focused on the effects of IRS1 and IRS2 phosphorylation on the insulin-signaling pathway. Both positive and negative phosphorylation sites finely regulate IRS1 and IRS2 activity and are a paradigm of the flexibility of insulin and IGF signaling (36). The final serine/threonine phosphorylation state of IRS proteins is a consequence of the combined action of several kinases that are activated by different pathways in a spaciotemporal manner. Multiple site phosphorylation of these proteins by distinct kinases, such as JNK (37), GSK3 (38), ERK1, or mTOR (39), provides a large number of combinations of phosphorylating events that generate a very complex network (40). We show that CDK4 phosphorylates IRS2 at the new Ser388 site. Moreover, we show that this phosphorylation renders IRS2 more active. Our results add more complexity to the understanding of the physiology of the phosphorylation of the IRS proteins. Phosphorylation by CDK4 may also have an impact on the phosphorylation of IRS2 by other kinases; however, the relative contribution of CDK4 to the final activation or inhibition of IRS compared with other kinases and the identification of which serine/threonine residues are the most critical in regulating IRS function in response to insulin remain to be elucidated. Similarly, we still do not understand why CDK4 activates IRS2 whereas AKT inhibits it through a negative feedback loop. The same stimulus, insulin, triggers concomitantly inhibitory and stimulatory phosphorylations in IRS. The fine regulation of these positive versus negative phosphorylation events requires further investigation. Interestingly, we were able to observe the stimulation of IRS2 Ser388 phosphorylation with insulin not only in adipocytes, but also in other cell types, such as C2C12 myotubes and primary hepatocytes. IRS2 Ser388 phosphorylation could also be detected in Min6 cells, but was not so insulin responsive. As shown in Supplemental Figure 6, A–C, upon insulin stimulation, IRS2 Ser388 phosphoryla-

tion was stronger after 1 hour of treatment, which is in agreement with our findings in mature adipocytes. These results open interesting perspectives into the contribution of CDK4 to IRS2 Ser388 phosphorylation in other insulin-sensitive tissues; CDK4 could, for instance, participate in the control of de novo lipid synthesis in liver upon insulin stimulation.

RNAi-mediated depletion of CDK6, the CDK4 ortholog, suggests that this kinase is also able to phosphorylate IRS2 at Ser388 in mature adipocytes upon insulin stimulation, but to a lesser extent (Supplemental Figure 6D). The effects of CDK6 on IRS2 in other tissues remain to be studied.

Defects in insulin action and insulin secretion are both features of type 2 diabetes. In line with previous publications reporting that CDK4 regulates β cell growth (11) and insulin secretion in β cells (41), it would be interesting to explore the relative contribution of this IRS2 Ser388 phosphorylation in β cell function. The involvement of IRS2 in the pathogenesis of type 2 diabetes is highlighted by the phenotype of *Irs2*⁻/⁻ mice. Indeed, these animals develop type 2 diabetes with impaired peripheral insulin signaling and pancreatic β cell function without compensation by IRS1 (42).

Third, the importance of our findings goes beyond the control of adipocyte biology in normal physiology. Here, we also report a significant ($P = 0.0362$) correlation between CCND3 expression and BMI in human subjects. Our model is further supported by the observed increase in the phosphorylation of the Ser388 of IRS2 in human obese subjects (BMI > 27). Insulin resistance is a major feature in various metabolic disorders, such as obesity and type 2 diabetes. We show here an inverse correlation of IRS2 Ser388 levels in VAT with the blood glucose levels from the subjects (Figure 7H). This strongly supports the notion that this phosphorylation participates in glucose homeostasis in humans.

In conclusion, our results demonstrate that CDK4 is a regulator of adipocyte insulin signaling. By combining experimental data from cellular and mouse models and data obtained using human samples, our study provides insights into the complex pathogenesis of obesity and insulin resistance.

Methods

Materials. All experiments with the CDK4 inhibitor (PD0332991, Azasynth Co.) were done using 1 μM of PD0332991 in mature 3T3-L1 adipocytes. All chemicals, unless stated otherwise, were purchased from Sigma-Aldrich. Actrapid human recombinant insulin was purchased from Novo Nordisk Pharma SA. AKT inhibitor (catalog 124017) was purchased from Calbiochem and used at 10 μM for 30 minutes. ¹⁴C-acetate, and γ-³³P-ATP were purchased from PerkinElmer.

Animals. The generation of *Cdk4ⁿᶜ* and *Cdk4^R24C/R24C* mice has been previously described (11, 13). The 8- to 12-week-old male db/+ and db/db as well as C57BL/6J (B6) mice were obtained from Janvier. *E2f1⁺/⁺* and *E2f1⁻/⁻* mice (B6;129S4-E2f1tm1 Meg/J) were purchased from The Jackson Laboratory. *Cdk4^flox/flox* mice were generated for this study in collaboration with Cyagen Biosciences. The targeting vector included a Neo resistance cassette flanked by FRT sites as well as CRE-dependent lox P sites in introns 1 and 8 (Supplemental Figure 1I).

C57BL/6 embryonic stem cells were used for gene targeting, and the positive cells were bred into albino B6 female mice. This strategy allowed us to have a pure B6 background. *Cdk4^flox/+* mice were then crossed with mice expressing Flp recombinase (B6.Cg-Tg[Pgk1-FLPo]10Sykr/J) in order to remove the Neo resistance cassette. With one subsequent cross with B6 animals, the Flp transgene was removed and the obtained *Cdk4^flox/+* mice were then intercrossed in order to generate the *Cdk4^flox/flox* mice used in this study.

Animals were maintained in a temperature-controlled animal facility with a 12-hour light/12-hour dark cycle and had access to food and water according to the Swiss Animal Protection Ordinance (OPAn). Only male animals were used in this study. For the GTT, mice were starved for 16 hours and then injected i.p. with glucose (2 g/kg). Tail vein blood glucose was measured at the indicated times. For the insulin tolerance test (ITT), 6-hour–fasted mice were injected i.p. with 0.75 U/kg insulin and tail vein blood glucose was then measured at the indicated times. For the in vivo insulin-stimulation assay, mice were fasted overnight and injected in the portal vein or i.p. with 0.75 U/kg insulin or an equal volume of saline. After 3 or 50 minutes, the mice were sacrificed via cervical dislocation. For insulin level measurements, tail vein blood was collected under fed conditions 2 hours after the beginning of the 12-hour dark cycle.

Plasmid constructs and mutagenesis. pDONR-IRS2 was subcloned from pBS mouse IRS-2 (Addgene plasmid catalog 11372) (43) and generated using the pDONR221 vector of Gateway Cloning Technology (Invitrogen). Flag-IRS2 and GST-IRS2 were obtained using the pDEST pCMV14-3XFlag and pGEX-2T vectors of Gateway Cloning Technology starting from the above-described pDONR-IRS2 constructs. A similar strategy was used to obtain the truncated versions of GST-IRS2. The Flag-PIK3R1 and Flag-PDPK1 plasmids were obtained from the Montpellier Genomic Collection (MGC). pDONR-hRB 379–928aa was subcloned from pCMV human RB1 and generated using the pDONR221 vector of Gateway Cloning Technology. pGEX-2T hRB 379–928aa was obtained using the pDEST pGEX-2T from Gateway Cloning Technology. The different serine-to-alanine mutants of GST-IRS2 were generated using a QuikChange Site-Directed Mutagenesis Kit (Stratagene).

Cell culture. 3T3-L1 and 293T were obtained from ATCC. *Irs2⁻/⁻* cells were cultured in DMEM with 10% FBS (PAA Laboratories) in 5% CO_2 in an incubator set at 37°C. Two days after reaching confluence, 3T3-L1 cells were differentiated with DMEM, 10% FBS, 0.5 mM 3-isobutyl-1methylxanthine (IBMX), 1.7 μM insulin, 1 μM dexamethasone, and 1 μM rosiglitazone for 2 days. From day 3 onward, the cells were incubated with DMEM, 10% FBS, and 10 μg/ml insulin, and the medium was changed every 2 days until day 8 of differentiation. 3T3-L1 mature adipocytes were maintained in medium containing FBS only. For insulin (100 nM) or isoproterenol (100 nM) treatments, fully differentiated 3T3-L1 adipocytes were incubated in serum-free DMEM containing 0.2% fatty acid–free BSA. Primary hepatocytes were obtained from B6 mice. Mouse hepatocytes were harvested and cultured as previously described (44). Min6 cells were provided by Christian Widmann (Department of Physiology, Université de Lausanne, Lausanne). They were maintained as previously described (45) and incubated in DMEM supplemented with 15% FBS and 5 mM glucose overnight. The day after, cells were incubated in serum-free DMEM containing 0.1% fatty acid–free BSA for 6 hours. C2C12 myoblasts were obtained from ATCC and were cultured in low-glucose DMEM with 10% FBS in 5% CO_2 in an incubator set at 37°C. For myotube differentiation, C2C12 myoblasts were seeded in 6-cm plates. When the cells reached 95% confluency, the culture medium was switched to DMEM containing 2% horse serum. The medium was changed every 2 days until day 5 of

differentiation. C2C12 myotubes were incubated in α-MEM overnight to induce starvation. Primary hepatocytes, Min6 cells, and C2C12 myotubes were stimulated with insulin (100 nM).

Proteins extraction, coimmunoprecipitation assays, and immunoblot analyses. For endogenous immunoprecipitation experiments between CDK4 and IRS2, mature 3T3-L1 adipocytes were lysed in a buffer containing 0.3% CHAPS, 40 mM Hepes, pH 7.5, 120 mM NaCl, 1 mM EDTA, 10 mM pyrophosphate, 10 mM glycerophosphate, and protease inhibitor cocktail. Lysates were precleared with protein A/G–agarose beads (Life Technologies) and 4 μg of control antibody (HA antibody) for 1 hour. After this step, anti-CDK4 antibodies or HA antibodies were added to the precleared lysates overnight to immunoprecipitate CDK4 or for the control immunoprecipitation, respectively. For endogenous immunoprecipitation experiments, mature 3T3-L1 adipocytes or eWAT from mice was lysed in a buffer containing 20 mM Tris, pH 7.5, 150 mM NaCl, 1 mM EDTA, 1% Triton X-100, 1 mM Na_3VO_4, 1 mM β-glycerophosphate, 50 mM NaF, and protease inhibitor cocktail. Whole protein extracts were precleared with protein A/G–agarose beads (Life Technologies) for 1 hour, and anti-CDK4 antibody (Santa Cruz Biotechnology Inc., sc-260AC) and negative control (Rabbit IgG) (Santa Cruz Biotechnology Inc., sc-2345) were added to immunoprecipitate CDK4 overnight at 4°C. For IRS2 and PIK3R1 immunoprecipitation experiments from mature adipocytes and mice, whole protein extracts were precleared with protein A/G–agarose beads (Life Technologies) and 4 μg of control antibody (HA antibody) for 1 hour. Then anti-IRS2 anti-PIK3R1 antibody and negative control (HA antibody) were added to the precleared lysates for immunoprecipitation overnight at 4°C. Immunoprecipitation experiments in 293T cells were performed using the same buffer as above. Anti-CDK4 antibody (Santa Cruz Biotechnology Inc., sc-601) and negative control (rabbit IgG) (Santa Cruz Biotechnology Inc., sc-2027) were used for the immunoprecipitation. Flag-PIK3R1, Flag-PDKP1, and Flag-IRS2 were transfected with Lipofectamine 2000 (Invitrogen) and immunoprecipitated with Flag beads (Sigma-Aldrich A2220). Proteins were extracted with the same lysis buffer described above and subjected to SDS-PAGE electrophoresis. Protein extractions from the different tissues (eWAT, BAT, brain, muscle, heart, kidney, lung, spleen, and liver) were prepared using M-PER mammalian extraction buffer (Thermo Scientific) containing 1:100 Halt phosphatase inhibitor cocktail (Thermo Scientific) and 1:100 Halt protease inhibitor cocktail, EDTA-free (Thermo Scientific). All the tissues were snap-frozen and then ground with Liquid N2 before lysis. The following antibodies were used for Western blot analysis: anti-CCND1 (NeoMarkers Rb-010-P0), anti-CCND3 (clone sc-6283), anti-CDK4 (clone sc-260), anti-HSL (clone sc-25843), anti-HA (clone sc-805), anti-IRS2 (clone sc-8299) (Santa Cruz Biotechnology Inc.); anti-CCND2 (clone ab3085), anti-CDK4 (clone DSC-35), anti-Ki67 (clone ab15580) (Abcam); anti–LMNA (clone 2032), anti–pHSL Ser573 (clone 4139), anti–RB1 Ser780 (clone 9307), anti–pAKT Thr308 (clone 4056), anti–pAKT Ser473 (clone 4060), anti-AKT (clone 9272), anti-CDK6 (clone DCS83) (Cell Signaling Technology); anti-Flag (clone F3165), anti-actin (clone A2066), anti-tubulin (clone T6199) (Sigma-Aldrich); anti-PI3K3R1 (clone 06-195) (Upstate); and anti-IRS2 (Millipore MABS15). The phosphospecific antibody against IRS2 Ser388 was synthesized and purchased from GenScript.

Kinase assays. 3T3-L1 mature adipocytes were incubated overnight in serum-free DMEM containing 0.2% fatty acid–free BSA and either stimulated with insulin (100 nM) or left untreated with lysates

of these cells used to immunoprecipitate CDK4, as described above. Additionally, CDK4 was immunoprecipitated from eWAT collected from mice that had fasted for 16 hours and were injected i.p. with insulin (0.75 U/kg) for 30 minutes. Kinase assays were performed using immunoprecipitated CDK4 and 500 ng of recombinant RB1 protein (Santa Cruz Biotechnology Inc.) as a substrate in kinase buffer (25 mM Tris/HCl, pH 7.5, 150 mM NaCl, 10 mM $MgCl_2$, 1 mM DTT, 5 mM $Na_4P_2O_7$, 50 mM NaF, 1 mM vanadate, and protease inhibitor cocktail) with 40 μM ATP and 8 μCi γ-[33P]ATP for 30 minutes at 30°C. Recombinant CDK4/CCND3 (ProQinase) was used as positive control. Boiling the samples for 5 minutes in the presence of denaturing sample buffer stopped the reaction. Samples were subsequently subjected to SDS-PAGE, and the gels were then dried in a gel dryer for 1 hour and exposed to an x-ray film at –80°C.

When using GST-purified proteins as substrates, kinase assays were performed using 500 ng of recombinant RB1 protein (Santa Cruz Biotechnology Inc.) as a positive control and recombinant CDK4/CCND3 kinase (ProQinase) and incubated in kinase buffer (described above) supplemented with 40 μM ATP and 8 μCi γ-[33P]ATP for 30 minutes at 30°C.

PamChip peptide microarrays for kinome analysis following insulin stimulation. For kinome analysis, STK microarrays were purchased from PamGene International BV. Each array contained 140 phosphorylatable peptides as well as 4 control peptides. Sample incubation, detection, and analysis were performed in a PamStation 12 according to the manufacturer's instructions. Briefly, extracts from *Cdk4*^{+/+} and *Cdk4*[nc] mice or mature 3T3-L1 adipocytes were made using M-PER mammalian extraction buffer (Thermo Scientific) containing 1:50 Halt phosphatase inhibitor cocktail (Thermo Scientific) and 1:50 Halt protease inhibitor cocktail, EDTA-free (Thermo Scientific), for 20 minutes on ice. The lysates were then centrifuged at 15,871 *g* for 20 minutes to remove all debris. The supernatant was aliquoted, snap-frozen in liquid nitrogen, and stored at –80°C until further processing. Prior to incubation with the kinase reaction mix, the arrays were blocked with 2% BSA in water for 30 cycles and washed 3 times with PK assay buffer. Kinase reactions were performed for 1 hour with 5 μg of total extract for the mouse experiment or 2.5 μg of total extract for the mature adipocyte and 400 μM ATP at 30°C. Phosphorylated peptides were detected with an anti-rabbit–FITC antibody that recognizes a pool of anti–phospho serine/threonine antibodies. The instrument contains a 12-bit CCD camera suitable for imaging of FITC-labeled arrays. The images obtained from the phosphorylated arrays were quantified using the BioNavigator software (PamGene International BV), and the list of peptides whose phosphorylation was significantly different between control (3 minutes of insulin treated in *Cdk4*^{+/+} mice or 5 minutes of insulin stimulation in cells starved in the presence of DMSO) and test (3 minutes of insulin treated in *Cdk4*[nc] mice or 5 minutes of insulin stimulation in cells starved in the presence of PD0332991) conditions was uploaded to GeneGo for pathway analysis. The list of the significantly different peptides is shown in Supplemental Figure 3, C and D. The BioNavigator software was used to perform the upstream STK analysis that is shown in Figure 4D.

Statistics. All statistics are described in the figure legends. The results were expressed as mean ± SEM. Pearson's correlation coefficient was calculated to test for correlation between 2 parameters. Comparisons between 2 groups were performed with an unpaired

2-tailed Student's *t* test, and multiple group comparisons were performed by 1-way ANOVA followed by Tukey's test and 2-way ANOVA followed by Tukey's test. $P < 0.05$ was considered significant.

Study approval. All animal care and treatment procedures were performed in accordance with Swiss guidelines and were approved by the Canton of Vaud SCAV (authorization VD 2627.b). For human samples, the protocol concerning the use of biopsy from patients was approved in agreement with Spanish regulations, either by the Ethics and Research Committee of Virgen de la Victoria Clinical University Hospital or by the Institutional Ethics Committee of the Joan XXIII University Hospital. All patients provided written informed consent.

Supplemental data. Additional methods information is available in Supplemental Experimental Procedures. The sequences of the primers used for RT-qPCR are available in Supplemental Table 1.

Author contributions

LF designed the project. SL, ICLM, PDD, XE, JCA, CC, AG, QL, LMC, BD, JSA, EB, SH, AA, and PD designed and carried out the experiments. The design and execution of the PamGene experiment was done by ICLM. VJ and FB provided the AAV8 vectors. LZ performed the tail-vein injections. CRK provided pBS mouse IRS-2 and *Irs2−/−* cells. JV and FJT provided human VAT samples. SL, ICLM, and LF wrote the manuscript.

Acknowledgments

Address correspondence to: Lluis Fajas, Department of Physiologie, Université de Lausanne, CH-1005 Lausanne, Switzerland. Phone: 41.21.692.55.10; E-mail: lluis.fajas@unil.ch.

1. Saltiel AR, Kahn CR. Insulin signalling and the regulation of glucose and lipid metabolism. *Nature*. 2001;414(6865):799–806.
2. White MF. Insulin signaling in health and disease. *Science*. 2003;302(5651):1710–1711.
3. Rask-Madsen C, Kahn CR. Tissue-specific insulin signaling, metabolic syndrome, and cardiovascular disease. *Arterioscler Thromb Vasc Biol*. 2012;32(9):2052–2059.
4. Vazquez-Vela ME, Torres N, Tovar AR. White adipose tissue as endocrine organ and its role in obesity. *Arch Med Res*. 2008;39(8):715–728.
5. Koch L, et al. Central insulin action regulates peripheral glucose and fat metabolism in mice. *J Clin Invest*. 2008;118(6):2132–2147.
6. Abel ED, et al. Adipose-selective targeting of the GLUT4 gene impairs insulin action in muscle and liver. *Nature*. 2001;409(6821):729–733.
7. Choi YH, et al. Alterations in regulation of energy homeostasis in cyclic nucleotide phosphodiesterase 3B-null mice. *J Clin Invest*. 2006;116(12):3240–3251.
8. Matsushime H, et al. Identification and properties of an atypical catalytic subunit (p34PSK-J3/cdk4) for mammalian D type G1 cyclins. *Cell*. 1992;71(2):323–334.
9. Connell-Crowley L, Harper JW, Goodrich DW. Cyclin D1/Cdk4 regulates retinoblastoma protein-mediated cell cycle arrest by site-specific phosphorylation. *Mol Biol Cell*. 1997;8(2):287–301.
10. Malumbres M, Barbacid M. Cell cycle, CDKs and cancer: a changing paradigm. *Nat Rev Cancer*. 2009;9(3):153–166.
11. Rane SG, et al. Loss of Cdk4 expression causes insulin-deficient diabetes and Cdk4 activation results in beta-islet cell hyperplasia. *Nat Genet*. 1999;22(1):44–52.
12. Serrano M, Hannon GJ, Beach D. A new regulatory motif in cell-cycle control causing specific inhibition of cyclin D/CDK4. *Nature*. 1993;366(6456):704–707.
13. Martin J, et al. Genetic rescue of Cdk4 null mice restores pancreatic beta-cell proliferation but not homeostatic cell number. *Oncogene*. 2003;22(34):5261–5269.
14. Abella A, et al. Cdk4 promotes adipogenesis through PPARgamma activation. *Cell Metab*. 2005;2(4):239–249.
15. Sarruf DA, Iankova I, Abella A, Assou S, Miard S, Fajas L. Cyclin D3 promotes adipogenesis through activation of peroxisome proliferator-activated receptor gamma. *Mol Cell Biol*. 2005;25(22):9985–9995.
16. Fajas L, Landsberg RL, Huss-Garcia Y, Sardet C, Lees JA, Auwerx J. E2Fs regulate adipocyte differentiation. *Dev Cell*. 2002;3(1):39–49.
17. Jimenez V, et al. In vivo adeno-associated viral vector-mediated genetic engineering of white and brown adipose tissue in adult mice. *Diabetes*. 2013;62(12):4012–4022.
18. Sotillo R, et al. Wide spectrum of tumors in knock-in mice carrying a Cdk4 protein insensitive to INK4 inhibitors. *EMBO J*. 2001;20(23):6637–6647.
19. Rodriguez-Diez E, et al. Cdk4 and Cdk6 cooperate in counteracting the INK4 family of inhibitors during murine leukemogenesis. *Blood*. 2014;124(15):2380–2390.
20. Zechner R, et al. FAT SIGNALS — lipases and lipolysis in lipid metabolism and signaling. *Cell Metab*. 2012;15(3):279–291.
21. Fry DW, et al. Specific inhibition of cyclin-dependent kinase 4/6 by PD 0332991 and associated antitumor activity in human tumor xenografts. *Mol Cancer Ther*. 2004;3(11):1427–1438.
22. Hilhorst R, Houkes L, Mommersteeg M, Musch J, van den Berg A, Ruijtenbeek R. Peptide microarrays for profiling of serine/threonine kinase activity of recombinant kinases and lysates of cells and tissue samples. *Methods Mol Biol*. 2013;977:259–271.
23. Thirone AC, Huang C, Klip A. Tissue-specific roles of IRS proteins in insulin signaling and glucose transport. *Trends Endocrinol Metab*. 2006;17(2):72–78.
24. Malumbres M, Barbacid M. Mammalian cyclin-dependent kinases. *Trends Biochem Sci*. 2005;30(11):630–641.
25. Viglietto G, et al. Cytoplasmic relocalization and inhibition of the cyclin-dependent kinase inhibitor p27(Kip1) by PKB/Akt-mediated phosphorylation in breast cancer. *Nat Med*. 2002;8(10):1136–1144.
26. Zhou BP, Liao Y, Xia W, Spohn B, Lee MH, Hung MC. Cytoplasmic localization of p21Cip1/WAF1 by Akt-induced phosphorylation in HER-2/neu-overexpressing cells. *Nat Cell Biol*. 2001;3(3):245–252.
27. Reuveni H, et al. Therapeutic destruction of insulin receptor substrates for cancer treatment. *Cancer Res*. 2013;73(14):4383–4394.
28. Baserga R. The insulin receptor substrate-1: a biomarker for cancer? *Exp Cell Res*. 2009;315(5):727–732.
29. Heilmann AM, et al. CDK4/6 and IGF1 receptor inhibitors synergize to suppress the growth of p16INK4A-deficient pancreatic cancers. *Cancer Res*. 2014;74(14):3947–3958.
30. Vora SR, et al. CDK 4/6 inhibitors sensitize PIK3CA mutant breast cancer to PI3K inhibitors. *Cancer Cell*. 2014;26(1):136–149.
31. Muranen T, Meric-Bernstam F, Mills GB. Promising rationally derived combination therapy with PI3K and CDK4/6 inhibitors. *Cancer Cell*. 2014;26(1):7–9.
32. Miller ML, et al. Drug synergy screen and network modeling in dedifferentiated liposarcoma identifies CDK4 and IGF1R as synergistic drug targets. *Sci Signal*. 2013;6(294):ra85.
33. Turner NC, et al. Palbociclib in hormone-receptor-positive advanced breast cancer. *N Engl J Med*. 2015;373(3):209–219.
34. Asghar U, Witkiewicz AK, Turner NC, Knudsen

ES. The history and future of targeting cyclin-dependent kinases in cancer therapy. *Nat Rev Drug Discov*. 2015;14(2):130–146.

35. Menendez JA, Lupu R. Fatty acid synthase and the lipogenic phenotype in cancer pathogenesis. *Nat Rev Cancer*. 2007;7(10):763–777.

36. Copps KD, White MF. Regulation of insulin sensitivity by serine/threonine phosphorylation of insulin receptor substrate proteins IRS1 and IRS2. *Diabetologia*. 2012;55(10):2565–2582.

37. Solinas G, Naugler W, Galimi F, Lee MS, Karin M. Saturated fatty acids inhibit induction of insulin gene transcription by JNK-mediated phosphorylation of insulin-receptor substrates. *Proc Natl Acad Sci U S A*. 2006;103(44):16454–16459.

38. Sharfi H, Eldar-Finkelman H. Sequential phosphorylation of insulin receptor substrate-2 by glycogen synthase kinase-3 and c-Jun NH2-terminal kinase plays a role in hepatic insulin signaling. *Am J Physiol Endocrinol Metab*. 2008;294(2):E307–E315.

39. Fritsche L, et al. Insulin-induced serine phosphorylation of IRS-2 via ERK1/2 and mTOR: studies on the function of Ser675 and Ser907. *Am J Physiol Endocrinol Metab*. 2011;300(5):E824–E836.

40. Boura-Halfon S, Zick Y. Phosphorylation of IRS proteins, insulin action, and insulin resistance. *Am J Physiol Endocrinol Metab*. 2009;296(4):E581–E591.

41. Blanchet E, et al. E2F transcription factor-1 regulates oxidative metabolism. *Nat Cell Biol*. 2011;13(9):1146–1152.

42. Withers DJ, et al. Disruption of IRS-2 causes type 2 diabetes in mice. *Nature*. 1998;391(6670):900–904.

43. Tsuruzoe K, Emkey R, Kriauciunas KM, Ueki K, Kahn CR. Insulin receptor substrate 3 (IRS-3) and IRS-4 impair IRS-1- and IRS-2-mediated signaling. *Mol Cell Biol*. 2001;21(1):26–38.

44. Benhamed F, et al. The lipogenic transcription factor ChREBP dissociates hepatic steatosis from insulin resistance in mice and humans. *J Clin Invest*. 2012;122(6):2176–2194.

45. Annicotte JS, et al. The CDK4-pRB-E2F1 pathway controls insulin secretion. *Nat Cell Biol*. 2009;11(8):1017–1023.

3. Article 3 : E2F1 inhibits circulating cholesterol clearance by regulating PCSK9 expression in the liver

E2F1 inhibits circulating cholesterol clearance by regulating PCSK9 expression in the liver

Qiuwen Lai[1,*], Pierre-Damien Denechaud[1,*], Cédric Le May[2] and Lluis Fajas[1,#]

[1]Department of Physiology, Université de Lausanne (UNIL), Lausanne, Switzerland.
[2]Institut du Thorax, Inserm UMR1087 - CNRS UMR6291, Nantes, France

* Contributed equally
# Corresponding author

Contact:
Lluis Fajas Coll:
E-mail: Lluis.Fajas@unil.ch
Phone: +41 21 692 5510

Conflict of interest statement:
The authors have declared that no conflict of interest exists

ABSTRACT

Cholesterol accumulation in the liver is an early event in nonalcoholic fatty liver disease (NAFLD). Here, we found that E2F1 plays a crucial role in maintaining cellular cholesterol homeostasis by regulating cholesterol uptake via PCSK9 (proprotein convertase subtilisin/kexin type 9), an enzyme that promotes LDLR (low density lipoprotein receptor) degradation upon activation. E2F1-/- mice display reduced total plasma cholesterol levels and increased cholesterol content in the liver. In this study, we show that E2F1 deletion in cellular and mouse models leads to a marked decrease in PCSK9 expression and increase in LDLR expression. In addition to the up regulation of LDLR, we report that E2F1-/- hepatocytes exhibit increased LDL uptake. ChIP-Seq and PCSK9 promoter reporter experiments confirmed that E2F1 binds to and transactivates the PCSK9 promoter. Interestingly, E2F1-/- mice fed a high cholesterol diet (HCD) display a fatty liver phenotype and liver fibrosis. Collectively, these data indicate that E2F1 regulates cholesterol uptake and that the loss of E2F1 leads to abnormal cholesterol accumulation in the liver and the development of fibrosis in response to a high cholesterol diet.

Keywords: Cholesterol/E2F1/LDLR/Metabolism/PCSK9

BRIEF SUMMARY

Unexpected role for E2F1 in controlling cholesterol uptake, which provides a fundamental framework for exploring new therapeutic approaches against liver fibrosis.

INTRODUCTION

There are eight E2F genes (E2F1-8) in mammals, which can be widely classified based on their transcriptional properties, cell cycle properties, and interaction partners (1). Among the E2Fs, E2F1 is the best-studied transcription factor controlling the G1/S transition during the cell cycle. The activity of E2F1 is dependent on its binding partners: dimerization protein (DP) and the retinoblastoma family of proteins (RB) (2). Upon cell cycle entry, cyclin-dependent kinases 4/6 (cdks) phosphorylate RB, leading to release of the E2F1-RB repressor complex (3), resulting in activation of E2F1-mediated transcriptional regulation of target genes, such as thymidine kinase (Tk), dihydrofolate reductase (Dhfr), cyclin D and cyclin E. In addition to cell cycle control, E2F1 also participates in the control of oxidative, glucose and lipid metabolism (4-6). Moreover, the E2F1-/- mouse model exhibits decreased plasma total cholesterol levels, suggesting that E2F1 may also be implicated in regulating cholesterol homeostasis (7). Here, we elucidate a novel mechanism explaining how E2F1 participates in controlling sterol balance.

Cholesterol is an essential building block for the cell membrane and is a precursor of metabolites such as bile acids, steroid hormones and oxysterols, which have important biological functions in physiology. Cholesterol is a highly insoluble molecule that must be transported in the form of lipoprotein particles. There are four main types of circulating lipoproteins: chylomicron (CM), very low density lipoprotein (VLDL), low density lipoprotein (LDL) and high density lipoprotein (HDL). Perturbation of the cholesterol balance leading to high plasma LDL levels and low HDL levels is a risk factor for cardiovascular diseases (CVDs). Thus, interventions aimed at decreasing plasma LDL levels have become an efficient strategy to protect against CVDs.

The liver is one of the primary organs that maintains whole-body cholesterol homeostasis (8). In the liver, cholesterol is packaged in VLDL and then enters the circulation, where VLDL undergoes lipolysis to form LDL. The uptake of LDL and

other ApoE/ApoB lipoproteins is mediated by LDLR. LDL binds to LDLR and is endocytosed into cells (9). In addition to regulating endogenous synthesis, LDLR levels are crucial for maintaining the optimal cellular cholesterol balance (10). LDLR levels are transcriptionally controlled by sterol regulatory element-binding protein 2 (SREBP2) and post-transcriptionally controlled by proprotein convertase subtilisin/kexin 9 (PCSK9), an enzyme that binds to LDLR and promotes its degradation. Inhibition of PCSK9 prevents LDLR degradation, resulting in increased availability of LDLR to facilitate LDL clearance. Hence, PCSK9 inhibitors have been developed as novel drugs for CVDs (11).

In this study, we elucidate a new mechanism upstream of PCSK9-mediated LDLR degradation. We show that E2F1 acts as a positive regulator of PCSK9 to control cholesterol uptake. In the absence of E2F1-induced PCSK9 regulation, there is an increase in LDLR-mediated uptake and over-accumulation of cholesterol in cells. E2F1-/- mice fed a high cholesterol diet (HCD) display increased α-collagen and α-sma gene expression, which is typically observed during liver fibrosis development. Taken together, our results show that in addition to SREBP2, E2F1 acts to control LDLR via PCSK9 in response to sterol signals to prevent over-accumulation of sterols in the cell, particularly during high cholesterol dietary intake.

RESULTS

E2F1-/- mice exhibit decreased plasma cholesterol levels and increased cholesterol content in the liver and colon tissues

Previous results from our laboratory indicated that E2F1 is a major regulator of lipid metabolism (5). By analyzing the plasma lipid profile, we found that E2F1 knockout mice (E2F1-/-) display lower plasma total cholesterol, HDL-cholesterol, and LDL-cholesterol levels compared with wild-type mice (E2F1+/+) fed a normal chow diet (Figure 1A). These results were confirmed via FPLC separation of lipoproteins (Supplemental Figure 1) and suggested that deletion of E2F1 disrupts cholesterol homeostasis.

We quantified the cholesterol and bile acid content in the feces to elucidate whether the observed reduction in circulating cholesterol levels was secondary to decreased cholesterol excretion. No differences were observed between the E2F1+/+ and E2F1-/- mice (Figure 1C-D). We next investigated whether the cholesterol content in the tissues was altered in these mice. Interestingly, the E2F1-/- mice exhibited consistently higher levels of cholesterol in the liver, BAT and colon compared with E2F1+/+ mice (Figure 1B). No major differences in cholesterol content were detected in the other tissues tested. These findings suggested that the reduction of plasma cholesterol levels observed in the E2F1-/- mice was potentially due to increased cholesterol uptake.

E2F1 participates in the transcriptional regulation of genes involved in cholesterol metabolism

As a transcription factor, E2F1 controls the expression of its target genes. We analyzed our previously published E2F1 ChIP high-throughput DNA sequencing (ChIP-seq) data from primary cultures of mouse hepatocytes infected with adenovirus-E2F1 (5) to identify potential E2F1 targets that regulate cholesterol homeostasis. We found that E2F1 binds to the regulatory regions of several

cholesterol-related genes (Figure 2A), including mevalonate kinase, 7 dehydrocholesterol reductase and proprotein convertase subtilisin/kexin type 9 (PCSK9). PCSK9 is a promising target because it is a key regulator of cholesterol homeostasis that controls cholesterol uptake (12). ChIP-qPCR experiments in a human hepatocellular liver carcinoma cell line (HepG2) confirmed our ChIP-seq data and showed that endogenous E2F1 specifically binds to the PCSK9 promoter (Figure 2B). In addition, the functional occupancy of E2F1 on the human PCSK9 promoter was assessed through Renilla-based reporter analyses. Consistently, transient transfections revealed that E2F1 was able to transactivate the PCSK9 promoter (Figure 2C). Collectively, our results indicate that E2F1 binds and transactivates the PCSK9 promoter.

E2F1 is a positive regulator of PCSK9

We decided to focus on the liver and hepatocytes to further characterize the effects of E2F1 on PCSK9 transcription because the liver is the central organ for cholesterol homeostasis. The first interesting observation was that PCSK9 expression was regulated by E2F1. In agreement with previous studies (13), hepatic PCSK9 mRNA expression was increased in the livers of mice in the fed state (Figure 3A). However, this induction was significantly reduced in the livers of E2F1-/- mice compared with E2F1+/+ mice. No differences in PCSK9 expression were observed in the fasting state (Figure 3A). PCSK9 protein expression in hepatic samples derived from E2F1-/- mice was also markedly reduced in the fed state (Figure 3B). In accordance with the typical role of PCSK9 in inducing LDLR degradation, LDLR protein expression was increased in the livers of E2F1-/- mice compared with E2F1+/+ mice, as assessed by immunofluorescence (Figure 3C). These results were confirmed in primary hepatocyte cultures. Basal PCSK9 mRNA and protein expression was reduced in primary E2F1-/- hepatocytes (Figure 3D, 3E). As expected, incubation of these cells with cholesterol decreased PCSK9 expression

(Figure 3D). This reduction was even more pronounced in E2F1-/- hepatocytes (Figure 3D). Consistent with the previous *in vivo* observations, LDLR protein expression, analyzed through immunofluorescence, was increased in E2F1-/- cells (Figure 3F). Strikingly, and possibly as a result of increased LDLR expression and activity, the cholesterol content was increased in E2F1-/- hepatocytes (Figure 3G, 3H). We investigated the rate of cholesterol biosynthesis in the cells to determine whether the higher cholesterol content of E2F1-/- hepatocytes was due to an increase in *de novo* cholesterol synthesis. E2F1-/- hepatocytes exhibited a lower rate of cholesterol biosynthesis compared with E2F1+/+ hepatocytes (Figure 3I). These results confirmed that the high cholesterol levels observed in E2F1-/- cells are due to an increase in sterol uptake, and not endogenous biosynthesis.

Increased LDL uptake in E2F1 KO HepG2 cells

We generated an E2F1KO HepG2 cell line using CRISPR technology in which the E2F1 protein was successfully removed to validate our results obtained from mouse hepatocytes in a human cell model (Supplemental Figure 2). No changes in PCSK9 expression were observed in the E2F1KO HepG2 and control cells upon culture in complete serum (Figure 4A, 4B). Interestingly, the expression of both PCSK9 mRNA and protein was decreased in E2F1KO cells cultured with delipidated serum (DL) compared with the control cells (Figure 4A, 4B). Consistent with the decrease in PCSK9 expression, LDLR protein expression was increased in E2F1KO cells grown under DL conditions (Figure 4B). The increased LDLR expression contributed to the increased LDL uptake in E2F1KO cells grown in the same DL conditions (Figure 4C). Because cholesterol accumulation inhibits cholesterol biosynthesis, E2F1KO cells consistently showed a decrease in the capacity to synthesize cholesterol (Figure 4D). Taken together, these results supported the hypothesis that E2F1 acts as a positive regulator of hepatic PCSK9 in human/mouse hepatocytes. The reduction of PCSK9 expression in E2F1-deficient cells/tissues

6

facilitates LDL-cholesterol uptake, which contributes to the accumulation of cellular cholesterol and the decrease in endogenous cholesterol biosynthesis (Figure 4E).

Abnormal cholesterol homeostasis in E2F1-/- mice

We challenged the mice through five weeks of feeding with a high-cholesterol diet (HCD) to further investigate the participation of E2F1 in the regulation of cholesterol metabolism *in vivo*. As previously described (Figure 1), E2F1-/- mice showed reduced plasma cholesterol levels compared with E2F1+/+ mice before the change of diet (Figure 5A). The HCD led to a time-dependent increase in plasma cholesterol levels in both genotypes (Figure 5A). At the end of the 5-week HCD treatment, we did not observe any difference in plasma total, HDL- or LDL-cholesterol levels between E2F1+/+ and E2F1-/- mice (Figure 5A-C). In contrast, we observed major morphological differences in the livers of these mice. Surprisingly, H&E staining of liver sections revealed that E2F-/- mice showed ballooning of the hepatocytes, which is an early sign of steatohepatitis (Figure 5D). Moreover, the neutral lipid content, as determined by Oil Red O staining, was also increased in the livers of the E2F1-/- mice compared with the E2F1+/+ mice (Figure 5D), suggesting that E2F1 deletion leads to an increase in lipid accumulation in this tissue. Filipin staining, a marker of the cholesterol content, was also stronger in E2F1-/- livers (Figure 5D-E). Strikingly, the expression of PCSK9 at both the mRNA and protein levels was diminished in the livers of E2F1-/- mice compared with E2F1+/+ mice fed the HCD (Figure 5F-G, Supplemental Figure 3). This result was in accord with the increased LDLR expression observed in the livers of the E2F1-/- mice (Figure 5H-I). In addition, we found that the hepatic expression of E2F1 in the HCD-fed mice was markedly increased compared with the chow-fed mice (Supplemental Figure 4), suggesting that E2F1 expression is diet dependent and plays a role in controlling homeostasis by controlling PCSK9 expression. In summary, these results supported

the hypothesis that E2F1 deletion in mice fed the HCD resulted in an increase in LDLR expression and cholesterol accumulation in the liver.

High dietary cholesterol promotes liver fibrosis in E2F1-/- mice

Morphological observations of the livers of E2F1-/- mice suggested early signs of steatohepatitis development. Therefore, we performed trichrome staining on histological liver sections. Stronger staining was observed in the livers of the E2F1-/- mice compared with the E2F1+/+ mice, suggesting the presence of fibrosis in the liver of these mice fed the HCD (Figure 6A). Liver fibrosis is characterized by increased production of extracellular matrix, such as α-collagen type I. Furthermore, during the progression of liver fibrosis, hepatic stellate cells undergo transdifferentiation to a myofibroblast-like phenotype that expresses a high level of smooth muscle actin (*a*-sma) (14). Accordingly, the mRNA levels of both fibrosis biomarker genes (α-collagen type I and *a*-sma) were also increased in the E2F1-/- mice (Figure 6B). We checked inflammation gene markers, such as IL6 and TNFα, and did not find any significant differences that could reveal a modification of inflammation between the E2F1+/+ and E2F1-/- mice (Figure 6B). We also observed that the total BA levels in fecal material were modestly decreased in E2F1-/- mice fed the HCD compared with E2F1+/+ mice, suggesting that E2F1 deletion led to an increase in cholesterol uptake and, possibly, a reduction in cholesterol breakdown to BA (Supplemental Figure 5A). No differences in fecal neutral sterol levels were detected between E2F1+/+ and E2F1-/- mice (Supplemental Figure 5B). These data suggested that E2F1 could protect mice from the early stages of steatohepatitis development by regulating optimal cholesterol uptake (Figure 7).

8

DISCUSSION

Deregulation of lipid and lipoprotein metabolism is associated with nonalcoholic fatty liver disease (NAFLD) (15). NAFLD is the most common liver disease in the Western countries and affects approximately 30% of the US population. The pathology of NAFLD involves various stages, beginning with lipid accumulation in the liver (simple steatosis) and progressing to chronic inflammation that may lead to nonalcoholic steatohepatitis (NASH), hepatic fibrosis, cirrhosis, and hepatocellular carcinoma (16). Although the underlying mechanism that induces inflammation and fibrosis remains unclear, several studies have established that perturbed cholesterol homeostasis is central to the development of NASH (17, 18). Here, we show that the transcription factor E2F1, which is primarily known for its roles in cell cycle regulation, plays a role in cholesterol homeostasis. We identified a new transcriptional target of E2F1, PCSK9, which is characterized as playing a role in the regulation of LDLR degradation and cholesterol uptake. Consequently, E2F1-/- mice display reduced PCSK9 expression in the liver, leading to a decrease in plasma total cholesterol levels and an increase in the cholesterol content of the liver and other tissues. These results initially led us to consider that E2F1 deletion might prevent CVD. Surprisingly, further analysis highlighted that hypercholesterolemia was not prevented by an HCD (Figure 5A). Instead, E2F1-/- mice presented early signs of liver fibrosis (Figure 6), likely due to excessive cellular cholesterol accumulation.

E2F1 has recently been implicated in liver fibrosis (19) in a study in which Zhang and co-workers detected increased E2F1 expression in human fibrotic/cirrhotic livers and in a mouse model of hepatobiliary injury. We observed similar E2F1 induction in the livers of mice fed an HCD (Figure EV4). Nevertheless, in contrast to our observations, the authors reported that E2F1-/- mice were protected from liver fibrosis induced by DDC supplementation. Fibrosis initiation in this specific model (DCC) is dependent on bile acid accumulation and toxicity and

not on lipid accumulation, as observed when mice are fed an HCD diet, which may explain the differences observed between these two models.

We showed that E2F1 regulates PCSK9 mRNA expression, which is a promising therapeutic target for lowering plasma LDL-cholesterol levels. Indeed, recent clinical trials revealed that treatment with a PCSK9 inhibitor was effective in clearing as much as 70% of plasma LDL-C, with a good safety profile (20). The transcriptional regulation of PCSK9 relies largely on the nutritional status and cholesterol cellular content. Other transcription factors, including SREBP2, SREBP1c and HNF1a, control PCSK9 expression (13, 21). Interestingly, we previously showed that E2F1 is activated by insulin and controls SREBP-1c gene expression in the liver (5), suggesting that cross-talk exists between these pathways.

In the present work, we have illustrated that hepatic PCSK9 mRNA expression is reduced in response to a high cholesterol diet compared with a normal chow diet (Figure 5F), suggesting that under these conditions, PCSK9 inhibition is required to increase LDLR activity and, thus, cholesterol uptake. Interestingly, when we challenged mice with the HCD, PCSK9 expression was further decreased in E2F1-/- mice. Strikingly, we found that hepatic E2F1 expression was increased in response to the HCD compared with the chow diet. Based on these results, we can conclude that induction of E2F1 in mice fed a high cholesterol diet is required to repress LDLR-mediated cholesterol uptake through PCSK9 activation. Further supporting this conclusion, when E2F1 was deleted and mice were fed the HCD, hepatic PCSK9 expression was detected at very low levels. Hence, we can speculate that E2F1-mediated regulation of PCSK9 expression is a compensatory mechanism to avoid excessive cholesterol accumulation in cells. Indeed, excess intracellular cholesterol levels are toxic to cells (22). However, the obvious effect of decreased PCSK9 expression is a reduction in plasma LDL-C levels. The promising outcomes from phase II and III clinical trials using PCSK9 monoclonal antibodies for treatment have gained significant attention, in the hope that a PCSK9 inhibitor may represent a

magic bullet for CVDs (23). Most crucially, our data highlight the observation that although inhibiting PCSK9 is beneficial for reducing circulating LDLC levels, efficient uptake by the LDL system must be accompanied by a competent sterol excretion system to avoid excessive cholesterol accumulation in the liver.

In conclusion, our study supports the hypothesis that E2F1-induced PCSK9 expression is important to moderately control the amount of LDLR and support cellular cholesterol homeostasis (Figure 7). In our model, we established that E2F1 regulates the availability of the LDLR through PCSK9 in response to dietary status. In addition to SREBP2 activation, the high level of E2F1 expression during feeding conditions induces PCSK9 expression, which in turn reduces available LDLR levels. This mechanism prevents cholesterol that is simultaneously derived from LDLR-mediated uptake and synthesis from overwhelming cells, maintaining the whole-body cholesterol balance. However, during high cholesterol dietary intake, SREBP2 activity is inhibited to limit cholesterol loading from the synthesis and uptake pathways. In this case, E2F1 acts as an alternative regulator to control optimal LDLR-mediated sterol clearance through PCSK9.

METHODS

Animal experiments. E2F1+/+ and E2F1-/- mice (B6; 129S4-E2f1tm1Meg/J) were purchased from The Jackson Laboratory. Mice were fed normal chow or a high cholesterol diet (HCD) (Cat: TD.88051, Harlan) and housed under a 12 h light/dark cycle. All mice in the fed and overnight fasting groups were euthanized at 10 am. Organs and blood samples were collected for all experiments. All animal experiments were approved by the Canton of Vaud SCAV (authorization VD2627 and VD3046).

Cell culture and transfection. The HepG2 cell line was purchased from the American Type Culture Collection (ATCC). E2F1 was knocked out using CRISPR/Cas9 technology. LentiCRISPR v2 was a gift from Feng Zhang (Addgene plasmid 52961); a description of the plasmid can be found in Sanjana, Shalem et al. 2014. Both the pMD2.G and psPAX2 plasmids were gifts from Didier Trono (Addgene plasmid 12259 and 12260, respectively). The target sequences for the E2F1 guide were 5'CACCGTCTGACCACCAAGCGCTTCC-3' and 5'-AACGGAAGCGCTTGGTGGTCAGAC-3'. The oligos were synthesized and cloned into the digested LentiCrispR vector in accordance with the protocol described by Shalem et al (24). Lentiviral production was based on the standard protocol established by Salmon and Trono (25). For lentivirus infection, HepG2 cells were infected with 2 ml of the obtained virus for 72 hours. Infected HepG2 cells were treated with 5 μg/ml puromycin for five consecutive days, with fresh medium (DMEM/Glutamax plus 10% FBS) added every two to three days during the treatment period to select for the positive, infected cells. Western blotting was performed to ensure that the E2F1 protein (Cat: sc-193, Santa Cruz Biotechnology) was not expressed. For the experiments, we treated the cells with either 10% delipidated FBS (DL) (Cat: S5394, Sigma) or 10% FBS. The HepG2 cell line was transfected with a PCSK9 promoter reporter (*Renilla*) and an empty vector plasmid (Cat: S712669, Cat: S790005, Switchgear), using X-tremeGene (Cat: 06366236001, Roche).

We isolated mouse primary hepatocytes in accordance with the protocol described in Benhamed, Denechaud et al. 2012. For the experiments, we treated the cells with DMSO (control) or 0.065 mM water-soluble cholesterol (Cat: C4951, Sigma) overnight.

Histology. Liver tissues were fixed in 4% neutral buffered formalin and embedded in OCT freezing medium. The tissues were cut and stained with H&E for morphological analysis, Oil Red O to detect neutral lipids or trichrome to detect fibrosis. The tissues were sectioned and stained by the Mouse Pathology Facility at UNIL, Switzerland.

Fecal analysis. Feces of singly housed mice or pooled feces from E2F1+/+ and E2F1-/- mice were collected after 24 h and dried at 70°C. Fecal samples were used to quantify bile acid and neutral sterol levels using gas-liquid chromatography-mass spectrometry, as previously described (26) or as otherwise indicated using a commercial kit (Cat: 80470, Crystal Chem; Cat: 113009910026, Diasys). All gas-liquid chromatography-mass spectrometry analyses were performed by Albert K Groen at the University of Groningen, The Netherlands.

Real-time quantitative PCR analysis. Total mRNA was extracted from 20-30 mg of liver or cultured cells using an RNeasy kit (Cat: 74106, Qiagen) according to the manufacturer's protocol. One microgram of the RNA was subsequently reverse-transcribed and quantified via real-time quantitative PCR using an ABI 7900HT instrument. All presented data were based on the standard curve method and normalized to mouse RS9 levels.

Classical ChIP in HepG2 cells. ChIP was performed as previously described (5). Briefly, cells were fixed with a 1% formaldehyde solution and lysed with a cell lysis solution. The isolated nuclear extract was sheared through 20 cycles of sonication (30s on 30s off /cycle). A DNA gel was run to verify that isolated chromatin was sheared into small fragments spanning approximately 300-800 bp. Magnetic beads were pre-cleared with BSA and salmon sperm, followed by

incubation with the E2F1 antibody (Cat: sc-193, Santa Cruz Biotechnology) for 1 hour at 4°C with rotation. The isolated chromatin was immunoprecipitated with the prepared magnetic beads overnight at 4°C. The immunoprecipitated chromatin was washed and, together with the input samples, reverse cross-linked at 65°C overnight. The DNA was subsequently purified with a MinElute column (Cat: 28206, Qiagen). Finally, E2F1 DNA binding was quantified via qPCR.

High-throughput ChIP-seq. The ChIP-seq experiment was performed as previously described (5). The sequencing data are available in the NCBI Gene Expression Omnibus (GEO) database (GEO GSE74006) (5)

Lipid analysis. Lipids were extracted using the Folch method (Folch, Lees et al. 1957). Briefly, 30-50 mg of liver tissue were ground in 1 ml of PBS, followed by the addition of 5 ml of a chloroform:methanol (2:1) solution. The sample was vortexed vigorously and centrifuged at 1,000 rpm. The lower chloroform phase containing the lipids was transferred to a new glass tube, and the sample was dried using nitrogen gas. Cholesterol and triglyceride concentrations were quantified with commercial kits (Cat: 113009910026 and DIA0060, Diasys). Fast protein liquid chromatography (FPLC) was performed as previously described (27).

LDL-C uptake assay. LDL-C uptake was determined according to the manufacturer's protocol (Cat: ab133127, Abcam). Briefly, 4,000 E2F1+/+ and E2F1-/- cells/well were plated in 96-well plates and cultured in medium supplemented with 10% FBS or 10% delipidated FBS for 24 hours. After treatment, 75 μl of diluted LDL-DyLight 550 was added to each well, followed by incubation for 4 hours at 37°C in a 5% CO_2 incubator and subsequent cell fixation. All images were captured using Biotek Cytation 3 at 200x magnification. The images were quantified using Fiji software.

Cholesterol biosynthesis assay. Approximately $5x10^5$ cells were plated in 6-well plates and treated overnight. After treatment, the cells were washed twice with PBS. Fresh serum-free medium supplemented with 2 μCi of tritium-labeled acetic

14

acid and 2.5 mM cold-labeled sodium acetate (Cat: S5636, Sigma) was added to all wells, followed by incubation for four hours at 37°C in a 5% CO_2 incubator. After a four-hour incubation, the cells were scraped in 500 μl of ice-cold 2% NaCl, and 0.045 μCi of C14 radiolabeled cholesterol was added to the cell lysate as an internal control. Lipids were isolated from 400 μl of the cell lysate using Folch's method (chloroform:methanol, 2:1), and the remaining 100 μl of the cell lysate was used to quantify protein concentrations. The isolated lipids were dried under nitrogen gas and re-suspended in 150 μl of Folch reagent. Fifty microliters of the sample was loaded onto a TLC silica plate, and the plate was stained with iodine vapor following the separation of lipids. The cholesterol band was identified based on co-migration with a cholesterol standard. The cholesterol bands were excised and placed into glass scintillation vials to measure tritium and C14 radioactivity using a liquid scintillation counter. The results were normalized to the amount of protein and C14 counts (internal control).

Immunoblotting. Protein samples were separated via SDS-PAGE and transferred to a nitrocellulose membrane. The membrane was blocked in 5% milk diluted in TBST and incubated with a primary antibody overnight at 4°C. The blot was subsequently washed and incubated with the corresponding secondary antibody for one hour at RT with shaking. The immunoblot was revealed using ECL and imaged using ChemiDoc XRS software. The following antibodies were used: E2F1 (Cat: sc-193, Santa Cruz Biotechnology), LDLR (Cat: ab30532, Abcam), PCSK9 (Cat: ab31762, Abcam), β-actin (Cat: A2066, Abcam), *a*-tubulin (Cat: T6199, Sigma).

LDLR immunostaining. The mouse liver was cryosectioned at a thickness of 10 μm. Tissue sections were fixed in 4% formalin and blocked in 1% BSA/TBST for one hour. The LDLR primary antibody (Cat: ab30532, Abcam) was diluted in blocking solution, followed by incubation overnight at 4°C. After incubation, the tissue sections were washed three times in PBS and incubated with an Alexa Fluor 488-conjugated anti-rabbit IgG antibody (cat: A21206, Life Technologies) for one hour at RT. The

tissue sections were subsequently washed three times in PBS and incubated with DAPI for three minutes, then washed again. The samples were mounted using mounting medium and analyzed under a fluorescent microscope.

Filipin staining. Cultured cells or mouse liver cryosections were fixed in 4% formalin for ten minutes at RT. The samples were washed three times with PBS and incubated with 1.5 mg glycine/ml PBS for 10 minutes at RT to quench the formalin. The samples were subsequently stained with the filipin working solution (0.05 mg/ml in PBS) for two hours at RT. Then, the samples were washed with PBS and viewed under a fluorescence microscope.

Statistics. All data are expressed as the mean ± SEM. Statistical significance was assessed with a 2-tailed, unpaired t-test or one-way ANOVA, as appropriate, using Prism 6 software (GraphPad Software). Differences were considered statistically significant at $P < 0.05$. All experiments were performed on at least three independent occasions, unless stated otherwise.

AUTHOR CONTRIBUTIONS

QL: designed the project, assembled the data, analyzed and interpreted the results, and wrote and approved the manuscript. PDD: designed the project, analyzed the data and critically reviewed the manuscript. CLM performed the FPLC analysis. LFC: designed the project and wrote and approved the manuscript. All authors read and provided comments on the manuscript

ACKNOWLEDGEMENTS

REFERENCES

1. Biswas AK, and Johnson DG. Transcriptional and nontranscriptional functions of E2F1 in response to DNA damage. *Cancer Res.* 2012;72(1):13-7.
2. Dyson N. The regulation of E2F by pRB-family proteins. *Genes Dev.* 1998;12(15):2245-62.
3. Frolov MV, and Dyson NJ. Molecular mechanisms of E2F-dependent activation and pRB-mediated repression. *J Cell Sci.* 2004;117(Pt 11):2173-81.
4. Blanchet E, Annicotte JS, Lagarrigue S, Aguilar V, Clape C, Chavey C, Fritz V, Casas F, Apparailly F, Auwerx J, et al. E2F transcription factor-1 regulates oxidative metabolism. *Nat Cell Biol.* 2011;13(9):1146-52.
5. Denechaud PD, Lopez-Mejia IC, Giralt A, Lai Q, Blanchet E, Delacuisine B, Nicolay BN, Dyson NJ, Bonner C, Pattou F, et al. E2F1 mediates sustained lipogenesis and contributes to hepatic steatosis. *J Clin Invest.* 2016;126(1):137-50.
6. Fajas L, Landsberg RL, Huss-Garcia Y, Sardet C, Lees JA, and Auwerx J. E2Fs regulate adipocyte differentiation. *Dev Cell.* 2002;3(1):39-49.
7. Hsieh MC, Das D, Sambandam N, Zhang MQ, and Nahle Z. Regulation of the PDK4 isozyme by the Rb-E2F1 complex. *J Biol Chem.* 2008;283(41):27410-7.
8. Accad M, and Farese RV, Jr. Cholesterol homeostasis: a role for oxysterols. *Curr Biol.* 1998;8(17):R601-4.
9. Brown MS, and Goldstein JL. A receptor-mediated pathway for cholesterol homeostasis. *Science.* 1986;232(4746):34-47.
10. Ishibashi S, Brown MS, Goldstein JL, Gerard RD, Hammer RE, and Herz J. Hypercholesterolemia in low density lipoprotein receptor knockout mice and its reversal by adenovirus-mediated gene delivery. *J Clin Invest.* 1993;92(2):883-93.
11. Borghi C, and Cimminiello C. [The new lipid-lowering drugs: focus on monoclonal antibodies]. *G Ital Cardiol (Rome).* 2016;17(4):14-21.
12. Lipari MT, Li W, Moran P, Kong-Beltran M, Sai T, Lai J, Lin SJ, Kolumam G, Zavala-Solorio J, Izrael-Tomasevic A, et al. Furin-cleaved proprotein convertase subtilisin/kexin type 9 (PCSK9) is active and modulates low density lipoprotein receptor and serum cholesterol levels. *J Biol Chem.* 2012;287(52):43482-91.
13. Costet P, Cariou B, Lambert G, Lalanne F, Lardeux B, Jarnoux AL, Grefhorst A, Staels B, and Krempf M. Hepatic PCSK9 expression is regulated by nutritional status via insulin and sterol regulatory element-binding protein 1c. *J Biol Chem.* 2006;281(10):6211-8.
14. Schuppan D, and Kim YO. Evolving therapies for liver fibrosis. *J Clin Invest.* 2013;123(5):1887-901.
15. Fon Tacer K, and Rozman D. Nonalcoholic Fatty liver disease: focus on lipoprotein and lipid deregulation. *J Lipids.* 2011;2011(783976.

16. Arguello G, Balboa E, Arrese M, and Zanlungo S. Recent insights on the role of cholesterol in non-alcoholic fatty liver disease. *Biochim Biophys Acta.* 2015;1852(9):1765-78.

17. Ioannou GN. The Role of Cholesterol in the Pathogenesis of NASH. *Trends Endocrinol Metab.* 2016;27(2):84-95.

18. Musso G, Gambino R, and Cassader M. Cholesterol metabolism and the pathogenesis of non-alcoholic steatohepatitis. *Prog Lipid Res.* 2013;52(1):175-91.

19. Zhang Y, Xu N, Xu J, Kong B, Copple B, Guo GL, and Wang L. E2F1 is a novel fibrogenic gene that regulates cholestatic liver fibrosis through the Egr-1/SHP/EID1 network. *Hepatology.* 2014;60(3):919-30.

20. Poirier S, and Mayer G. The biology of PCSK9 from the endoplasmic reticulum to lysosomes: new and emerging therapeutics to control low-density lipoprotein cholesterol. *Drug Des Devel Ther.* 2013;7(1135-48.

21. Dubuc G, Chamberland A, Wassef H, Davignon J, Seidah NG, Bernier L, and Prat A. Statins upregulate PCSK9, the gene encoding the proprotein convertase neural apoptosis-regulated convertase-1 implicated in familial hypercholesterolemia. *Arterioscler Thromb Vasc Biol.* 2004;24(8):1454-9.

22. Tabas I. Consequences of cellular cholesterol accumulation: basic concepts and physiological implications. *J Clin Invest.* 2002;110(7):905-11.

23. Giunzioni I, Tavori H, Covarrubias R, Major AS, Ding L, Zhang Y, DeVay RM, Hong L, Fan D, Predazzi IM, et al. Local effects of human PCSK9 on the atherosclerotic lesion. *The Journal of pathology.* 2016;238(1):52-62.

24. Shalem O, Sanjana NE, Hartenian E, Shi X, Scott DA, Mikkelsen TS, Heckl D, Ebert BL, Root DE, Doench JG, et al. Genome-scale CRISPR-Cas9 knockout screening in human cells. *Science.* 2014;343(6166):84-7.

25. Salmon P, and Trono D. Production and titration of lentiviral vectors. *Curr Protoc Neurosci.* 2006;Chapter 4(Unit 4 21.

26. Dikkers A, Freak de Boer J, Annema W, Groen AK, and Tietge UJ. Scavenger receptor BI and ABCG5/G8 differentially impact biliary sterol secretion and reverse cholesterol transport in mice. *Hepatology.* 2013;58(1):293-303.

27. Le May C, Kourimate S, Langhi C, Chetiveaux M, Jarry A, Comera C, Collet X, Kuipers F, Krempf M, Cariou B, et al. Proprotein convertase subtilisin kexin type 9 null mice are protected from postprandial triglyceridemia. *Arteriosclerosis, thrombosis, and vascular biology.* 2009;29(5):684-90.
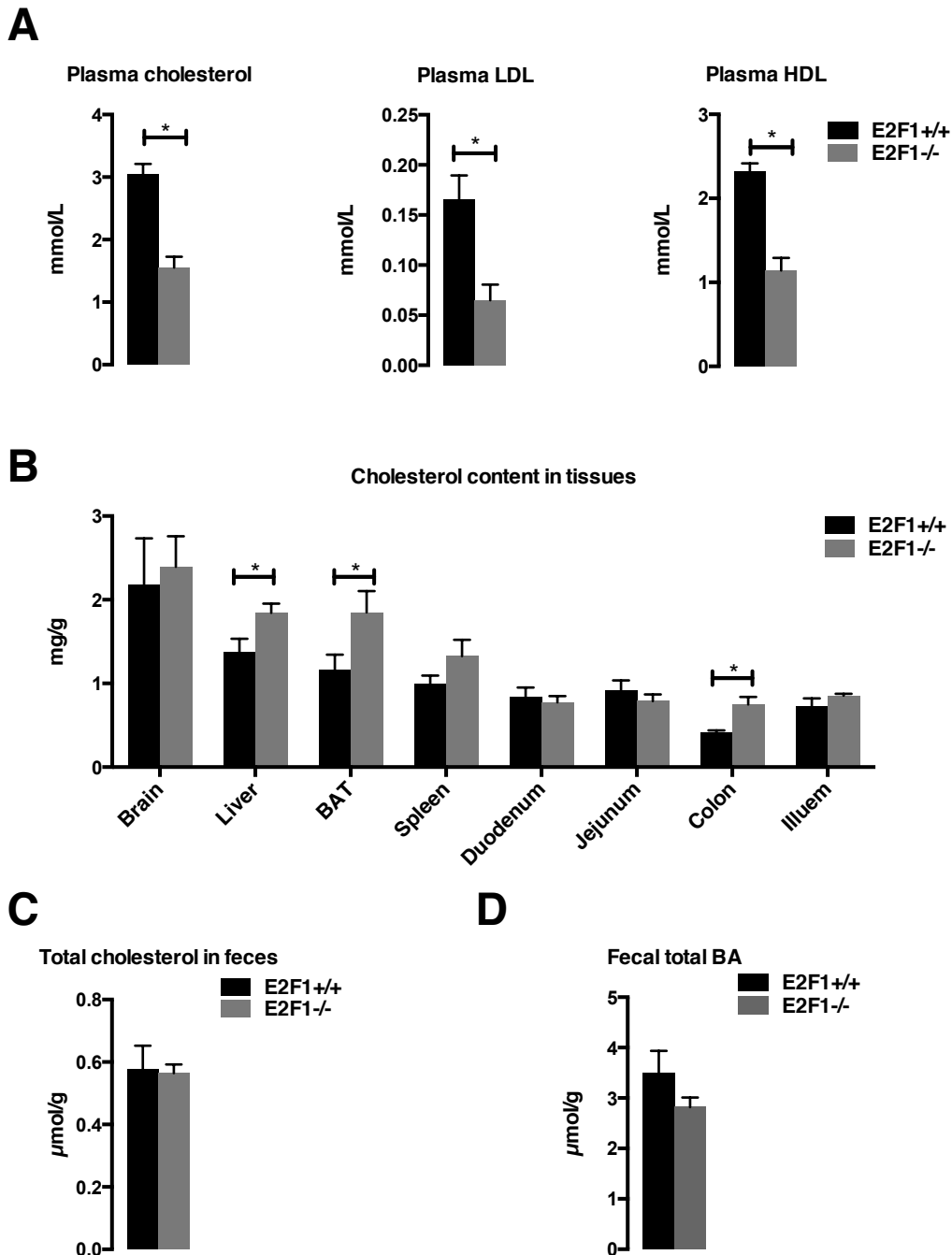
Figure 1. Decreased total plasma cholesterol levels and increased cholesterol content in the liver and colon tissues of E2F1-/- mice

(A) Plasma lipid profiles of E2F1+/+ and E2F1-/- mice fed a normal chow diet.

(B) Quantification of the cholesterol content of various tissues from the E2F1+/+ and E2F1-/- mice that were fed a chow diet.

**(C)** Quantification of total free cholesterol levels in feces collected from individual mice using commercial kits.

(D) Quantification of total bile acid levels in feces collected from individual mice using commercial kits.

All data are presented as the means ± standard errors of the mean (SEM) from a minimum of five mice per group. An asterisk denotes a significant difference at P<0.05.

A

| ENSEMBL_GENE_ID	GENE_ID	Gene Name
ENSMUSG00000018167	Stard3	START domain containing 3
ENSMUSG00000018861	Fdxr	ferredoxin reductase
ENSMUSG00000020538	Srebf1-c	sterol regulatory element binding transcription factor 1-c
ENSMUSG00000020919	Stat5b	signal transducer and activator of transcription 5B
ENSMUSG00000021259	Cyp46a1	cytochrome P450, family 46, subfamily a, polypeptide 1
ENSMUSG00000021273	Fdft1	farnesyl diphosphate farnesyl transferase 1
ENSMUSG00000021594	Srd5a1	steroid 5 alpha-reductase 1
ENSMUSG00000023832	Acat2	acetyl-Coenzyme A acetyltransferase 2
ENSMUSG00000023921	Mut	methylmalonyl-Coenzyme A mutase
ENSMUSG00000024087	Cyp1b1	cytochrome P450, family 1, subfamily b, polypeptide 1
ENSMUSG00000024687	Osbp	oxysterol binding protein
ENSMUSG00000024799	Tm7sf2	transmembrane 7 superfamily member 2
ENSMUSG00000026675	Hsd17b7	hydroxysteroid (17-beta) dehydrogenase 7
ENSMUSG00000030670	Cyp2r1	cytochrome P450, family 2, subfamily r, polypeptide 1
ENSMUSG00000031393	Mecp2	methyl CpG binding protein 2
ENSMUSG00000031604	Sc4mol	sterol-C4-methyl oxidase-like
ENSMUSG00000031708	Tecr	Trans-2,3-Enoyl-CoA Reductase
ENSMUSG00000032245	Cln6	ceroid-lipofuscinosis, neuronal 6
ENSMUSG00000037295	Ldlrap1	low density lipoprotein receptor adaptor protein 1
ENSMUSG00000039050	Osbpl2	oxysterol binding protein-like 2
ENSMUSG00000039529	Atp8b1	ATPase, class I, type 8B, member 1
ENSMUSG00000040374	Pxmp3	peroxisomal membrane protein 3
ENSMUSG00000041939	Mvk	mevalonate kinase; similar to mevalonate kinase
ENSMUSG00000044252	Osbpl1a	oxysterol binding protein-like 1A
ENSMUSG00000044254	**Pcsk9**	**proprotein convertase subtilisin/kexin type 9**
ENSMUSG00000045294	Insig1	insulin induced gene 1
ENSMUSG00000046873	Mbtps2	membrane-bound transcription factor peptidase, site 2
ENSMUSG00000058454	Dhcr7	7-dehydrocholesterol reductase
ENSMUSG00000059743	Fdps	Farnesyl Diphosphate Synthase

B
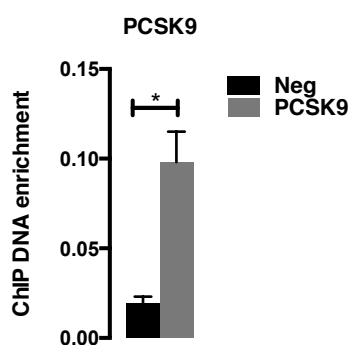
C
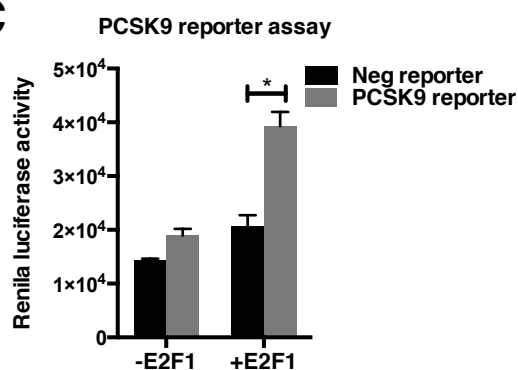
Figure 2. E2F1 binds and transactivate PCSK9 promoter activity
(A) List of cholesterol-related genes enriched in E2F1 ChIP-seq analysis of primary culture of hepatocytes Ad-E2F1. PCSK9 is highlighted in bold.
(B) PCSK9 was enriched via E2F1 ChIP-IP performed in the HepG2 cell line. The experiments were independently repeated three times, and representative data are shown (N=3).
(C) Human PCSK9 promoter reporter activity in HepG2 cells transfected with E2F1 or the empty plasmid (N=3).
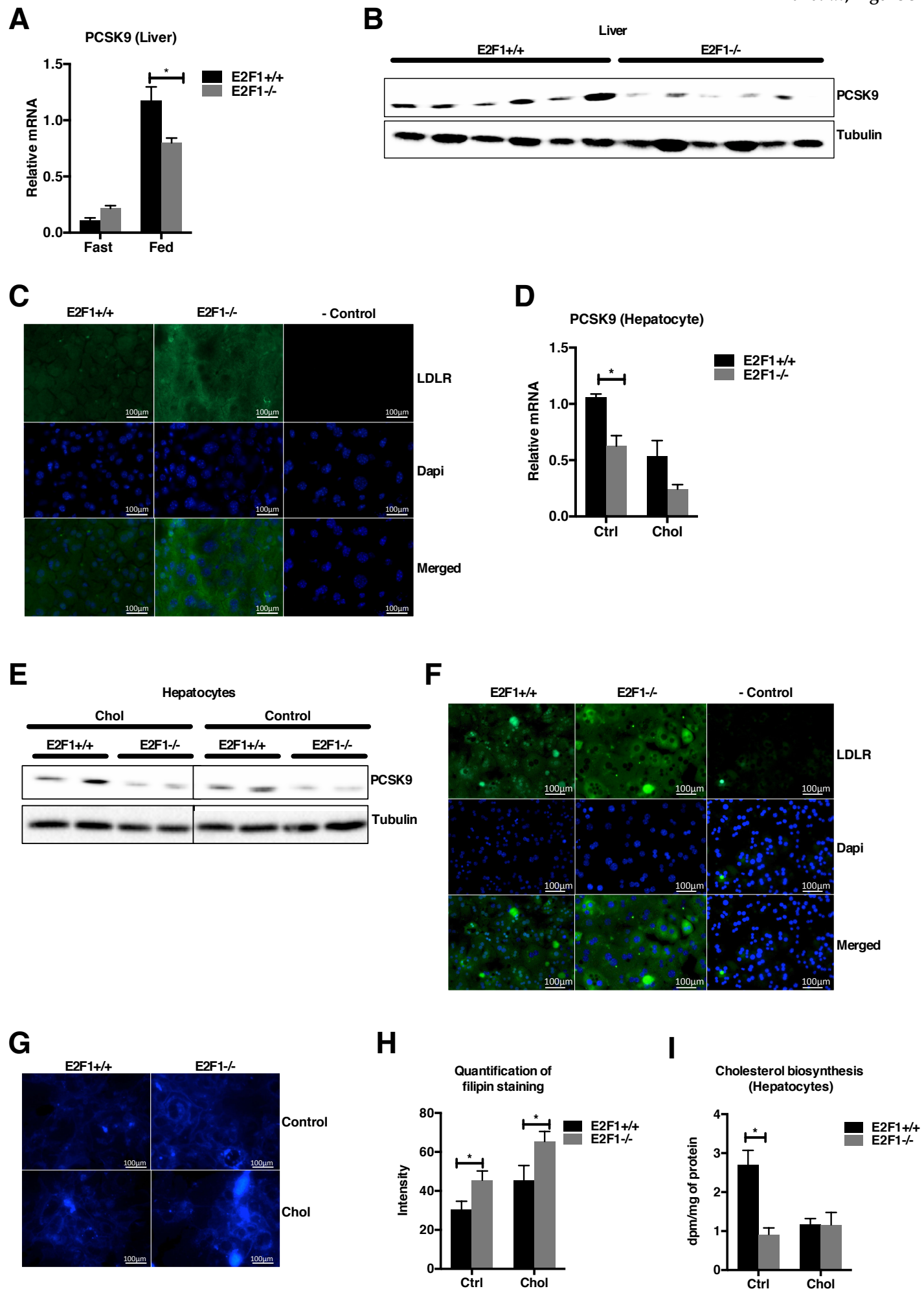
Figure 3. Loss of E2F1 decreases PCSK9 expression and increases hepatic LDLR protein expression in hepatocytes

(A) Relative expression of PCSK9 mRNA in liver tissues from E2F1+/+ and E2F1-/- mice that were fed a normal chow diet or fasted overnight.

(B) Western blot of PCSK9 in the livers of E2F1+/+ and E2F1-/- mice.

(C) Representative images of LDLR immunostaining in livers from E2F1+/+ and E2F1-/- mice that were fed a chow diet. LDLR is stained in green; nuclei are stained in blue. Scale bar: 100 µm.

(D) Relative expression of PCSK9 mRNA in primary E2F1+/+ and E2F1-/- mouse hepatocytes treated with medium supplemented with DMSO (control) or 0.065 mg/ml cholesterol (chol).

(E) Representative images of PCSK9 western blots from primary E2F1+/+ and E2F1-/- mouse hepatocytes. Tubulin was used as a loading control (N=2).

(F) Representative images of LDLR immunostaining in primary E2F1+/+ and E2F1-/- mouse hepatocytes (N=3). The experiment was independently repeated three times. LDLR is stained in green; Nuclei are stained in blue. Scale bar: 100 µm.

(G) Filipin staining of E2F1+/+ and E2F1-/- mouse hepatocytes (N=3).

(H) Quantification of the intensity of filipin staining.

(I) Quantification of the rate of cholesterol biosynthesis in E2F1+/+ and E2F1-/- mouse hepatocytes treated with medium supplemented with DMSO (control) or 0.065 mg/ml cholesterol.

All data are presented as the means ± standard errors of the mean (SEM) of three independent experiments, unless otherwise indicated. An asterisk denotes a significant difference at $P<0.05$.
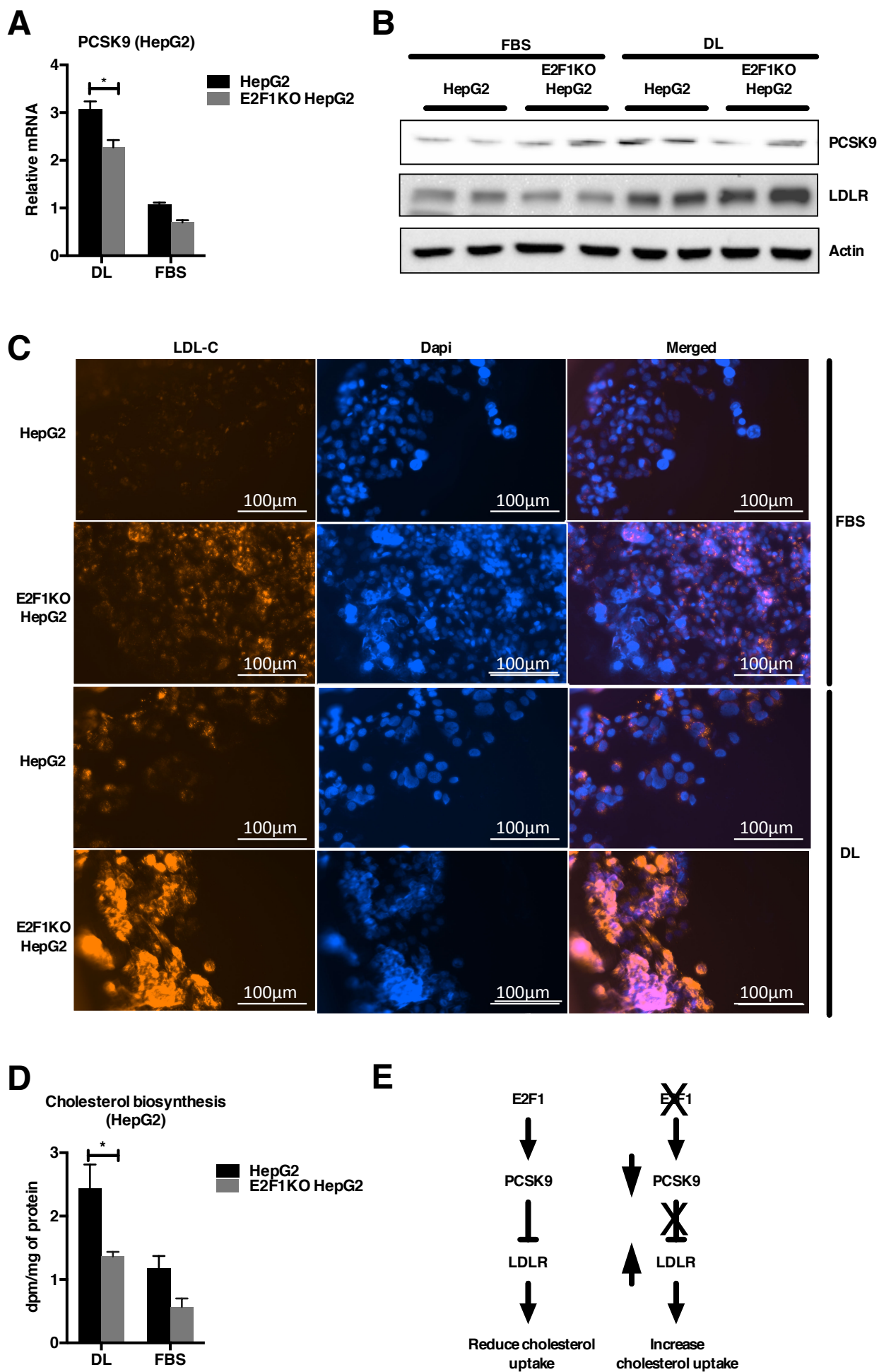
Figure 4. E2F1KO HepG2 cells show increased LDL-C uptake and decreased cholesterol biosynthesis
(A) Relative expression of PCSK9 mRNA in HepG2 and E2F1KO HepG2 cells treated with medium supplemented with 10% FBS or 10% delipidated serum (DL).
(B) Representative images of PCSK9 and LDLR western blots from HepG2 and E2F1KO HepG2 cells (N=3).
(C) Representative images of LDL-C uptake in HepG2 and E2F1KO HepG2 cells cultured in medium supplemented with 10% FBS or 10% delipidated serum (N=3). Red fluorescence denotes LDL-C, and nuclei are stained in blue. Scale bar: 100 μm.
(D) Quantification of the rate of cholesterol biosynthesis in HepG2 and E2F1KO HepG2 cells treated with medium supplemented with 10% FBS or 10% delipidated serum.
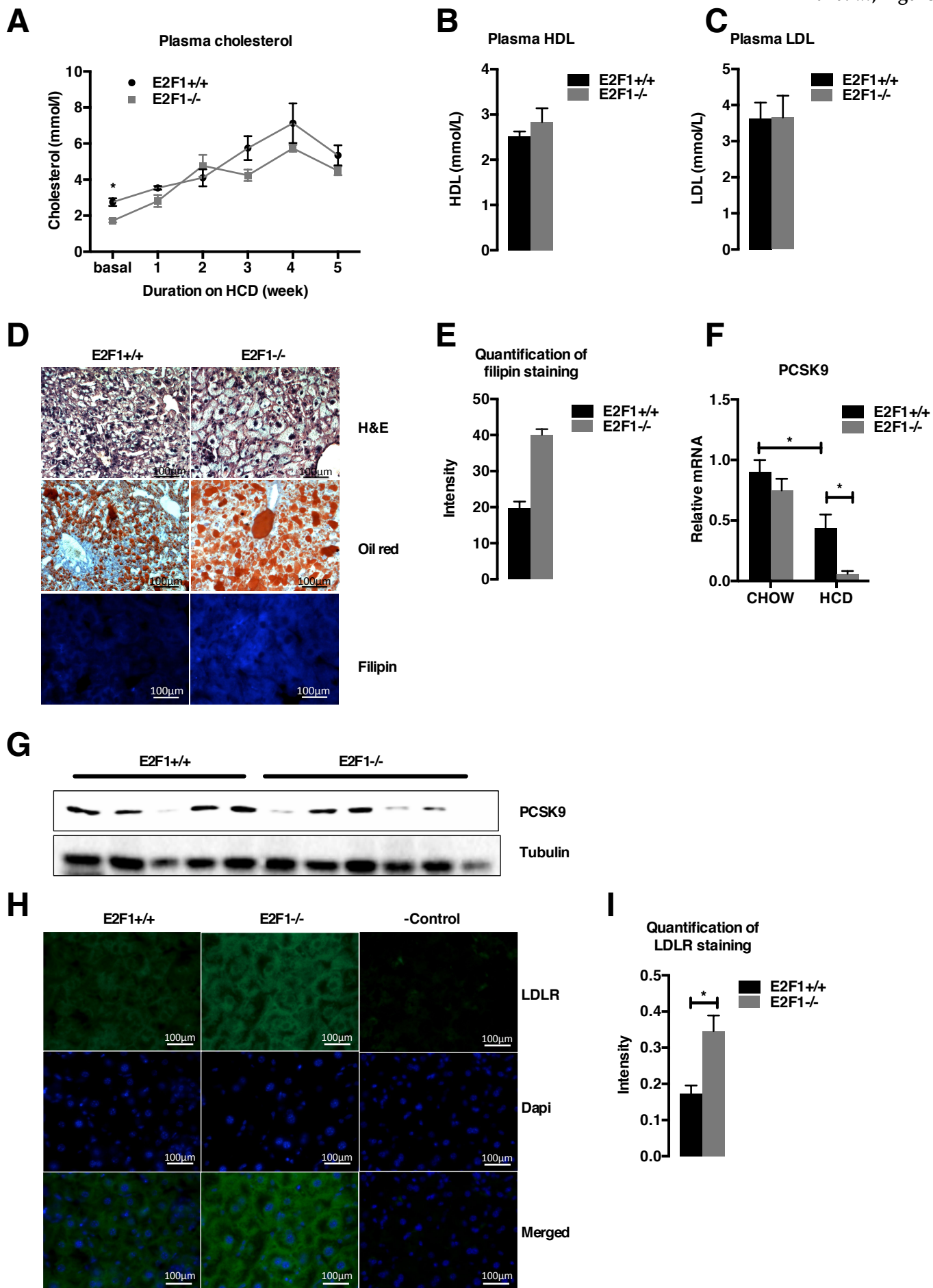
Figure 5. Cholesterol homeostasis and liver phenotype in E2F1-/- mice fed a HCD

(A) Plasma cholesterol profiles of E2F1+/+ and E2F1-/- mice before and after five weeks of being fed a high cholesterol diet (1.25% cholesterol).

(B-C) Plasma HDL and LDL-cholesterol levels after the five weeks of the HCD.

(D) H&E, Oil Red O and filipin staining of E2F1+/+ and E2F1-/- liver sections. Scale bar: 100 μm.

(E) Quantification of the intensity of filipin staining in the liver.

(F) Relative expression of PCSK9 mRNA in liver tissues from E2F1+/+ and E2F1-/- mice that were fed on chow or HCD for five weeks.

(G) Western blot of PCSK9 in the liver tissues of E2F1+/+ and E2F1-/- mice that were fed an HCD for five weeks. Tubulin was used as a loading control.

(H) Representative immunostaining of LDLR in the livers of E2F1+/+ and E2F1-/- mice that were fed an HCD. Scale bar: 100 μm.

(I) Quantification of LDLR staining in the livers from the E2F1+/+ and E2F1-/- mice that after five weeks of HCD. Fluorescence intensity was normalized to the number of cells.

All data are presented as the means ± standard errors of the mean (SEM) from a minimum of five mice per group. The asterisk denotes a significant difference at $P<0.05$.
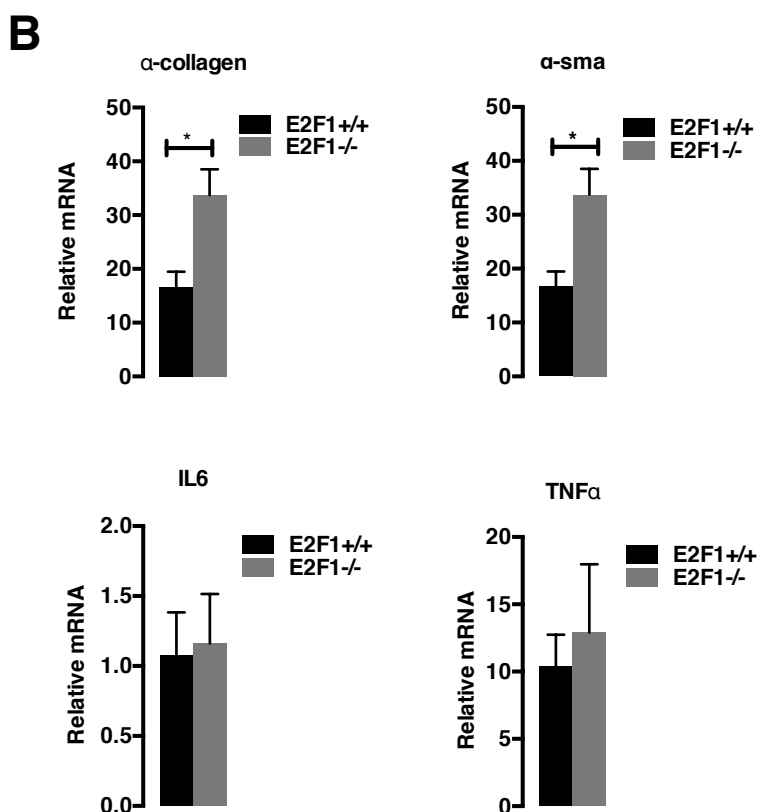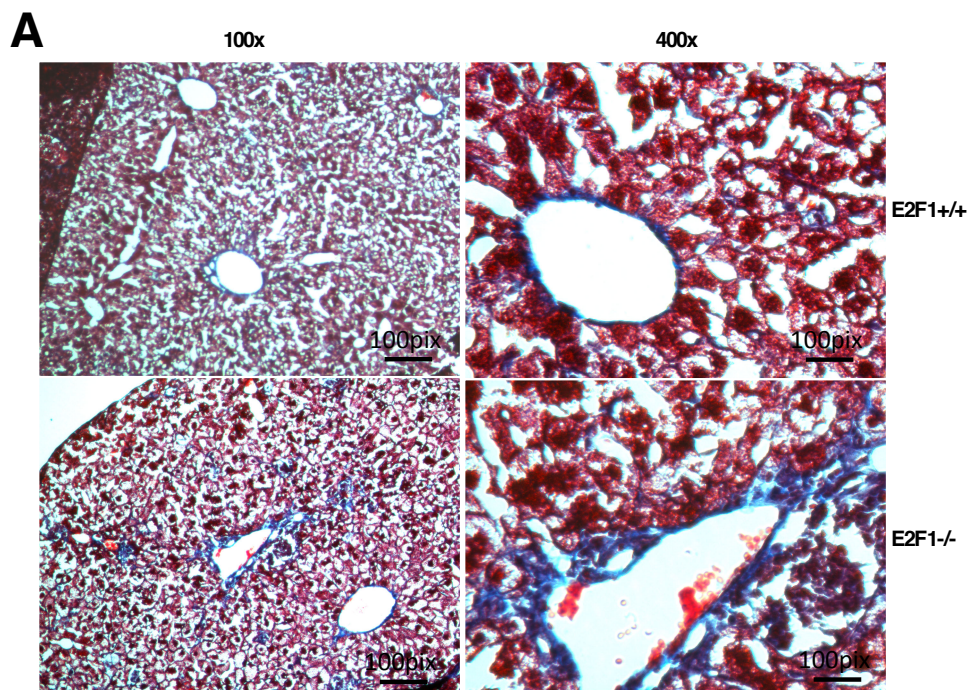
Figure 6. E2F1-/- mice exhibit more pronounced liver fibrosis after 5 weeks on the HCD
(A) Representative images of trichrome staining of livers from the E2F1+/+ and E2F1-/- mice that were fed a HCD for five weeks. Blue denotes collagen staining. Scale bar: 100 μm.
(B) Relative mRNA expression of fibrosis-inflammation related genes in the liver tissues from the E2F1+/+ and E2F1-/- mice that were fed an HCD for five weeks. All data are presented as the means ± standard errors of the mean (SEM) from a minimum of five mice per group. An asterisk denotes a significant difference at P<0.05.
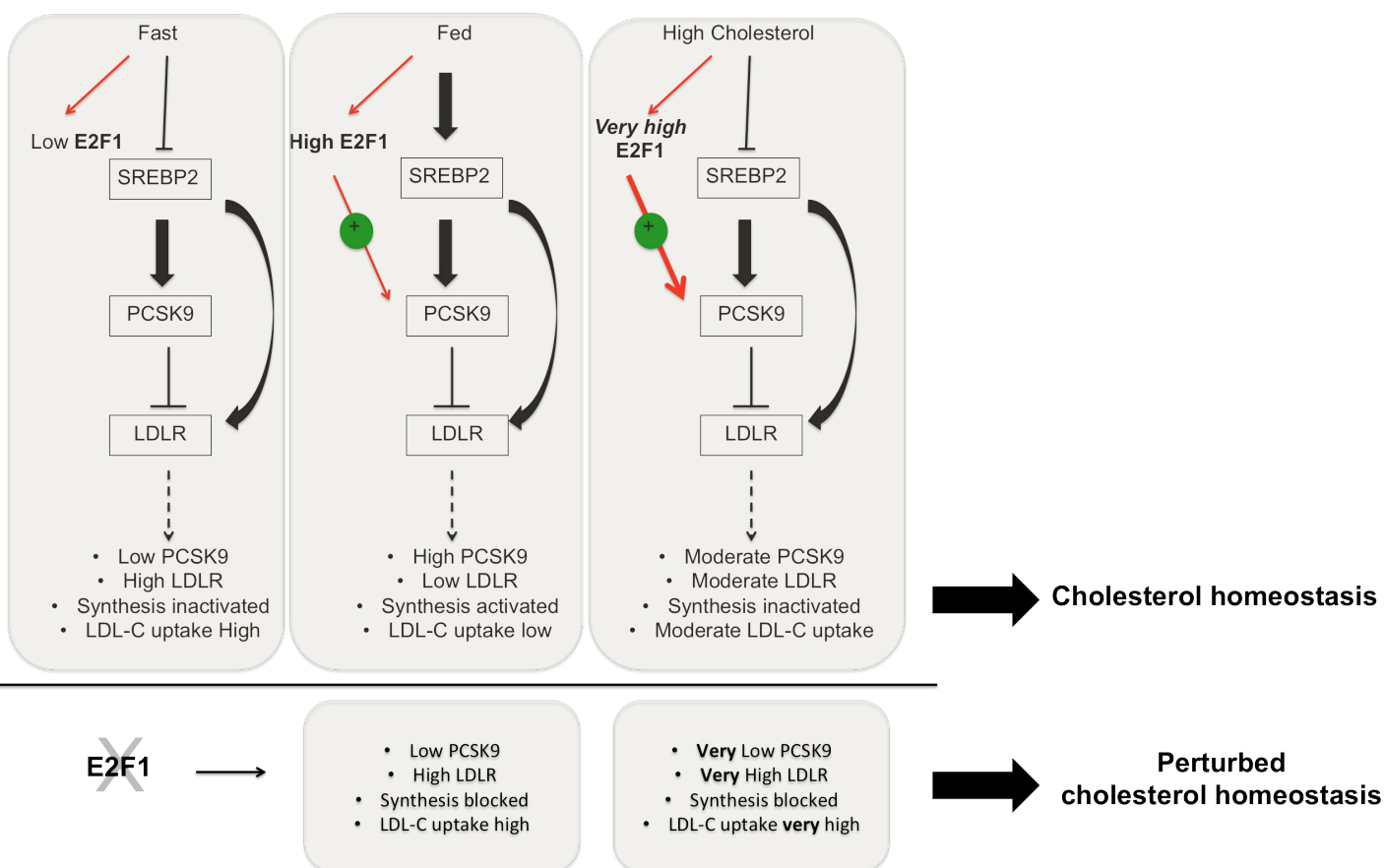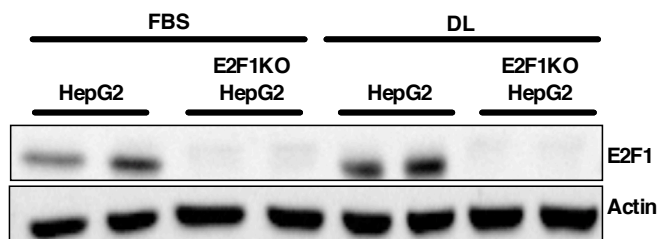
Figure 7. Proposed model: E2F1 regulation of PCSK9 in response to diets
E2F1 expression is diet dependent. E2F1 and SREBP2 work in a synergistic manner to regulate LDLR availability to PCSK9 and consequently LDL-cholesterol uptake.
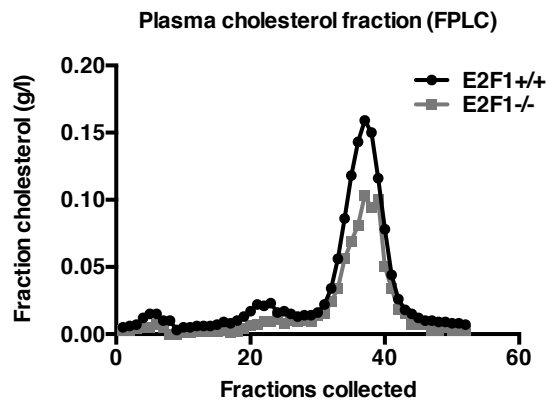
Supplemental Figure 1: FPLC separation of pooled plasma cholesterol in E2F1+/+ and E2F1-/- chow-fed mice.


Supplemental Figure 2: E2F1 expression was completely ablated in the HepG2 cell line. Representative images of E2F1 western blots from HepG2 and E2F1KO HepG2 cells (N=3).

Western blot quantification
PCSK9
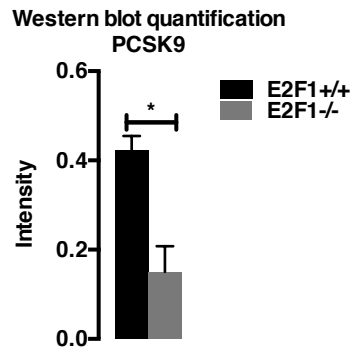
Supplemental Figure 3: Quantification of PCSK9 western blots of liver tissues from E2F1+/+ and E2F1-/- mice that were fed an HCD for five weeks. The obtained values were normalized to tubulin.
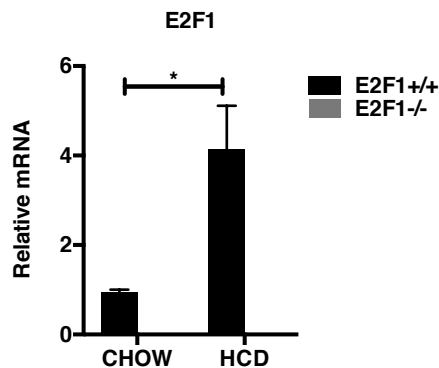
E2F1

Supplemental Figure 4: Relative expression of E2F1 mRNA in the livers of E2F1+/+ and E2F1-/- mice that were fed with either standard chow or an HCD for five weeks. All data are presented as the means ± standard errors of the mean (SEM) for a minimum of five mice per group. An asterisk denotes significant a difference at P<0.05.

A

Total bile acid in feces

B

Fecal neutral sterol
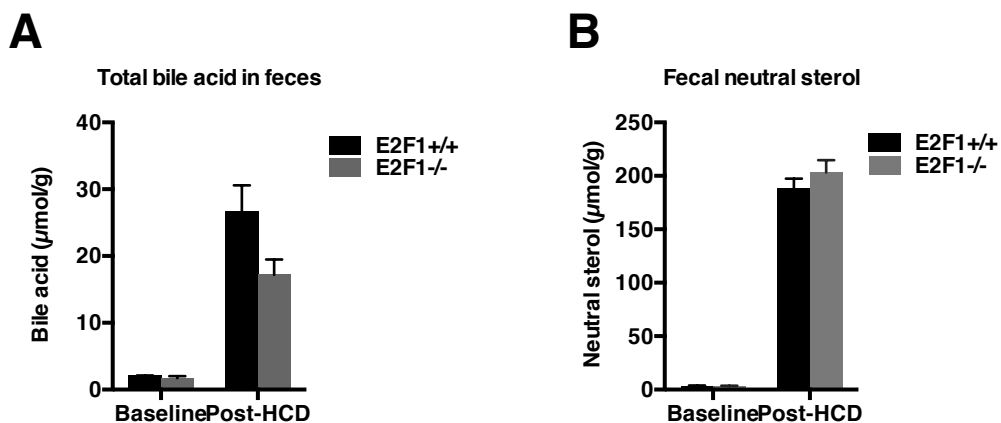
Supplemental Figure 5: Fecal analysis of E2F1+/+ and E2F1-/- before and after five weeks of HCD. (A) Fecal total bile acid quantification in the E2F1+/+ and E2F1-/- before and after five weeks of HCD. (B) Fecal total neutral sterol quantification in the E2F1+/+ and E2F1-/- before and after five weeks of HCD. All data are presented as the means ± standard errors of the mean (SEM) for a minimum of five mice per group. An asterisk denotes significant a difference at P<0.05.

Summary

1. E2F-/- mice exhibit decreased plasma cholesterol levels and increase cholesterol content in the liver tissues.

2. E2F1 is a positive regulator of PCSK9 and control LDLR mediated cholesterol uptake.

3. E2F1-/- mice has an abnormal cholesterol homeostasis and display an accumulation of cholesterol in the livers.

4. High dietary cholesterol promotes liver fibrosis in E2F1-/- mice.

5. Our data suggests that PCSK9 inhibitor treatment is beneficial for lowering plasma lipid but excessive cholesterol uptake in the liver should not be overlooked.